Angular Momentum Distribution in Galactic Halos

Drehimpulsverteilung in galaktischen Halos

Adelheid Teklu

München 2014

Angular Momentum Distribution in Galactic Halos

Drehimpulsverteilung in galaktischen Halos

Master Thesis

at

Ludwig–Maximilians–Universität München

submitted by

Adelheid Teklu

born 3rd of February 1984 in Munich

supervised by

PD Dr. Klaus Dolag

Munich, September 29, 2014

Evaluator: PD Dr. Klaus Dolag

Contents

1. Introduction **1**

2. The Magneticum Pathfinder Simulations **8**

3. Classification of Galaxies and Properties of Disks **11**
3.1. Classification 11
3.1.1. The Circularity Parameter 13
3.1.2. Selection Criteria 13
3.1.3. Morphology 15
3.2. Rotation Curves 17

4. The Angular Momentum **19**
4.1. The Specific Angular Momentum 19
4.1.1. The Specific Angular Momentum of Gas and Stars 20
4.1.2. The Angular Momentum – Mass Relation 22
4.1.3. The Specific Angular Momentum of Gas and Dark Matter . . 24
4.1.4. Angular Momentum Profiles 30
4.2. Orientation of the Angular Momentum Vectors 31
4.2.1. The Angle between the Gas and the Star Component 32
4.2.2. The Angle between the Gas and the Dark Matter Component 32
4.2.3. The Angle between the Dark Matter and the Star Component 35
4.2.4. The Angle between the Dark Matter at Different Radii 37
4.3. The λ-Parameter 39
4.3.1. The λ – Distribution for Halos 39
4.3.2. The λ – Distribution for Single Components of the Halos . . . 45

Summary **55**

Acknowledgements **59**

A. Appendix: Angular Momentum-Mass Relation at $z = 0.99$ and $z = 0.47$ **61**

B. Appendix: Angular Momentum Profiles at $z = 0.99$ and $z = 0.47$ **63**

C. Appendix: Alignment Angles **64**
C.1. Tables for $z = 1.98$ and 0.07 64
C.2. Gas and Stars at $z = 0.99$ and $z = 0.47$ 66

C.3. Dark Matter and Gas at $z = 0.99$ and $z = 0.47$ 67
C.4. Dark Matter and Stars at $z = 0.99$ and $z = 0.47$ 68
C.5. Dark Matter at Different Radii at $z = 0.99$ and $z = 0.47$ 69

D. Appendix: λ – Distribution **70**
D.1. Table for the Overall λ-Distribution 70
D.2. λ for the Dark Matter Only 71
D.3. λ for Different Components at $z = 0.99$ and $z = 0.47$ 72

References **77**

1. Introduction

The Universe is filled with dark energy and matter, which contributes about 72 and 28 per cent, respectively, to the Universe's content. The major part of the matter is not visible but dark, since it is not interacting with light. Only about five per cent of the content of the Universe is made up of ordinary "baryonic" matter. In the state the Universe is today, most of this matter is in the form of diffuse gas and fills the space between the galaxies. Some fraction of it sits in the deep potential wells of galaxy clusters and is hot enough to be visible in the X-rays. Only a tiny part of this matter is condensed into stars. These stars make up the visible part of galaxies and can be detected with modern telescopes. Additionally, some galaxies still have some cold gas in the form of extended gas disks, while other galaxies contain some hot diffuse gas, which fills the entire potential well associated with the dark matter halo. There are different kinds of galaxies observed, which span a variety of morphological types. According to the so-called Hubble tuning fork (see Fig. 1.1) we can divide them into three main types: elliptical, spiral and irregular galaxies.

Elliptical galaxies (for historical reasons also called "early type galaxies") are dispersion dominated systems ("dynamically hot"), which consist mainly of old stars. Many of them also contain gas. Some have hot gas which is seen in the X-Ray, about 40 per cent also have cold gas (Young et al., 2014), which can build up a disk-like structure. Elliptical galaxies are mostly found in dense environments, i.e. in the centers of galaxy clusters or groups. The most massive galaxies in the Universe are ellipticals. They can be subdivided by their ellipticity $\varepsilon := 1 - b/a$, where a is the semi-major and b is the semi-minor axis. Hence, an E0 galaxy has a circular shape with $b/a = 1$, while an E7 has a large ellipticity with $b/a = 0.3$.

Spiral galaxies (also called "late type galaxies") are rotation dominated ("dynamically cold"). They consist of a gaseous as well as a stellar disk with spiral patterns, which contain mainly young stars, and a central stellar bulge, which consists mostly of an old stellar population. They are subdivided into normal (Sa - Sd) and barred (SBa - SBd) spirals. Mostly they are found in the field, i.e. in less dense environments (Dressler, 1980).

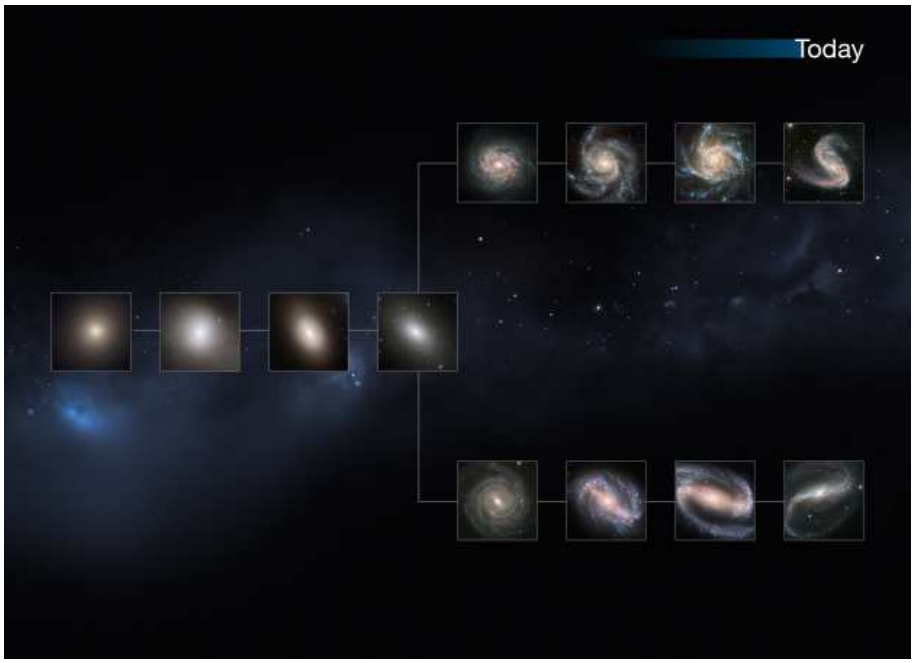

Fig. 1.1.: The Hubble tuning fork of galaxy classification at the present day. On the left side there are ellipticals, in the middle lenticulars and on the right side spiral galaxies. The upper branch shows normal spirals and the lower branch spirals with bars. Copyright: NASA, ESA, M. Kornmesser.

The third main class are the irregular galaxies, which do not have a real center and appear diffuse. Mostly, they are low mass objects which often belong to a larger galaxy or they are systems that have been disturbed by e.g. a merger.

Furthermore, as a transition between the ellipticals and the spirals there are S0 galaxies, also called lenticulars because of their lenticular shape. They have a bulge and a disk-like structure without spiral arms. For an introduction on galaxies and cosmology, see Hetznecker (2009) and Schneider (2008).

Naturally, the question arises, how the different types of galaxies formed and in particular, which properties determine a galaxy to become a disk or spheroid dominated system. For the formation of elliptical galaxies the following formation scenarios are proposed: One possibility is that they form by the major merger of two spiral galaxies (Toomre, 1977). Alternatively they can form by a series of minor mergers (e.g. (Meza et al., 2003)).

It is still not fully understood, how spiral galaxies form. The formation has been discussed in several studies for more than 30 years. The main focus is on the angular momentum. Initially the dark matter halo and the infalling gas have identical

angular momenta. During the formation of the galaxy the gas cools and condenses in the center of the halo to form a disk. Assuming that the angular momentum of the gas is conserved during this process, the angular momentum of the halo of a disk galaxy can be estimated directly from the angular momentum of the disk of the galaxy (Fall and Efstathiou, 1980; Fall, 1983; Mo et al., 1998).

For a better understanding we will briefly sketch the hierarchical growth of the structures in a cosmological context where we follow (Hetznecker, 2009). The first 30000 years after the Big Bang the Universe was dominated by radiation, i.e. photons. Due to the cosmic expansion the photons lost energy. Consequently, more and more neutral atoms could form without being destroyed again by the photons; the Universe becomes matter-dominated. Finally, 380000 years after the Big Bang baryons and photons decouple, which today can be seen as the Cosmic Microwave Background (CMB). However, the dark matter decouples about 300000 years earlier. Since it only interacts gravitationally it has time to form potential wells.
In hierarchical scenarios of structure formation (we follow Peebles (1993) and references therein), structures form by the gathering of clumps due to the gravitational force. The dark matter condenses at high redshift into small objects which grow to ever larger objects and finally build halos. The proto-galaxies are not totally spherically symmetric. The tidal torques of neighboring proto-galaxies give them their angular momentum of rotation. The gas cools and collapses within the dark matter halos to form the galaxies (White and Rees, 1978). Since the baryons and the dark matter gain the same amount of angular momentum through the tidal torques (Peebles, 1969; Doroshkevich, 1970) and the specific angular momentum of the gas should be conserved during the collapse, the disk is expected to have a similar specific angular momentum as that of the hosting halo (Fall and Efstathiou, 1980).

Since it is very difficult to observe these early stages of galaxy formation, we have to make use of numerical N-body simulations. Until recently, simulations suffered from the so called “angular momentum problem”, where the objects became too small compared to observations because the gas had lost too much angular momentum (e.g. Navarro and Benz (1991); Navarro and White (1994); Navarro and Steinmetz (1997)). As simulations got better in resolution and also included feedback from stars, supernovae (SNe) and active galactic nuclei (AGN), the gas was prevented

from cooling too soon. Hence, early star formation was suppressed and this numerical loss of angular momentum could be minimized. There are several studies that investigated the influence of star formation and the associated SN feedback on the formation of galactic disks (e.g. Brook et al. (2004); Okamoto et al. (2005); Governato et al. (2007); Scannapieco et al. (2008); Zavala et al. (2008)); they found that strong feedback at early times leads to the formation of more realistic disk galaxies.
Another parameter to describe the rotation of a system is the so-called spin parameter λ, which was introduced by Peebles (1969, 1971) and has since been investigated in several studies. With λ one can measure the degree of rotational support of the total halo. A completely rotationally-supported system would have $\lambda = 1$. It has the advantage that it is only weakly depending on the halo's mass and its internal substructures (Barnes and Efstathiou, 1987).

The impact of such parameters on galaxy formation has been investigated by many authors.
At first, simulations with only dark matter neglecting the baryons were employed. Bullock et al. (2001) defined a modified version of the λ-parameter by defining the energy of the halo via its circular velocity. In addition, they studied the alignment of the angular momentum of the inner and outer halo parts. They found that most halos were well-aligned but mentioned that about ten per cent of the halos were considerably misaligned. The misalignment angle of the angular momentum vectors at different radii was studied in more detail by Bailin and Steinmetz (2005). They showed that with increasing separation of the radii the misalignment of the vectors increases. In another study Macciò et al. (2008) focused on the spin parameter's dependence on the mass and the cosmology and did not find any dependencies on mass or cosmology. Trowland et al. (2013) studied the connection of the halo spin with the large scale structure. They confirmed that the spin parameter is not mass-dependent at low redshift but found an evolution, where at high redshift the overall values tend to be smaller.
Other authors included non-radiative gas in their analysis. The misalignment of the gas and dark matter angular momentum vectors and their spin parameters at redshift $z = 3$ were investigated by van den Bosch et al. (2002). They found the angular momentum vectors to be misaligned by a median angle of about 30°. But the overall distribution of the spin parameters of the gas and the dark matter were

found to be very similar. Another detailed study by Sharma and Steinmetz (2005) and Sharma et al. (2012) found that the spin parameter of gas is on average higher than that of the dark matter component and they reported a misalignment of the angular momentum of the gas and the dark matter of about 20°.
Chen et al. (2003) compared the spin parameter and the misalignment angles between the dark matter and gas angular momentum vectors obtained in simulations, which also allow the gas to cool. This enables one to additionally split the gas into a cold and a hot component. In their non-radiative model they confirmed that the spin parameter of the gas component has higher spin than the dark matter while in their simulations including cooling the two components had about the same amount of spin. The misalignments of the global angular momentum vectors were 22.8° and 25° for the cooling models and 23.5° for the non-radiative case. Stewart et al. (2011, 2013) focused on the specific angular momentum and the spin parameter in relation to the cold/hot mode accretion by following the evolution for individual halos over cosmic time and found that the spin of cold gas was the highest compared to all other components and about $3-5$ times higher than that of the dark matter. Scannapieco et al. (2009) investigated the evolution of eight individual halos and did not find a correlation between the spin parameter and the morphology of the galaxy inside the halo. Furthermore, they found that the disks have higher specific angular momentum than the hosting dark matter halos, while spheroids have lower specific angular momentum and that the disks can be destroyed by major mergers. In addition they saw a misalignment between stellar disks and infalling cold gas. Also, Sales et al. (2012) found no correlation between the spin parameter and the galaxy type and concluded that disks are predominantly formed in halos where the freshly accreted gas has similar angular momentum to that of earlier accretion, whereas spheroids tend to form in halos where gas streams in along misaligned cold flows. Kimm et al. (2011) studied the different behavior of the gas' and dark matter specific angular momentum by following the evolution of a Milky Way type galaxy over cosmic time. They also found that the gas has higher specific angular momentum and spin parameter than the dark matter. Hahn et al. (2010) investigated a sample of about 100 galactic disks and their alignment with their host halo at three different redshifts. Both the stellar and gas disks had a median misalignment angle of about 49° with respect to the hosting dark matter halo at $z = 0$.
Some works focused explicitly on the effect that baryons have on the dark matter halo by running parallel DM-only simulations. Bryan et al. (2013) did not find a

dependency of the spin parameter on mass, redshift or cosmology in their DM-only runs. In the simulations that included baryons and had strong enough feedback the overall spin was found to be affected only very little, while the baryons had a noticeable influence on the inner halo. Bett et al. (2010) investigated the specific angular momentum and the misalignment of the galaxy with its halo. They obtained a median misalignment angle of about 25° for the DM-only runs and about 30° for the run including baryons. The baryons were found to spin up the inner region of the halo.

Besides the properties of galaxies and their dark matter halos, the large scale structure also has an impact on the formation and evolution of galaxies. Recently, Welker et al. (2014) studied the alignment of the spin of the galaxies with their filaments in context with mergers. They find that halos experiencing major mergers have low spin, while in general minor mergers can increase the amount of angular momentum. If a halo does not undergo any mergers but only smooth accretion, the spin of the galaxy increases with time, in contrast to that of its hosting dark matter halo. The galaxies also realign with their filaments. Danovich et al. (2014) have investigated the buildup of the angular momentum in galaxies. They used a sample of 29 re-simulated galaxies at redshifts from $z = 4 - 1.5$. Overall the spin of the cold gas was about three times higher than that of the dark matter halo, in line with previous studies.

Observations indicate that the formation of galaxies is affected by the relation between mass and angular momentum (see Fall (1983)). The angular momentum of disk galaxies was found to be about six times higher than that of the ellipticals of equal mass. Romanowsky and Fall (2012) and Fall and Romanowsky (2013) revisited and extended this work analyzing 67 spiral and 40 early-type galaxies. They found that lenticular (S0) galaxies lie between spiral and elliptical galaxies in the so-called j_{star}-M_{star}-plane. The disks and bulges of spiral galaxies follow a similar relation, i.e. the bulges of spiral galaxies behave like "mini-ellipticals". Obreschkow and Glazebrook (2014) used data from high-precision measurements of 16 nearby spiral galaxies to calculate the specific angular momentum of the gas as well as the stars. They concluded that the mass and angular momentum are the two most important determining factors on the morphology of galaxies.

In this work we will analyze one simulation from the set of Magneticum Pathfinder

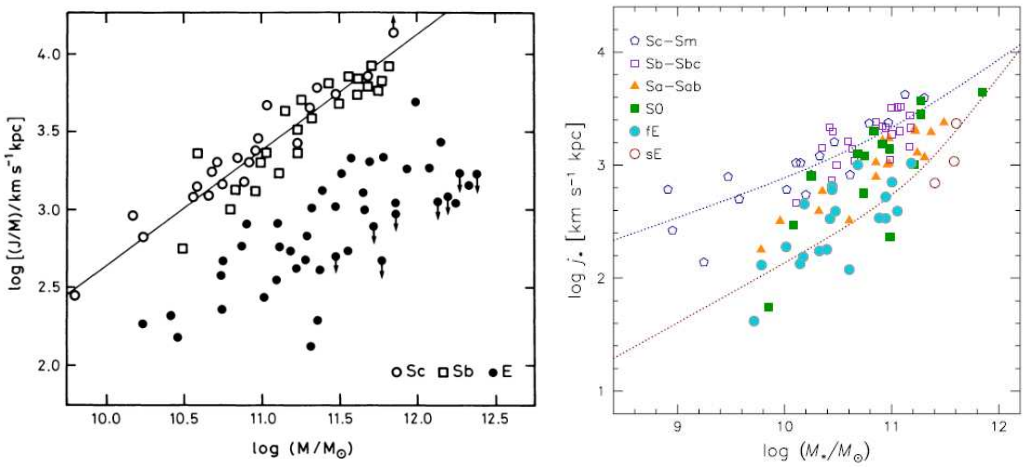

Fig. 1.2.: Left: The luminous mass against the specific angular momentum for observed elliptical and spiral galaxies. This picture is taken from Fall (1983). Right: The mass against the specific angular momentum for entire galaxies of elliptical, S0 and spiral galaxies. This picture is taken from Fall and Romanowsky (2013)

Simulations (Dolag et al., in prep.), which are introduced in chapter 2, and investigate how the baryonic component, especially the gas, influences the morphology of the galaxy. Therefore, in chapter 3 we classify the galaxies in the simulation using the circularity parameter ε. In chapter 4 we discuss the specific angular momentum of the different components of ellipticals as well as disks. Furthermore, we study the alignment of the angular momentum vectors of the baryonic and the dark matter component. Additionally, we analyze the differences in the spin parameter λ of ellipticals and disk galaxies caused by the interacting baryonic and dark matter components.

2. The Magneticum Pathfinder Simulations

In order to study the properties of galaxies in a statistically relevant manner we need both a large sample size and resolution high enough to resolve the morphology and underlying physics of galaxies. Since the newest generation of cosmological simulations can achieve both, they are a valuable tool for this study. We take the data for our studies from the Magneticum Pathfinder simulations, which are a set of cosmological hydrodynamic simulations with different volumes and resolutions (Dolag et al., in prep.), see Fig. 2.1 for an overview. The simulations were performed with an extended version of the N-body/SPH code GADGET-3 which is an updated version of GADGET-2 (Springel et al., 2001b; Springel, 2005), which includes various updates in the formulation of the SPH regarding the treatment of the viscosity and the used kernels (see Dolag et al. (2005) and Beck et al., in prep.).

They include a wide range of complex baryonic physics such as gas cooling and star formation (Springel and Hernquist, 2003), black hole seeding, evolution and AGN feedback (Springel et al., 2005; Fabjan et al., 2010; Hirschmann et al., 2014) as well as stellar evolution and metal enrichment (Tornatore et al., 2004, 2007). It also follows the thermal conduction at 1/20th of the classical spitzer value (Spitzer, 1962), following Dolag et al. (2004). The initial conditions are based on a standard ΛCDM cosmology with parameters according to the seven-year results of the Wilkinson Microwave Anisotropy Probe (WMAP7) (Komatsu et al., 2011). The Hubble parameter is $h = 0.704$ and the density parameters for the matter is $\Omega_M = 0.272$, for the dark energy $\Omega_\Lambda = 0.728$ and for the baryons $\Omega_b = 0.0451$. We use a normalization of the fluctuation amplitude at 8 Mpc of $\sigma_8 = 0.809$ and also include the effects of Baryonic Acoustic Oscillations. The largest and the smallest cosmological boxes simulate volumes of $(896\ \mathrm{Mpc/h})^3$ and $(12\ \mathrm{Mpc/h})^3$, respectively. The lowest resolution in mass of our largest box is $m_{\mathrm{DM}} = 1.3 \cdot 10^{10} M_\odot/h$ for dark matter particles and $m_{\mathrm{gas}} \simeq 2.6 \cdot 10^9 M_\odot/h$ for gas particles. The highest resolution in mass of our small-

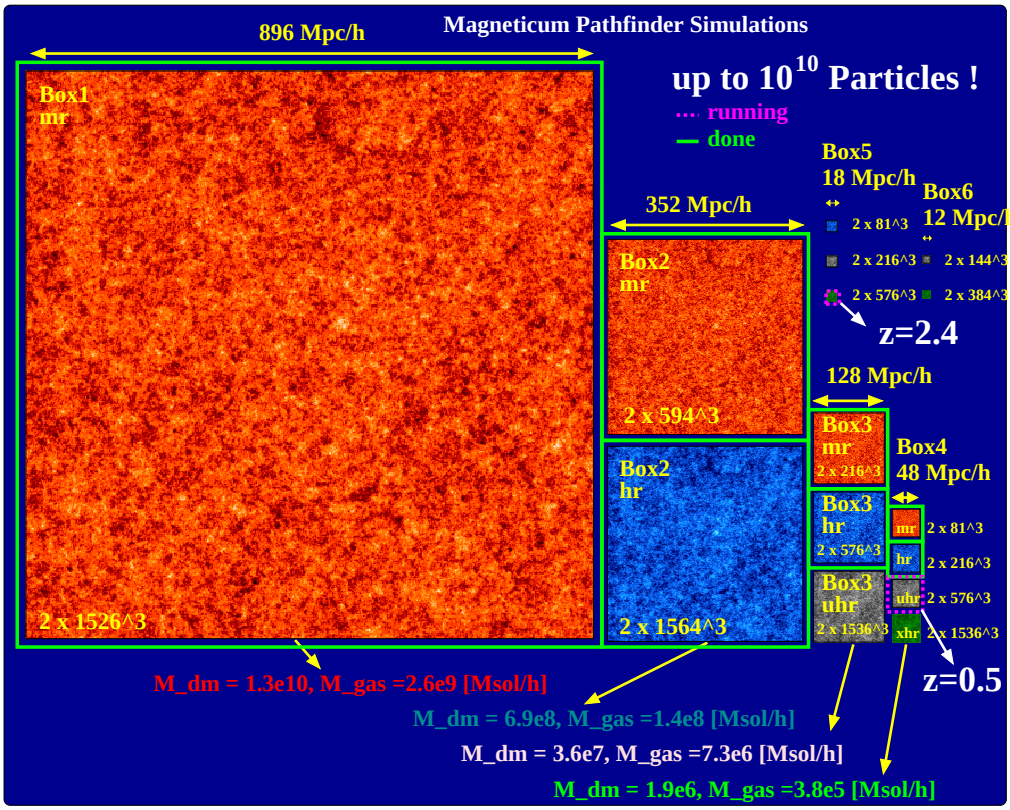

Fig. 2.1.: This is an overview of the Magneticum Pathfinder simulations with the different box sizes and resolutions. We used Box4 uhr and Box3 hr. This image is courtesy to K. Dolag.

est box is $m_{\rm DM} = 1.9 \cdot 10^6 M_\odot/h$ for dark matter particles and $m_{\rm gas} \simeq 3.9 \cdot 10^5 M_\odot/h$ for gas particles. There are six types of particles, of which the most important for our investigations are the gas, star and dark matter particles. The gas particles can each form up to four stars, so the mass of an individual gas particle changes during the evolution of time. In our simulations we use several state-of-the-art improvements of SPH such as spatially adaptive higher-order viscosity schemes, time step limiters and advanced kernel functions (for details see Beck et al., in prep). The Magneticum Pathfinder Simulations have already been successfully used in a wide range of numerical studies such as on the statistics of AGN (Hirschmann et al., 2014; Bachmann et al., 2014) or elliptical galaxies (Remus et al., 2013).

In this work we mainly used a medium-sized box ("Box4") with a volume of $(48\ \mathrm{Mpc/h})^3$ at ultra high resolution ("uhr"), which initially contains a total of $2 \cdot 576^3$ each dark matter and gas particles with masses of $m_{\rm DM} = 3.6 \cdot 10^7 M_\odot/h$ and $m_{\rm gas} = 7.3 \cdot 10^6 M_\odot$. The gravitational softening length for the dark matter

as well as the gas particles is 1.4 kpc/h and for the star particles it is 0.7 kpc/h. Additionally, we performed a dark matter-only run of Box4 uhr and also of the larger Box3 hr (high resolution), which has a volume of (128 Mpc/h)^3 and dark matter particles with masses of $m_{\rm DM} = 6.9 \cdot 10^8 M_\odot/h$. We use a standard Friends-of-Friends (Davis et al., 1985) and SUBFIND scheme for the detection of halos and subhalos (Springel et al., 2001a; Dolag et al., 2009). Therefore, at every simulation output time, we not only obtain the entire thermodynamical state of the simulation volume, but also a detailed catalog of structures and substructures and their corresponding virial properties. In the simulation the virial radius is evaluated according to the top-hat model obtaining the critical density above which the overdense region would collapse to a singularity (Eke et al., 1996). The simulations are split into 144 snap shots. We mainly use snap shots 036 ($z = 1.98$), 058 ($z = 0.99$), 096 ($z = 0.47$) and 136 ($z = 0.07$). For the dark matter only run we additionally use snap shot 044 ($z = 1.48$) of Box4 uhr and Box3 hr.

3. Classification of Galaxies and Properties of Disks

From our dataset we extract all halos in the virial mass range between $5 \cdot 10^{11} M_{\odot}$ and $2 \cdot 10^{13} M_{\odot}$. We choose the upper limit to exclude groups and clusters of galaxies, since the transition between the group/cluster halos and the individual galaxies is not clear. The lower limit is chosen to obtain a sample of halos which contain a significant amount of stellar mass and for which the resolution is sufficient to resolve the inner stellar and gas structures. Fig. 3.1 shows six galaxies within the chosen mass range. These galaxies were selected by eye in order to show that the galaxies in the simulations look like observed disk and elliptical galaxies. The middle panel is a picture of the full Box4 uhr at redshift $z = 0.47$.
After the extraction from our snap shot files, we transform the positions and velocities of all gas, stellar and dark matter particles into the center of mass frames of their corresponding host halos. Subsequently, we calculate the angular momentum $\mathbf{J}$ of the gas within the innermost ten per cent of the virial radius. Furthermore, we ignore all particles within the innermost one per cent of the virial radius, because of their potentially unknown contributions caused by bulge components or numerical resolution effects. We rotate the positions and velocities of all particles such that their z-components are aligned with the angular momentum vector $\mathbf{J}$.

3.1. Classification

Since we want to investigate the different behavior of the properties of the different morphological types of galaxies, we split the galaxies into ellipticals and disk galaxies. In the following section we therefore describe how we classify the galaxies according to their physical properties via the ε-parameter. We then show examples of the spatial distribution of elliptical and disk galaxies and take a look at the rotation curves of selected disk galaxies.

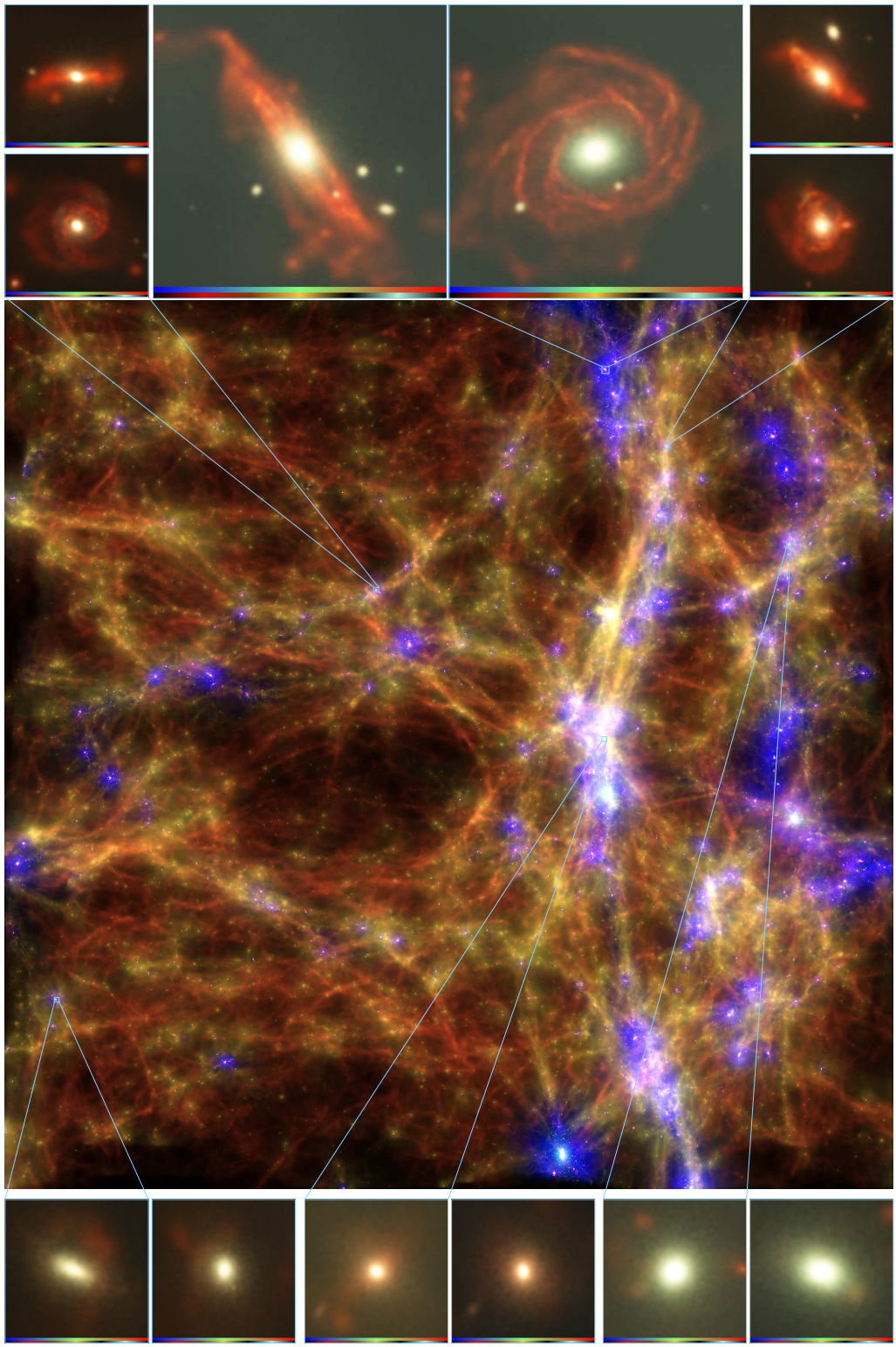

Fig. 3.1.: The panel in the center shows the complete Box4 uhr at $z = 0.47$. The galaxies in the upper panels look like observed spirals and those on the lower panels look like ellipticals. We color-code the stellar particles by their cosmological formation epoch and the gas particles by their temperature, where red is cold gas and blue is hot gas.

3.1.1. The Circularity Parameter

We use the circularity parameter ε to distinguish between different types of galaxies and to separate ellipticals from disks. The ε-parameter was first introduced by Abadi et al. (2003) as $\varepsilon_J = J_z/J_{\rm circ}(E)$. For our study we use the definition of Scannapieco et al. (2008) which is given by

$$\varepsilon = \frac{j_z}{j_{\rm circ}} = \frac{j_z}{rV_{\rm circ}}, \tag{3.1}$$

where j_z is the z-component of the specific angular momentum (see section 4.1 for the definition) of an individual particle and $j_{\rm circ}$ is the expected specific angular momentum of a particle assuming a circular orbit with radius r around the halo center of mass with an orbital velocity of $V_{\rm circ}(r) = \sqrt{GM(r)/r}$.

We compute the circularity ε for every individual particle between one and ten per cent of the virial radius. We perform this calculation for the stellar as well as the gas component. For our investigations we base our classification of galaxies on the specific angular momentum of both components, which allows us to capture rotationally supported gaseous disk structures or dispersion dominated spheroidal structures. Thus, our selection criterion is well able to distinguish between elliptical and disk galaxies.

3.1.2. Selection Criteria

For each selected halo we start to determine the galaxy type by computing the fraction f of particles that have an ε-value between -3 and 3 with a spacing of 0.1. Afterwards, we distinguish between elliptical and disk galaxies with the following selection criteria:

- We classify a galaxy as an elliptical galaxy if the majority of particles is in a close interval around the origin (i.e. $f(-0.3 \leq \varepsilon \leq 0.3) \geq 0.4$). In a dispersion dominated system there is usually a broad peak at $\varepsilon \simeq 0$ (see upper left panel of Fig. 3.2).

- We classify a galaxy as a disk galaxy if the majority of particles are off-centered from the origin (i.e. $f(0.7 \leq \varepsilon \leq 1.3) \geq 0.4$). In a rotation supported system there is usually a broad peak at $\varepsilon \simeq 1$ (see upper right panel of Fig. 3.2).

- All remaining galaxies, which fulfill neither of the two criteria, are classified as "others".

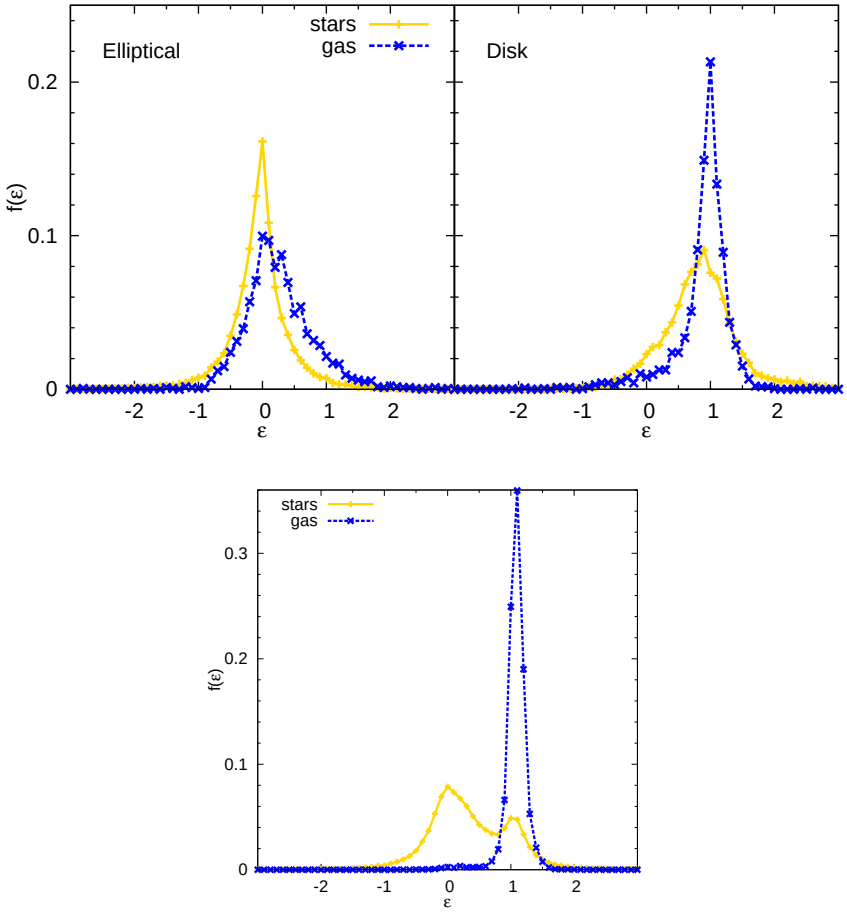

Fig. 3.2.: Exemplary distribution of the circularity parameter ε for an elliptical (upper left panel), a disk galaxy (upper right panel) and for a galaxy classified as disk in the gas and due to its dominant stellar bulge as elliptical in the star component (lower middle panel).

The total number of galaxies within the mass range between $5 \cdot 10^{11} M_{\odot}$ and $2 \cdot 10^{13} M_{\odot}$ selected from "Box4 uhr" at redshift $z = 0.07$ is 608 (for other redshifts see Table 3.1). In the gas as well as the star component 33 are classified as disks and 54 as ellipticals, while 521 could not be classified in such a way. These unclassified galaxies are merging objects, bulge dominated spirals, ellipticals with gas disks or irregular objects. An example is shown in the lower middle panel of Fig. 3.2. This galaxy has a dominant stellar bulge with an extended gaseous disk which builds up a disk of young stars. This is the galaxy shown in the upper middle panel of Fig. 3.1. In order to resolve the unclassified objects the classification could be refined

Tab. 3.1.: Total number of halos N in the selected mass range, the number of ellipticals ($N_{elliptical}$) and disks ($N_{\rm disk}$) classified by the circularity of the gas and stellar components at different redshifts.

Redshift	N	$N_{\rm elliptical}$	$N_{\rm disk}$
1.98	395	10	119
0.99	602	36	128
0.47	619	42	68
0.07	608	54	33

in such a way that we additionally divide into ellipticals which have a gaseous disk with new forming stars or galaxies which have a large stellar disk with only little gas (SO-galaxies). At high redshifts the fraction of disk and elliptical galaxies has the same tendency as the observations from Cappellari et al. (2011), who analyzed a sample of 871 nearby galaxies. They classified 8 per cent as ellipticals, 22 per cent as S0 and 70 per cent as disk galaxies. At lower redshifts our classification becomes more difficult since there are a lot of galaxies which have a very dominant stellar bulge but on the other hand also possess an extended gaseous disk containing many young stars (see again the galaxy in the middle upper panels of Fig. 3.1). Often, these objects are classified as ellipticals in the stellar component and as disk galaxies in the gas component, e.g. at $z = 0.07$ there are 146 objects classified that way. Furthermore, at this redshift 167 galaxies have a gas disk but could not be classified in the stellar component. Furthermore, the luminosity of the stars could be taken into account, since old stars which make up the bulge and the halo stars are not as luminous as young stars which build up the disk. Hence, in observations a galaxy with an old massive stellar bulge and a disk of young stars and an extended gas disk is very likely to be classified as a spiral galaxy.

3.1.3. Morphology

Fig. 3.3 (two left panels) shows an example of an elliptical galaxy, which fulfills the classification criteria in the gas and star component. The top row shows the projection onto the x-y-plane, the middle row onto the x-z-plane and the bottom row onto the y-z-plane. On the left hand side we plot the position of star particles color-coded by their stellar formation epoch (in the following simply called "age"), which is defined as $a = 1/(1+z)$, where z is the redshift, e.g. a star that has formed at redshift $z = 1$ has the age $a = 0.5$ and corresponds in this color-code to turquoise-

blue. Thus the youngest stars are blue and the oldest stars are red. The spatial distribution of stars is spheroidal and consists almost only of old and middle-aged stars. On the right hand side we plot the position of gas particles color-coded by their temperature. In the galaxy's center there is almost no gas left.

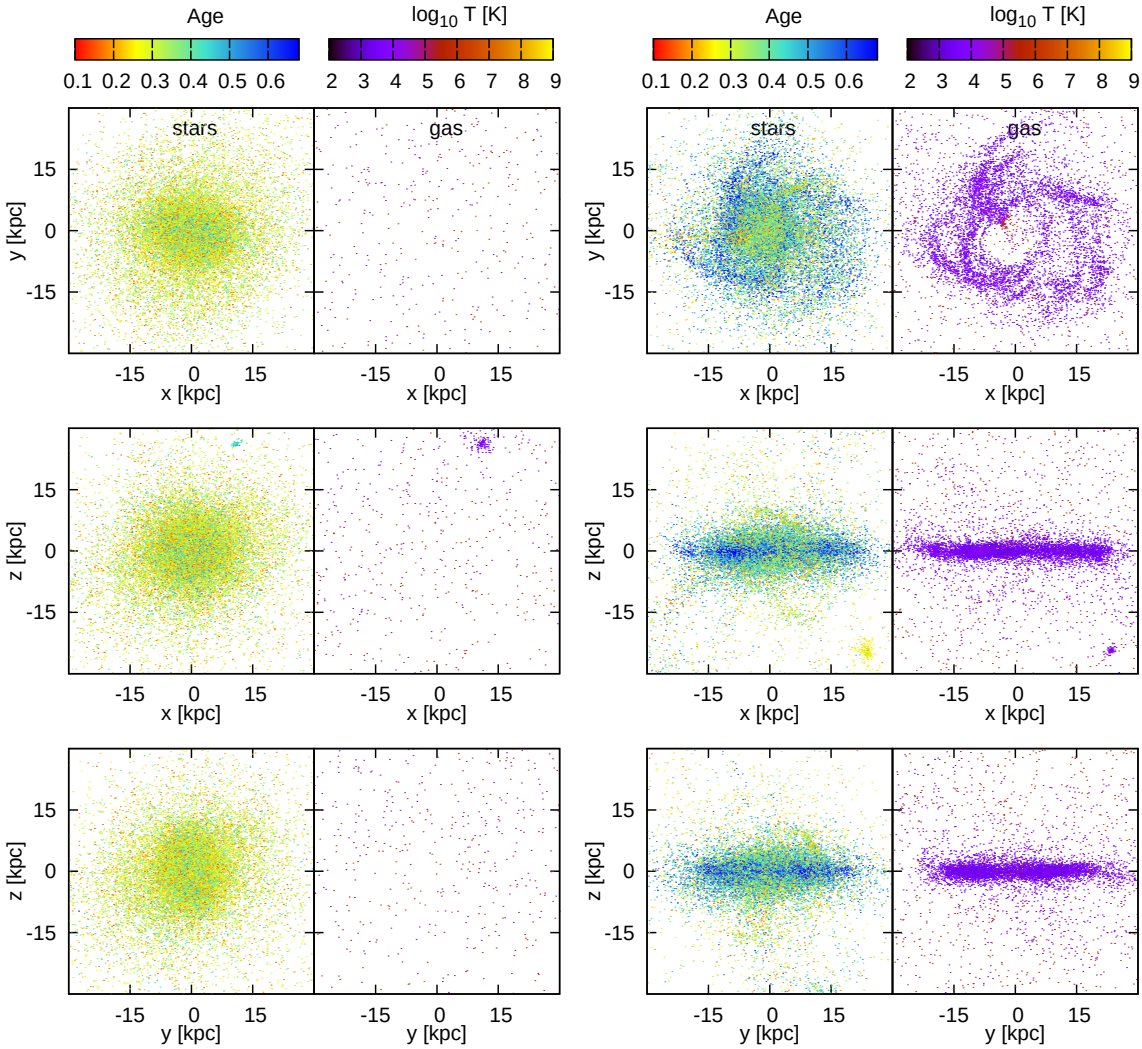

Fig. 3.3.: Exemplary spatial distribution of an elliptical (two left panels) and a disk galaxy (two right panels) at $z = 0.47$. The left panels show the stars color-coded by their age, where red are old and blue are young stars. The right panels show the distribution of the gas color-coded by the temperature, where blue is cold and red is hot gas.

Fig. 3.3 (two right panels) shows an example of a disk galaxy, which fulfills the classification criteria in the gas and star component. We find an old and middle-aged stellar population in a bulge at the center and additionally, a galactic disk

consisting of young and recently formed stars. The arrangement of the young stars corresponds to a spiral structure and thus is an indication of their formation within a disk and spiral structure. This is also supported by the spiral structure in the cold gas component, which is the raw material for star formation.

3.2. Rotation Curves

A good feature for comparing simulated galaxies with observations are their rotation curves. It is worth mentioning that rotation curves gave the first hint of the existence of dark matter, since the flat rotation curves of spiral galaxies could not only be explained with the mass of the visible matter (see e.g. Schneider (2008)).

Fig. 3.4 shows rotation curves of observed and simulated galaxies. In the top panel we plot rotation curves of a sample of 12 representative spiral galaxies of our local Universe. We took the data for the rotation curves (except for M83) from Yegorova et al. (2011), with original sources as follows. They used the Hα-data for UGC944, UGC1094, UGC3279 and UGC8220 from Vogt et al. (2004), for UGC1076, UGC10692 and AGC241056 from Catinella et al. (2006), for NGC5985 from Blais-Ouellette et al. (2004), for ESO601-G9 from Persic et al. (1996). They used the HI-data for ESO240-G11 from Kregel and van der Kruit (2004) and for M31 from Corbelli et al. (2010). The data for M83 was kindly provided by Peter Kamphuis and Baerbel Koribalski. In the bottom panel we plot rotation curves of a selected sample of 12 galaxies, which are classified as disks in both the gas and stellar component at a redshift of $z = 0.47$. The galaxies additionally were selected by eye. Thus, only galaxies which were undisturbed were selected.
We calculate the rotation curves directly from the velocities of the individual gas particles by projecting the velocity onto the tangential vector of a circle, which is symmetric around the origin, as done in the Bachelor thesis by Felix Schulze, 2012. The in this way obtained rotational velocity is then linearly binned along the radius with a bin size of $\Delta r = (0.2 \cdot R_{\rm vir})/100$. The spatial constraints are as follows. We only take into account particles within 20 per cent of the virial radius and we also employ a limit of ± 5 kpc in z-direction. Thus, we ensure that our computed rotation curves only contain contributions of particles, which clearly belong to the galactic disk. We show the curves beginning from 4 kpc away from the center of the galaxies for two reasons: firstly, the innermost few kpc, i.e. 2 times the softening length of the gas, namely 2.8 kpc/h, are spatially not resolved. Secondly, the feedback of the

AGN can blow out the gas in the center and thus the inner values of the rotational velocity only depend on few gas particles, which makes the values unusable. It is yet unclear, if these "holes" are realistic or if they are just an artifact due to too much feedback in the simulations. The rotation curves in the simulation are flat and begin to scatter in the region where the disk ends. Compared to the observations the selected rotation curves have smaller values.

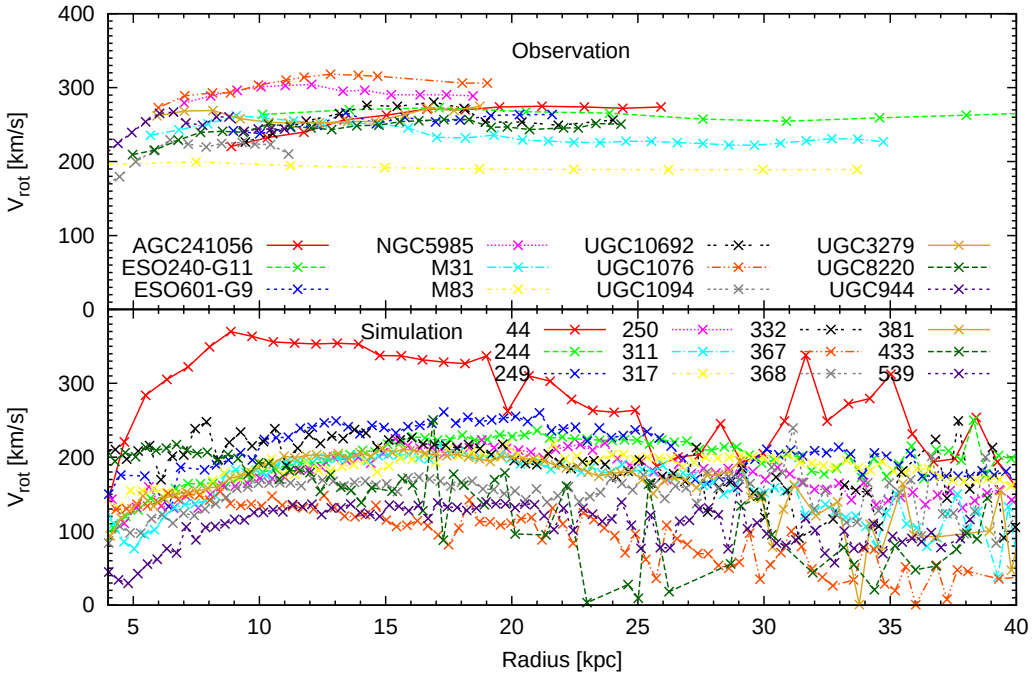

Fig. 3.4.: Observed and simulated galactic rotation curves. The upper panel shows observed rotation curves from a sample of nearby galaxies (see text). The lower panel shows rotation curves of 12 selected disks from the Magneticum simulation at redshift $z = 0.47$.

4. The Angular Momentum

We continue our investigations with a detailed study of the angular momentum of our selected sample of galaxies. The angular momentum plays a key role in the morphological differences between ellipticals and spirals. In a closed system without external forces, the angular momentum is a conserved quantity. However, in the context of galaxy formation and the interaction between collapsing objects and the large-scale structure, the assumption of the conservation is not necessarily fulfilled for a single galaxy. The total angular momentum of a galactic halo is given by

$$\mathbf{J} = \sum_{k} \left(\sum_{i \in N_k} m_{k,i}\, \mathbf{r}_{k,i} \times \mathbf{v}_{k,i} \right), \tag{4.1}$$

where k are the different components of matter (gas, stars and dark matter) and N_k is their corresponding particle number with the loop index i. We remark that in this chapter we plot either all four redshifts ($z = 1.98$, $z = 0.99$, $z = 0.47$ and $z = 0.07$) or present the highest and lowest redshifts and show the two redshifts in between in the appendix.

4.1. The Specific Angular Momentum

In our simulations, each particle carries its own mass. The initial mass is different for gas, star and dark matter particles. Later on, the mass of individual gas particles varies due to mass losses during star formation. Thus, we remove the mass dependence and use the specific angular momentum

$$\mathbf{j}_k = \frac{\sum_i m_{k,i} \mathbf{r}_{k,i} \times \mathbf{v}_{k,i}}{\sum_i m_{k,i}}, \tag{4.2}$$

where k are the species of matter, as above. Firstly, we calculate the angular momentum of each particle of a species. Afterwards, we sum over all individual particles and divide by the total mass of the corresponding species to obtain the absolute

value. For the calculation of the most inner region of the halo we only take particles within the inner ten per cent of the virial radius into account, which corresponds roughly to the size of the galaxies. We choose this radius as an approximate medium value, since smaller disks have a size of about five per cent while extended gaseous disks can reach out up to 20 per cent of the virial radius.

4.1.1. The Specific Angular Momentum of Gas and Stars

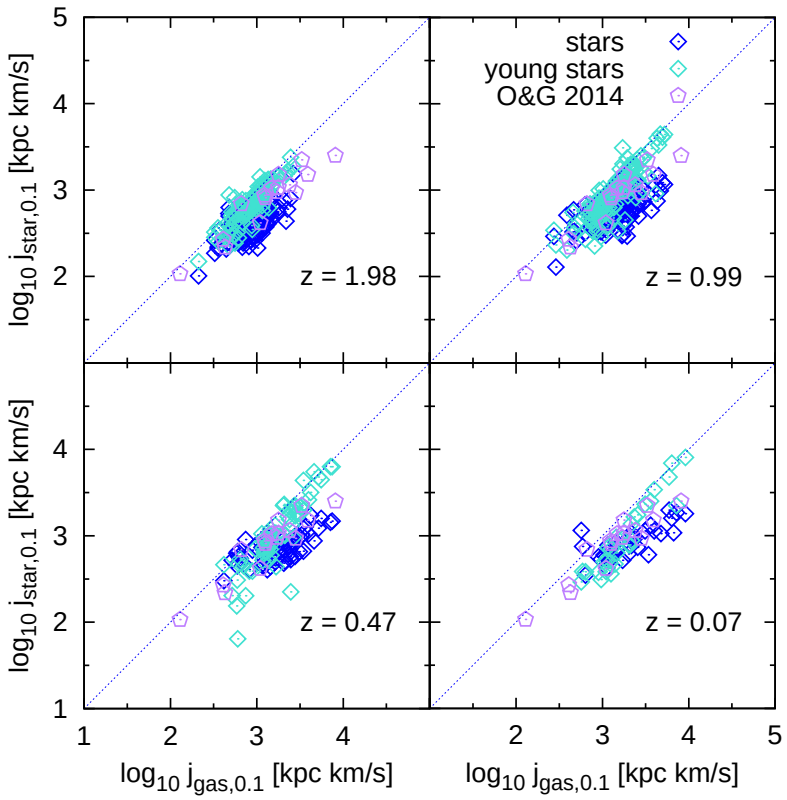

Fig. 4.1.: The specific angular momentum of the gas against the specific angular momentum of stars within ten per cent of the virial radius for galaxies which are classified as disks in the gas and star component (blue diamonds) at four redshifts as indicated in the plots. Additionally, we show the relation also for the young stars only (turquoise diamonds). We overplot observational data points calculated by Obreschkow and Glazebrook (2014) (purple pentagons). The values agree well with the observations and we note an overall spin up with cosmic time.

In Fig. 4.1 we cross-check our computed values and compare the relation between the specific angular momenta of gas and stars within the innermost ten per cent at

four redshifts with observations. We take the observational data from the THINGS (The HI Nearby Galaxy Survey, Walter et al., 2008) sample, which consists of 16 spiral galaxies in the local Universe, for which surface densities of stars and cold gas are available (Leroy et al., 2008). We obtained the values for the observed specific angular momenta from Obreschkow and Glazebrook (2014).
We took galaxies into account, which show an ε-distribution that peaks around 1 in both the gas and star component. Our simulations (blue symbols) agree well with the observations (purple symbols). The dotted line corresponds to equality of both values. We find that the specific angular momentum of the stars is slightly smaller than that of the gas (blue diamonds). Most probably, the specific angular momentum of the gas has partial contributions from freshly accreted gas, which has not lost its angular momentum yet. This becomes more evident by looking at the young stars (turquoise diamonds). For the young stars we consider those whose age is between $0.95 \cdot 1/(1+z)$ and $1 \cdot 1/(1+z)$ of that at the corresponding redshift. If we only take the young stars into account, we find almost an equality with the same specific angular momentum of the gas. At a lower redshift (lower right panel) the values of the specific angular momentum of the gas are slightly larger than at higher redshift (upper left panel). We assume this behavior to be caused by a spin-up of the cold gas with time. Hence, also the young stars have higher specific angular momentum. This appears in a slight trend for a separation of the young stars and the total star component, which have lower specific angular momentum than the gas.

So far we have only considered the halos hosting disk galaxies. In order to see if the ellipticals behave different we take a look at Fig. 4.2, which shows the specific angular momentum of the gas against that of the stars for disks (blue diamonds) as well as ellipticals (red circles). Compared to the disk galaxies the ellipticals have a lower specific angular momentum of the gas. Furthermore, most of the ellipticals have a much lower specific angular momentum of the stars compared to that of their gas. We suggest that, particularly at high z, most gas in ellipticals originates from the infalling substructures and hence its angular momentum is higher.

We can clearly see that the ellipticals and the disk galaxies show a different behavior in the relation between the angular momentum of the gas and stars. We also have seen that the gas gains angular momentum over time, especially in disk galaxies. The young stars of disk galaxies have approximately the same amount of angular momentum as the gas, from which they form.

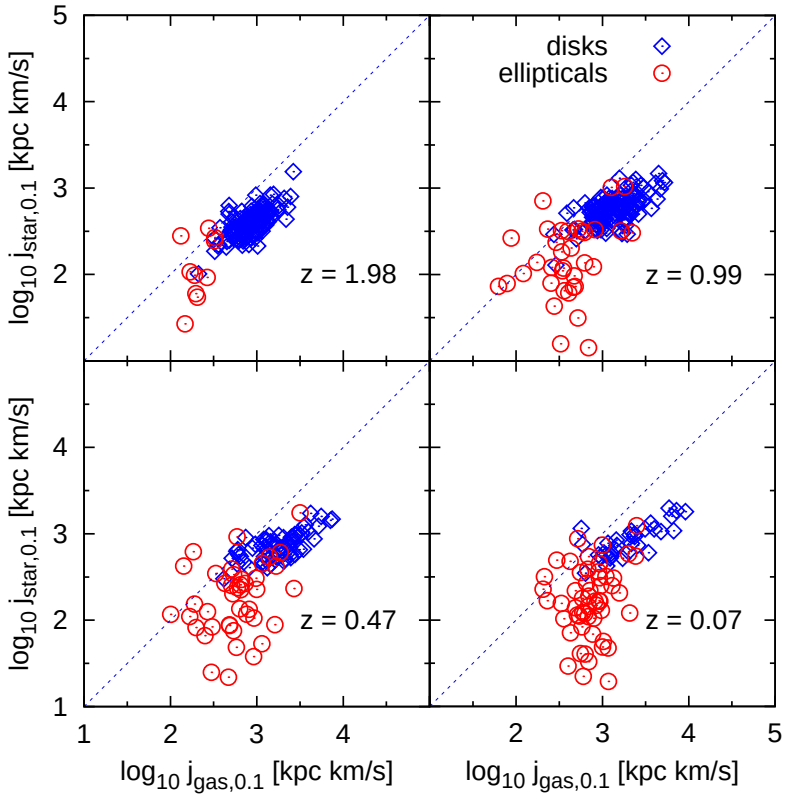

Fig. 4.2.: Specific angular momentum of the gas against the specific angular momentum of stars within ten per cent of the virial radius for galaxies that are classified in both components as disks (blue diamonds) or as elliptical galaxy (red circles).

4.1.2. The Angular Momentum – Mass Relation

The mass and the angular momentum of galaxies are proposed to be the most important ingredients in their formation history and the resulting morphology (Fall, 1983; Romanowsky and Fall, 2012; Obreschkow and Glazebrook, 2014). In this section, we compare the relation between the angular momentum and the mass of the stellar component of galaxies with observations, which is illustrated in Fig. 4.3. We take into account the mass as well as the angular momentum of the star particles within ten percent of the virial radius. The upper panels show our simulations at $z = 1.98$ while the lower panels show $z = 0.07$. The observational data is taken from Romanowsky and Fall (2012) (denoted as "R&F2012") and Obreschkow and Glazebrook (2014) (denoted as "O&G2014"). Romanowsky and Fall (2012) used a sample of 67 spiral and 40 elliptical galaxies. At low redshift the data from our simulations fit well with the observations, especially those of the disk galax-

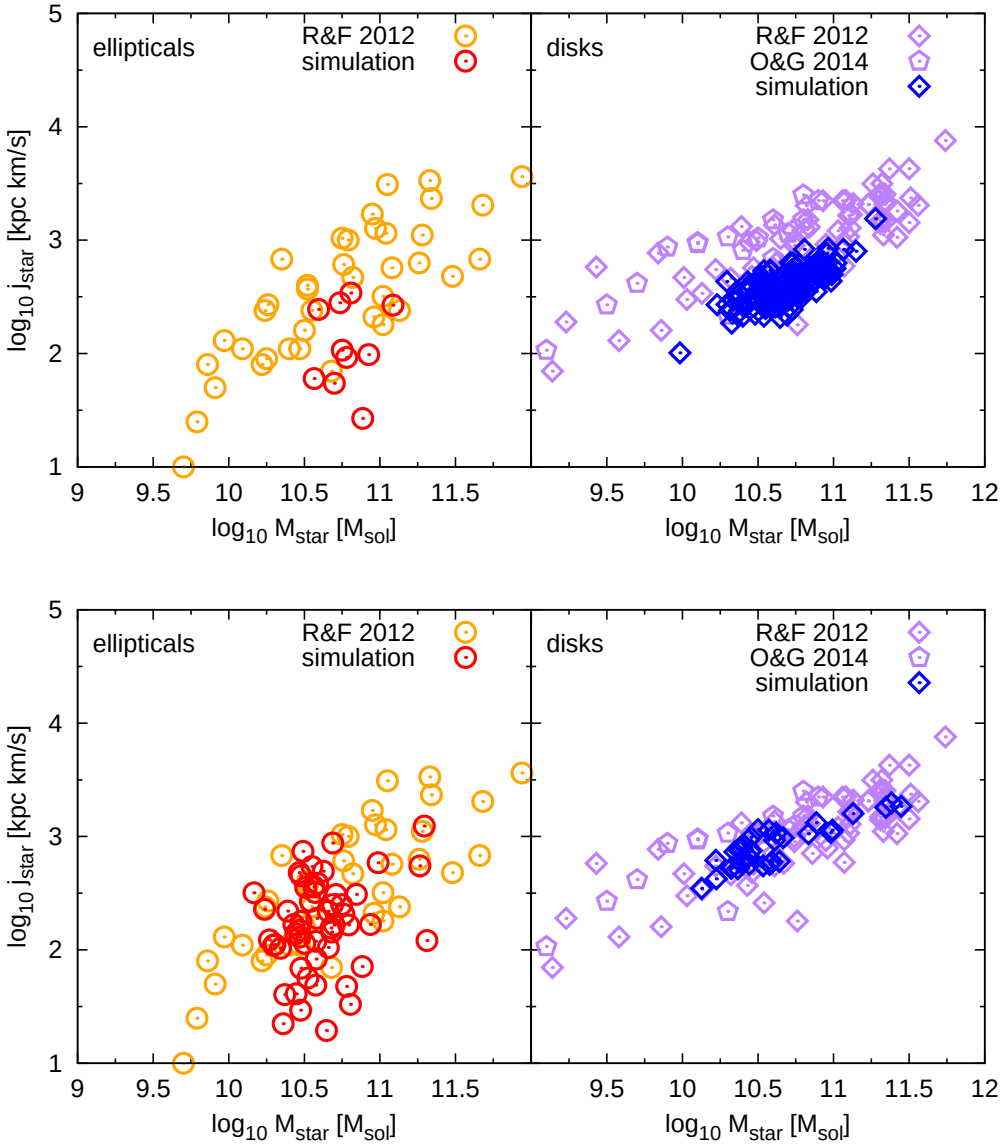

Fig. 4.3.: Stellar mass within the innermost ten per cent of the virial radius against the specific angular momentum of the stars within the central region at $z = 1.98$ (upper panels) and $z = 0.07$ (lower panels). The left panels show the simulated galaxies classified as ellipticals (red circles) compared to data from observed elliptical galaxies by Romanowsky and Fall (2012) (orange circles, denoted by "R&F 2012"). The right panels show disks in our simulation (blue diamonds) compared to observational data of spiral galaxies by Romanowsky and Fall (2012) (purple diamonds, denoted by "R&F 2012") and Obreschkow and Glazebrook (2014) (magenta pentagons, denoted by "O&G 2014").

ies (blue diamonds, lower right panel) which lie perfectly on the observational data points (purple symbols). In contrast to the disk galaxies, the ellipticals (red circles, lower left panel) show a large scatter which is also found in the observational data (orange symbols). When comparing the different redshifts we can see that at higher redshift the values for the ellipticals (red circles, upper left panel) as well as for the disk galaxies (blue diamonds, upper right panel) in our simulations are lower than that in observations (orange and purple symbols, respectively). This can be explained by the fact that the observational data represent nearby galaxies, which corresponds to low redshift. We want to remark that there are no galaxies in our simulations with stellar masses smaller than $\approx 10^{10} M_{\odot}$ and larger than $\approx 10^{11.5} M_{\odot}$ since we extracted only halos with virial masses between $5 \cdot 10^{11} M_{\odot}$ and $2 \cdot 10^{13} M_{\odot}$, as described earlier.

All in all, the results from the simulations fit well with the observational data. In particular, we are in agreement with (Fall, 1983), who find that the specific angular momentum of the galaxies increases with the disk-to-bulge ratio for a given mass. In forthcoming studies we will develop a more diverse classification that accounts for fast-rotating ellipticals and S0 galaxies which should lie in the gap between ellipticals and disk galaxies.

4.1.3. The Specific Angular Momentum of Gas and Dark Matter

We proceed with a detailed study of the angular momenta of dark matter and gas. In particular, we are interested in the scaling relations of the corresponding individual specific angular momenta of baryonic and non-baryonic matter. Previous studies (Fall, 1983; Mo et al., 1998) suggest an equality between the angular momentum of the dark matter halo and that of the gas components of their galaxies.

Firstly, we regard the specific angular momentum of the gas against dark matter within the entire virial radius. This is shown in Fig. 4.4 for the four redshifts as indicated in the plots. As noted in the introduction, previous numerical simulations suffered from a systematically too low angular momentum in the gas component compared to dark matter. However, in our simulations this problem does not occur any more. In fact, the specific angular momentum of the gas is even slightly higher than that of dark matter. The relation shows no difference between the two quantities for different galaxy types at higher redshifts. At the lowest redshift the specific angular momentum of the gas tends to be higher than that of the dark matter for el-

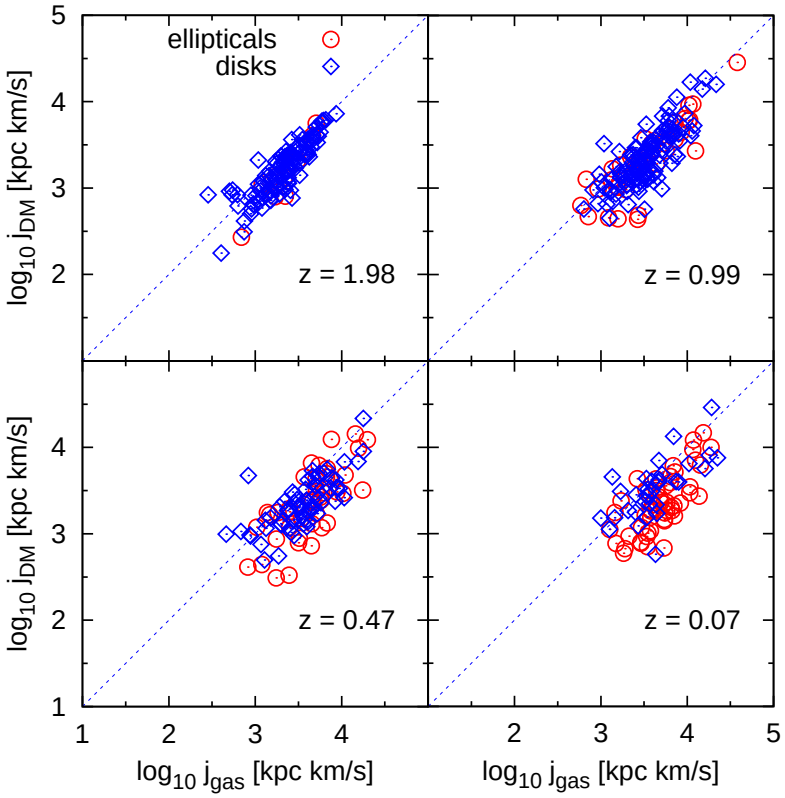

Fig. 4.4.: Specific angular momentum of the gas against specific angular momentum of dark matter within the entire virial radius at four different redshifts as indicated on the plots. The specific angular momentum is slightly higher for the gas but there is no difference between ellipticals (red) and disks (blue). In general, the values increase with decreasing redshift.

lipticals. Another trend which was seen in Fig. 4.1, where we compared the specific angular momenta of the gas and the stars, is the spin up of the angular momentum with time for both galaxy types.

Now we want to study the relation between the specific angular momentum of the gas of the galaxy, which resides within the innermost ten per cent of the virial radius, against that of total dark matter halo. Fig. 4.5 shows this relation for different redshifts as indicated in the plots. In general, we find the specific angular momentum of the dark matter to exceed the specific angular momentum of the gas. Most interesting, we identify a split-up between different types of galaxies: At redshift $z = 0.07$ the specific angular momentum of the gas in our sample of disks lies almost on the 1:1 relation with the specific angular momentum of the dark matter within

the entire virial radius. Still, there is a trend towards higher values of the specific angular momentum of dark matter compared to the gas. Averaged over all disks, the specific angular momentum of the gas in the central region is about 25 per cent lower than that of the dark matter. However, the specific angular momentum of the gas in our sample of ellipticals is about one order of magnitude smaller which is on average about 55 per cent less at $z = 0.07$. In the following sections, we refer to this split-up as the "angular momentum dichotomy in galactic halos". The split-up is also seen at the higher redshifts.

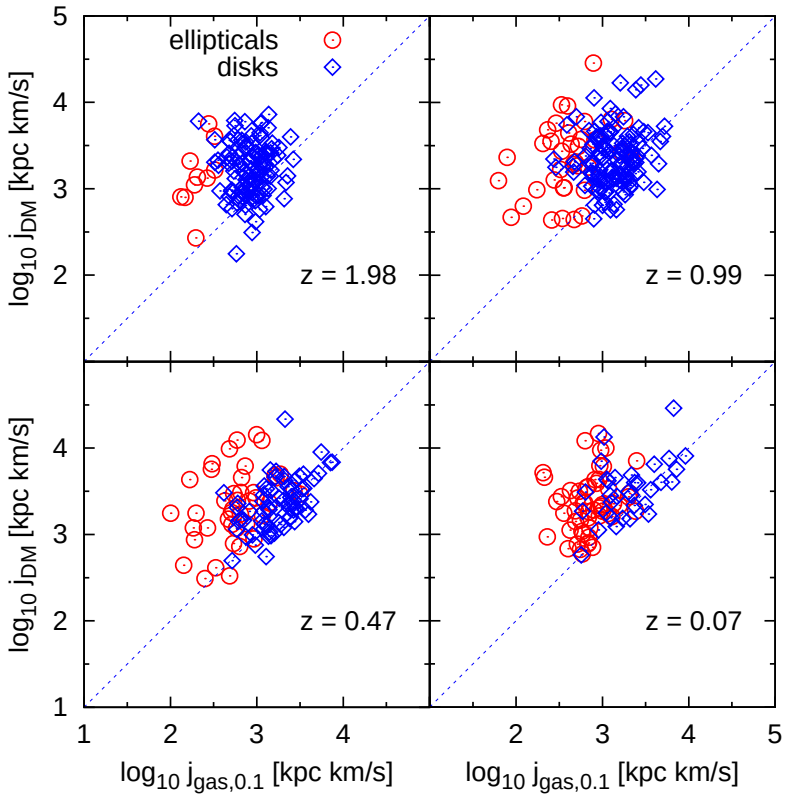

Fig. 4.5.: Specific angular momentum of the gas within ten per cent of the virial radius against specific angular momentum of dark matter within the entire virial radius. The specific angular momentum of the gas of the ellipticals is lower than that of the disks.

A possible explanation comes from the cold gas component, which dominates the gaseous disk in spiral galaxies. The cold gas has a higher specific angular momentum than the diffuse hot gas, which is more spherically distributed in a similar fashion to the dark matter. We will return to this assumption later on. The previously identified trend (see also Fig. 4.1), that with decreasing redshift the upper limit for

the specific angular momentum increases, supports the idea of a gas spin-up with time.

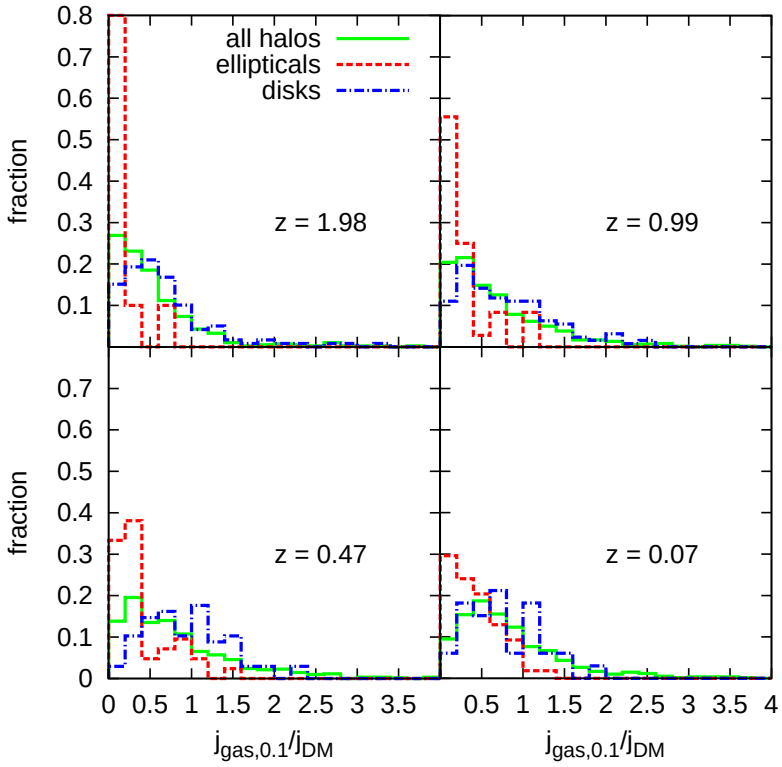

Fig. 4.6.: The fraction of the halos according to the fraction of the specific angular momentum of the gas the gas within ten per cent of the virial radius compared to the specific angular momentum of dark matter within the entire virial radius. While for ellipticals (red histogram) $j_{\mathrm{gas},0.1}$ is much smaller than j_{dm}, for disk galaxies (blue histogram) the distribution is broader.

In order to illustrate the scatters from the equality of the specific angular momentum of the dark matter halo and that of the gas within the galaxy, in Fig. 4.6 we show the fraction of the specific angular momentum of the gas in the inner region $j_{\mathrm{gas},0.1}$ with respect to the specific angular momentum of the dark matter halo j_{dm} for the four redshifts. The value 1 on the x-axis refers to the equality of the two quantities. Overall the distribution for all halos (green histograms) seems to broaden and move to higher x-values with decreasing redshift which supports the idea of the spin up of the gas component. This trend of broadening is also seen for the ellipticals (red histograms). At high redshift the specific angular momentum of the gas is always smaller than that of the dark matter. With decreasing redshift

the gas is spun up and there appear ellipticals whose angular momentum of the gas is higher than that of the surrounding dark matter halo. The distribution of the disk galaxies (blue histograms) is similar to that for all halos. There are always disk galaxies that have equal or even larger $j_{\mathrm{gas},0.1}$ than j_{DM}. At redshift $z = 0.47$ it looks like almost half of the disks have higher $j_{\mathrm{gas},0.1}$ than j_{DM}.

We now want to do some additional checks. Firstly, exemplary for redshift $z = 1.98$, we examine the specific angular momentum of the gas in the outer region, i.e. from ten to hundred per cent of the virial radius $j_{\mathrm{gas},0.9}$ compared to the dark matter halo's angular momentum, see Fig. 4.7. It looks almost the same as Fig. 4.4. This shows that for the overall specific angular momentum of the gas and the dark matter the outer parts are dominating.

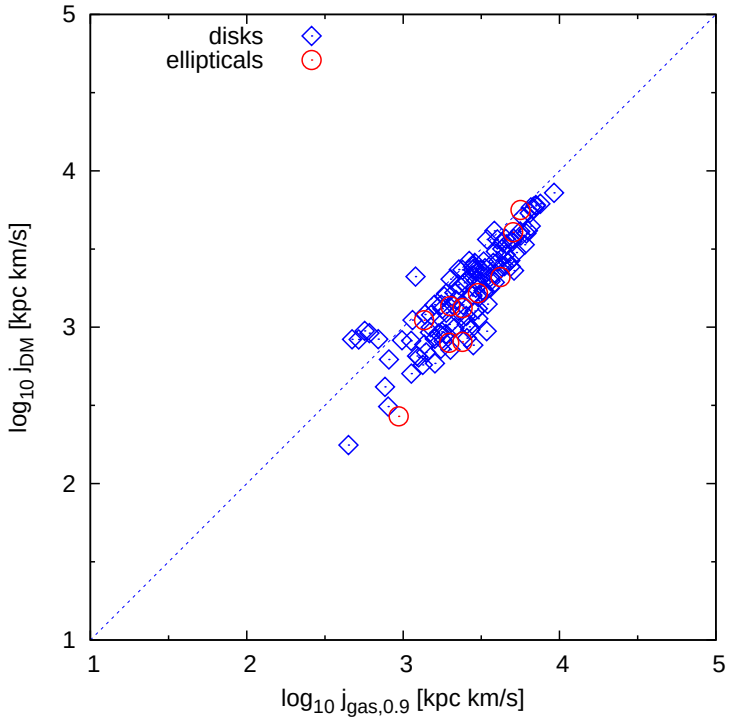

Fig. 4.7.: Specific angular momentum of the gas in the outer region, namely between ten per cent of the virial radius and the virial radius, against specific angular momentum of dark matter within the entire virial radius at redshift $z = 1.98$. There is no difference between ellipticals (red) and disks (blue).

We now return to the assumption that the cold gas has higher angular momentum than the hot gas. Therefore, the left panel of Fig. 4.8 shows the specific angular

momentum of the cold gas within the inner ten per cent of the virial radius and the right panel that of the hot gas within the inner region against that of the dark matter halo, exemplary for redshift $z = 1.98$. The cut between cold and hot gas was made at 10^5 K, i.e. cold gas is below that limit and hot gas has temperatures above this limit. The left panel almost looks the same as the plot for the corresponding redshift of Fig. 4.5 (upper left panel), where we have seen the specific angular momentum of the both gas components within the galaxy against that of the total dark matter halo, while the right panel does not show the splitting of the two galaxy types. This clearly shows that in the central region the cold gas is the dominant gas component.

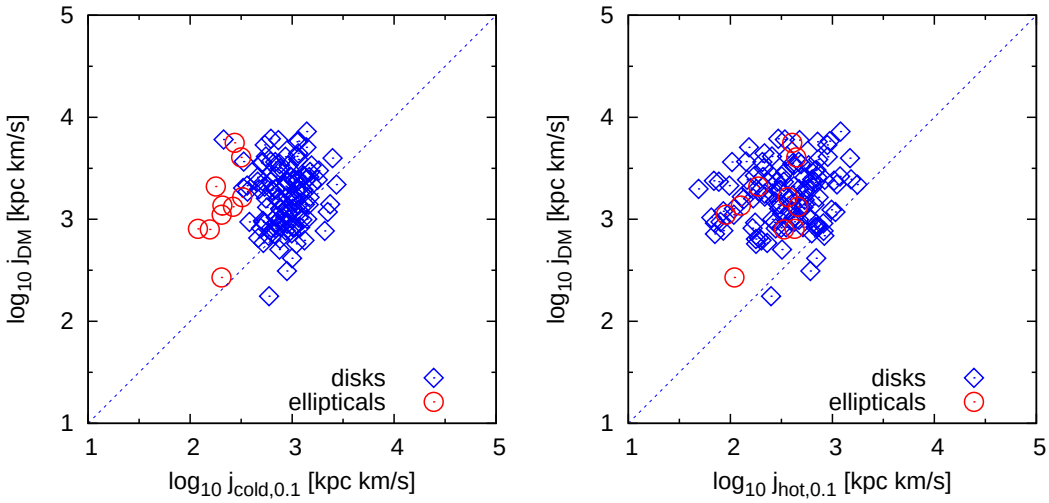

Fig. 4.8.: Specific angular momentum of the cold gas (left) and the hot gas (right) in the inner ten percent, each against specific angular momentum of dark matter within the entire virial radius at redshift $z = 1.98$. There is a splitting of disks (blue) and ellipticals (red) in the cold gas but no difference for the hot gas.

In this section we have learned that the main difference between elliptical and disk galaxies is the relation between the specific angular momentum of the gas and that of the dark matter. Whereas in disk galaxies the angular momentum of the gas is almost as high as that of the dark matter, especially at low redshift, it is much lower in elliptical galaxies. This shows that the cold gas in the disk galaxies transports high angular momentum material into the center, in contrast to the ellipticals, where we find mostly low angular momentum gas in the inner part. For observations at high redshifts this implies that one cannot directly estimate the angular momentum of the dark matter halo from the 1:1 relation but has to include a correction factor.

4.1.4. Angular Momentum Profiles

In order to illustrate and fathom the behavior of the specific angular momentum of the different components we turn to the radial profiles of the angular momentum. Fig. 4.9 shows the mean of our sample of elliptical (left panel) and disk galaxies (right panel) at redshifts $z = 1.98$ (two left panels) and $z = 0.07$ (two right panels), respectively. In the upper panels we plot the differential specific angular momenta of the different components against radius and in the lower panels we plot the individual mass fractions of the corresponding components against radius. The x-axis is linearly binned with a bin size of ten per cent of the virial radius of a halo. At redshift $z = 1.98$ the virial radius ranges approximately from 100 kpc to 300 kpc and at a redshift of $z = 0.07$ from 230 kpc to 750 kpc. The specific angular momentum

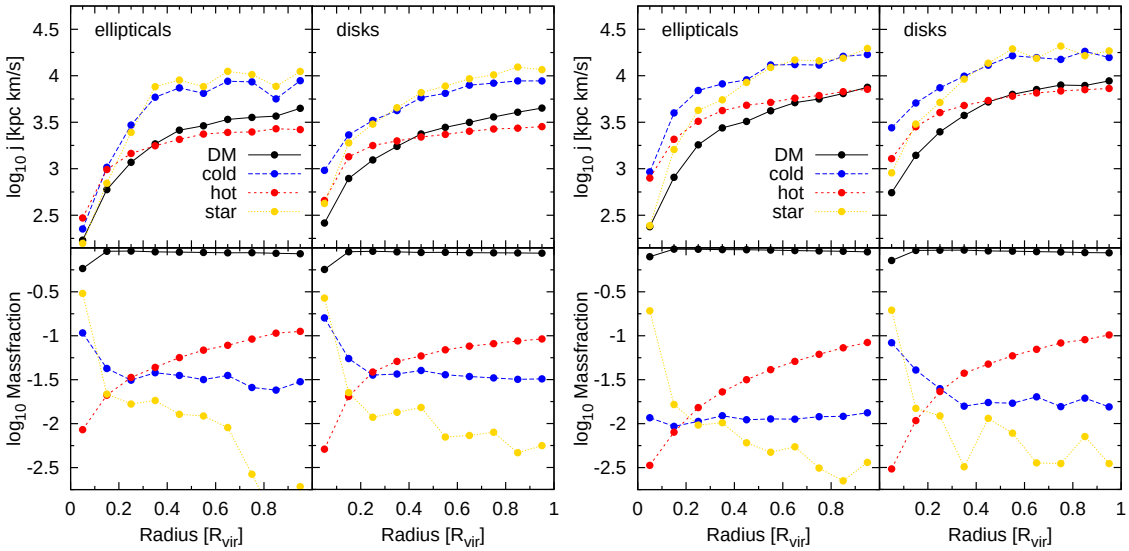

Fig. 4.9.: The specific angular momentum (top panels) and the mass fractions (bottom panels) against distance from the center for the cold gas (blue), hot gas (red), stars (yellow) and dark matter (black) of our sample of galaxies at $z = 1.98$ (two left panels) and $z = 0.07$ (two right panels). On each left hand side we show the analysis for the elliptical galaxies and on each right hand side that for the disk galaxies. At $z = 1.98$, in ellipticals the specific angular momentum of the cold gas drops below that of the hot gas in the center of the halos while for disks it remains higher. At $z = 0.07$, in ellipticals the specific angular momentum of the cold gas is only slightly higher than that of the hot gas in the center, while for disks it remains clearly higher. In the center of the ellipticals there is only little cold gas left.

of the two galaxy types increases from the center of the halo up to the virial radius. The specific angular momentum of the hot gas follows the dark matter, while the specific angular momentum of the stars follows that of the cold gas.

The main difference between the two galaxy types becomes clear in the central region: At redshift $z = 1.98$ the specific angular momentum of the cold gas of the ellipticals is lower than that of the hot gas, while for the disk galaxies it is higher than all other components. This confirms our previous interpretation of Fig. 4.5, where we find a split-up of the specific angular momentum of elliptical and disk galaxies in the gas component in the innermost region of the virial radius. Also taking into account the mass fraction makes it clear that the specific angular momentum of the gas in the innermost region is dominated by the cold gas because of the absence of hot gas in the center. On the other hand, the outer region is dominated by the hot gas, which behaves similar for ellipticals and disks, which also confirms our findings of Fig. 4.4, where there is no difference between the two galaxy types regarding the relation of the specific angular momenta of the gas and the dark matter, both within the entire virial radius. At redshift $z = 0.07$ the ellipticals have only little cold gas left in the center. As seen before in the lower right panel of Fig. 4.5 this gas spins up with decreasing redshift.

The radial profiles clearly show that in disk galaxies the cold gas transports high angular momentum material into the center, whereas in elliptical galaxies the gas in the central region has low angular momentum. Thus, we suspect that the star formation history is different for different galaxy types. In elliptical galaxies the specific angular momentum of the stars remains low, which indicates that there are almost no new stars formed and if so, they are formed out of the low angular momentum material. Hence, the specific angular momentum of the stars contains informations about the specific angular momentum of the gas from which they have formed.

4.2. Orientation of the Angular Momentum Vectors

In this section we want to study how the vectors of the baryonic components are oriented with respect to the dark matter and if it makes a difference for elliptical and disk galaxies. Therefore we calculate the (mis-)alignment angle θ.

The angle between two vectors of the species i and j is calculated by

$$cos\,(\theta) = \frac{\mathbf{J}_i \cdot \mathbf{J}_j}{|\mathbf{J}_i| \cdot |\mathbf{J}_j|}. \tag{4.3}$$

We then bin the angles from 0 to 180 degrees in 18 bins of a size of 10° and count the number of halos within each bin. For the plots the number of each galaxy type is normalized to unity. The values for redshift $z = 1.98$ are listed in Table C.1 and for redshift $z = 0.07$ in Table C.2.

4.2.1. The Angle between the Gas and the Star Component

Firstly, we want to investigate whether the angular momenta of the gas and the stars are aligned with each other. Fig. 4.10 shows the angle between the angular momentum vector of the gas against that of the stars. The left panels show both components within the entire virial radius while the right ones show both components in the inner ten per cent of the virial radius. The upper panels show redshift $z = 1.98$ and the lower ones $z = 0.07$. The gray dotted line is expected for a random distribution of the angles. When comparing the angles of the angular momentum vectors within the entire virial radius there is no difference between elliptical (red dashed histograms) and disk galaxies (blue dash-dotted histograms). In the central region it looks different: The disk galaxies have very well aligned gas and star angular momentum vectors with median values of 6.7° and 5.5° at redshift $z = 1.98$ and $z = 0.07$, respectively. This is in good agreement with Hahn et al. (2010) who found median angles of about 7° for their disks at $z = 0$. The ellipticals have a random distribution with median values of 82.6° and 85°, i.e. the gas and stellar components in elliptical galaxies are completely misaligned. On the other hand, this illustrates that the stellar and gaseous disk in disk galaxies are very well aligned, which is what we expect, since the stars form out of the gas and thus maintain the same orientation. In general, the gas and star components become less aligned with decreasing z. In contrast, the alignment for disks gets even slightly better.

4.2.2. The Angle between the Gas and the Dark Matter Component

Next, we want to study the alignments between the angular momentum of gas and dark matter. The upper left panel of Fig. 4.11 shows the misalignment angle

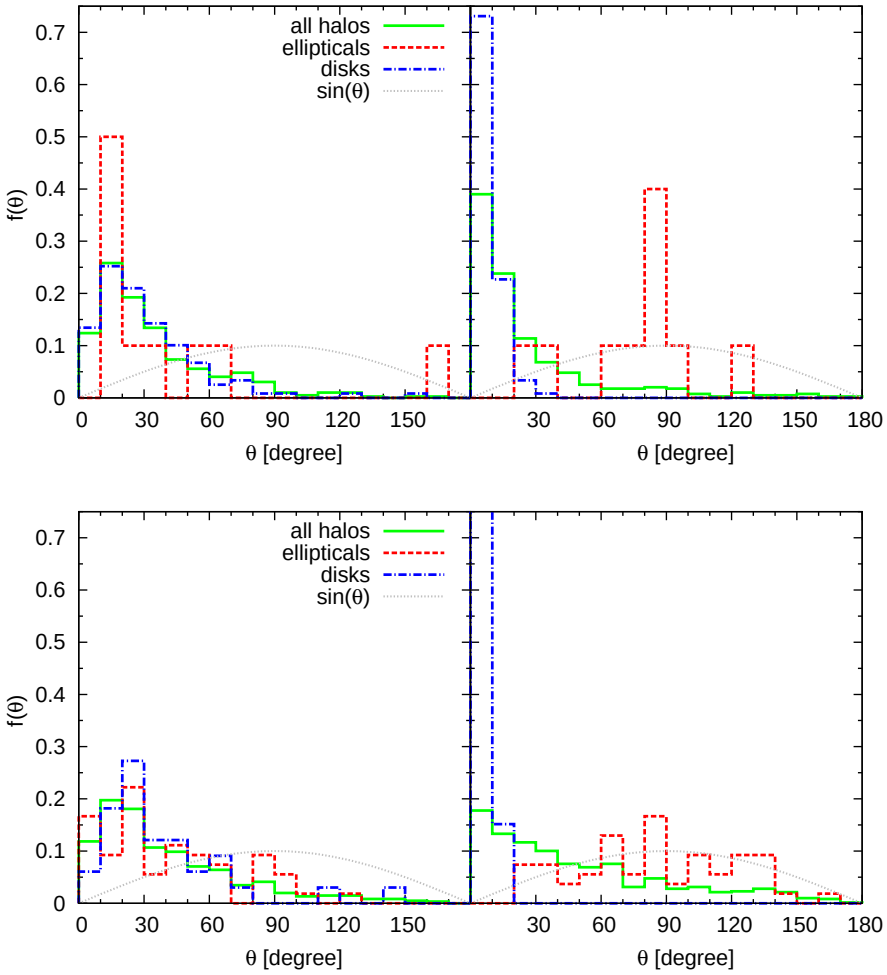

Fig. 4.10.: Left: The angle between the total angular momentum vectors of gas and stars within $R_{\rm vir}$. Right: The angle between the total angular momentum vector of gas and stars, both within the innermost ten per cent of the virial radius. The upper panels show redshift $z = 1.98$ and the lower panels $z = 0.07$.

between the angular momentum of the dark matter and the gas within the virial radius at redshift $z = 1.98$ and the lower left panel represents redshift $z = 0.07$. The gray dashed line is the expected distribution if the angles were spread randomly. The distribution of the angles does not show any significant difference between the galaxy types and are relatively well aligned. When considering all halos, at redshift $z = 1.98$ we find median and mean values of 12.8° and 19.6°, respectively and at redshift $z = 0.07$ we find median and mean values of 25.1° and 33°, respectively.

At higher redshifts this is in good agreement with Sharma and Steinmetz (2005) and Sharma et al. (2012), who find a mean misalignment angle of about 20°, and

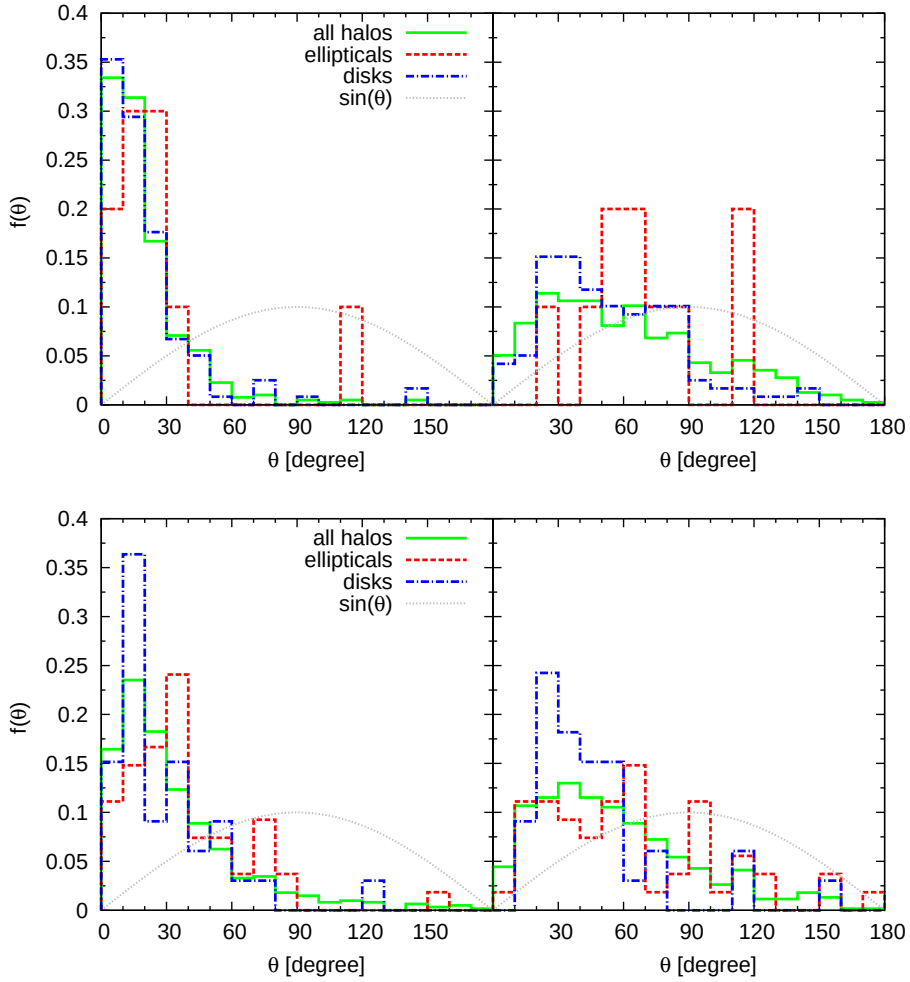

Fig. 4.11.: Left: The angle between the total angular momentum vectors of DM and gas within $R_{\rm vir}$. Right: The angle between the total angular momentum vector of DM in $R_{\rm vir}$ and the gas within the innermost ten percent of $R_{\rm vir}$. The upper panel shows $z = 1.98$ and the lower panels $z = 0.07$.

also with Chen et al. (2003), who obtained mean values of $22.8° - 25°$, depending on the used gas cooling physics. At lower redshift it better fits with the results of van den Bosch et al. (2002), who found slightly higher values, namely about 27° for the median and about 36° for the mean misalignment angle.

On the upper right panel of Fig. 4.11 the angle between the dark matter within the virial radius and that of the gas component in the central region is shown for redshift $z = 1.98$, and redshift $z = 0.07$ is shown on the lower right panel. At redshift $z = 1.98$, the median misalignment for all halos (green) is 53.4°, for the disks (blue) 47.2° and for the ellipticals (red) 65.7° while at redshift $z = 0.07$ the median

misalignment angles are slightly lower, namely for all halos it is 48.8°, for the disks 38.5° and for the ellipticals 55.6°. Sharma et al. (2012) found lower values for the gas within the innermost ten per cent of the virial radius compared to the total angular momentum vector of all halos, namely a median misalignment angle of about 30°. Hahn et al. (2010) compared the angular momentum of the gas component of the disk to the total angular momentum and obtained about 49° at $z = 0$. Interestingly we find a bimodality not only in the distribution of the different galaxy types but also in the distribution of the ellipticals. While the disks are comparatively aligned, the ellipticals also have an isotropically spread part.

We note that in all galaxies the angular momentum of the gas and the dark matter halo are better aligned with cosmic time.

4.2.3. The Angle between the Dark Matter and the Star Component

We now want to see if the angles between the angular momentum vectors of the dark matter and that of the stars reflect the orientation of the angular momentum vectors of the gas and the dark matter, since we have seen in Fig. 4.10 that the angular momentum vectors of the gas and that of the stars are very well aligned for disk galaxies and poorly aligned for ellipticals. The angle between the angular momentum vectors of the dark matter and that of the stars within the virial radius is shown on the left panels of Fig. 4.12. As median value for all halos we find 22.6° and as mean value 31.5° for the higher redshift (left upper panel). At the lower redshift (left lower panel) we find 23.9° as median and 31.2° as mean value. For comparison, Croft et al. (2009) calculated a median angle of 43.5° at redshift $z = 1$.

The upper right panel of Fig. 4.12 shows the angle between the angular momentum vector of the stars within the inner region and the dark matter within the entire virial radius at redshift $z = 1.98$. Since at this high redshift we have only a small sample of ellipticals (red) there is no obvious dichotomy between the galaxy types. In the lower right panel of Fig. 4.12, which shows a redshift of $z = 0.07$, we clearly see the dichotomy of the galaxy types. The disks (blue), which have a median misalignment angle of 42.5°, are better aligned than the ellipticals (red), whose misalignment angle has a median of 88.3°. Their distribution is nearly isotropic. A misalignment of the baryonic component of spheroid-dominated systems at different radii of the halo was also seen by Sales et al. (2012). Hahn et al. (2010) calculated

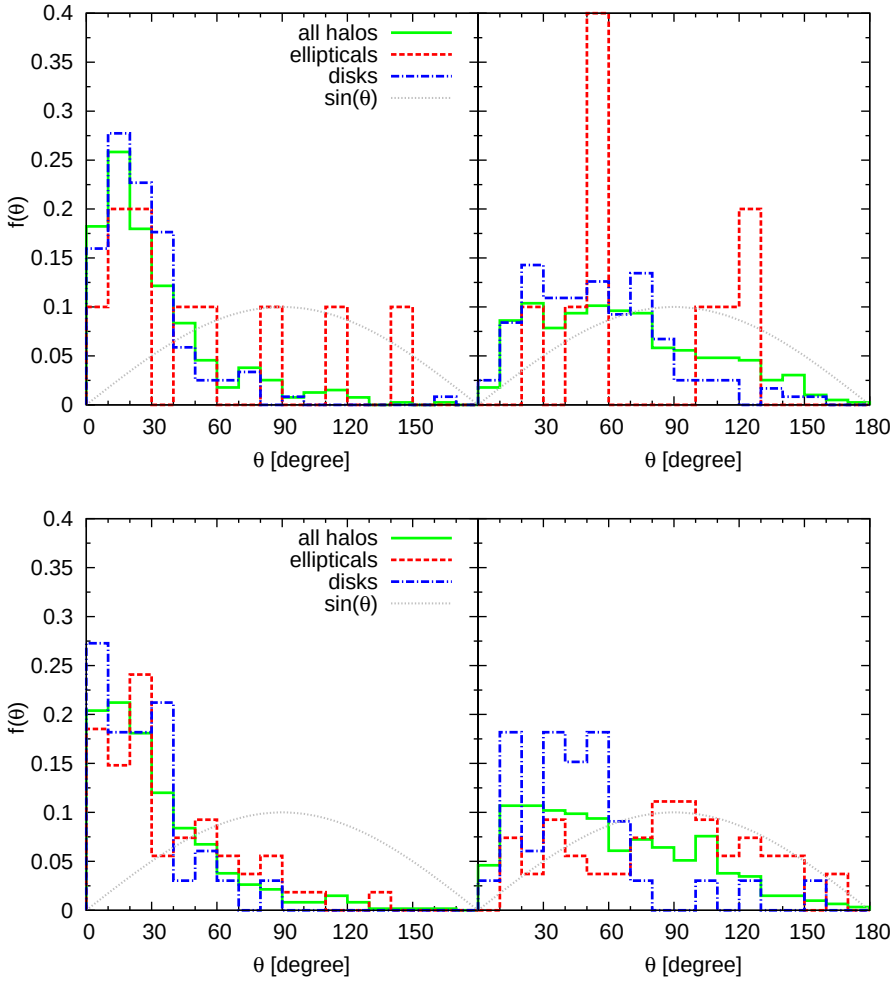

Fig. 4.12.: Left: The angle between the total angular momentum vectors of the dark matter and stars within $R_{\rm vir}$. Right: The angle between the total angular momentum vector of the dark matter in $R_{\rm vir}$ and the stars within the innermost ten per cent of the virial radius. The upper panels show redshift $z = 1.98$ and the lower ones $z = 0.07$.

a median angle of the stellar disk component and the total halo content of about 49° at $z = 0$.

The distribution of the alignment angles of the star component against that of the dark matter looks similar to that of the gas (Fig. 4.11) for the disk galaxies but the median values are slightly higher (see Table C.1 and C.2). We assume that this is attributed to the bulge component of the disk galaxy, which may not be completely aligned. For the ellipticals the alignment of the two baryonic components with the dark matter is also similar at high redshift but differs at low redshift, where the angular momentum of the gas is better aligned with that of the dark matter halo

than the stars' angular momentum vector with that of the dark matter. This agrees with the finding of Fig. 4.11 that the angular momenta of gas and stars in the galaxy get worse aligned with decreasing redshift.

4.2.4. The Angle between the Dark Matter at Different Radii

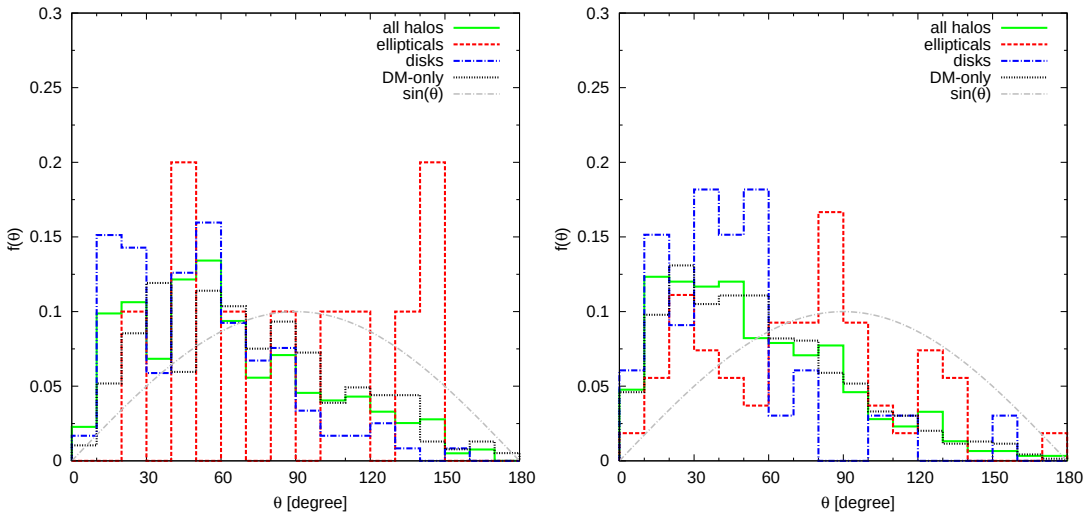

Fig. 4.13.: The angle between the total angular momentum vector of the dark matter in $R_{\rm vir}$ and that of the dark matter within the innermost ten per cent of the virial radius. The left hand side shows redshift $z = 1.98$ and the right one $z = 0.07$.

At last, we want to study whether the angular momentum of the total dark matter halo is aligned with that of the dark matter of its galaxy. Fig. 4.13 shows the angle between the vector of the total angular momentum over the virial radius against that of the inner part of the halo only for the dark matter for redshift $z = 1.98$ (left) and for $z = 0.07$ (right). For the baryon run at redshift $z = 1.98$ the median and mean values for all halos are 56.5° and 62.7°, respectively and we find a median angle of about 50° for the disk galaxies. At lower redshifts we calculate median and mean values for all halos of 46° and 54.5°, respectively and a median angle of about 40.6° for the disk galaxies. At high redshift our value is higher than the $\approx 34°$ found by Hahn et al. (2010) for the inner dark matter component with the total angular momentum of the halo at a redshift of $z = 1$. At $z = 0$ our results are agree well with their obtained median angle of 45°. In the DM-only run the values are higher with 66.4° for the median and 70.8° for the mean misalignment

angle at redshift $z = 1.98$ and slightly higher at redshift $z = 0.07$ with $51.2°$ for the median and $56.5°$ for the mean misalignment. This tendency was also seen by Bett et al. (2010) who found that in their run with baryons the vectors were slightly more aligned than in the DM-only case. The misalignment angle in our analysis is higher than their median angles of $15° - 30°$ for their run with baryons. This could be due to the fact that we only consider the inner ten per cent instead of 25 per cent. This seems plausible, since Bailin and Steinmetz (2005) found that the alignment becomes worse when the radii are further separated. Sales et al. (2012) found that the angular momentum of the baryonic component at different radii were misaligned for spheroidal systems, while they were well aligned for disk galaxies. Bullock et al. (2001) also concluded that a misaligned halo is less likely to host a spiral galaxy. We note that in general the angles become less misaligned with decreasing redshift. Interestingly, the distribution looks very similar to that of the angles between the angular momenta of stars in the galaxy and the dark matter halo (see Fig. 4.12).

An interpretation of the above findings could be, that disk galaxies preferentially form in halos, where the core is aligned with the outer parts of the halo. When the gas streams in, it does not transfer the angular momentum to the other components but keeps it and carries it to the central region. If gas flows into a halo with a misaligned core it loses angular momentum by transferring it to the components in the outer regions. Thus the gas does not form a disk and we get ellipticals. On the other hand, Sharma et al. (2012) showed that major mergers having misaligned angular momentum vectors can be responsible for misalignments. Welker et al. (2014) in addition proposed that anisotropic cold streams realign the galaxy with its hosting filament. However, Sales et al. (2012) suggested that disks form out of gas having similar angular momentum directions, which would favor the spherical hot accretion mode, while the accretion along cold flows that are mainly misaligned tend to build a spheroid.
In a further investigation we could trace back disk galaxies and see if the primordial alignment causes the inflowing matter to become a spiral or if it is the other way around, i.e. if the galaxy-type over cosmic time induces the alignment. We suspect that the environment has a significant impact on the formation of disk galaxies. In less dense environments, where the halos can evolve relatively undisturbed, the angular momentum of the galaxy remains aligned with that of its host halo and thus a disk can form.

4.3. The λ-Parameter

In the following section we want to study the dimensionless λ-parameter. For our investigations we use two different definitions for the calculation of the spin parameter λ. We will first discuss the general λ-parameter which is used for the total halo and then turn to the modified λ′-parameter for the evaluation of the different components and compare the baryon run with the dark matter only control run.

4.3.1. The λ – Distribution for Halos

The general λ-parameter, as defined by Peebles (1969, 1971) and adopted by e.g. Mo et al. (1998), is given by

$$\lambda = \frac{J|E|^{1/2}}{GM^{5/2}}, \tag{4.4}$$

where $E = -GM^2/2\,R_{\rm vir}$ is the total energy of the halo. The distribution of the λ-parameter can be fitted by a lognormal distribution of the following form:

$$P(\lambda) = \frac{1}{\lambda\sqrt{2\pi}\sigma}\, exp\left(-\frac{ln^2(\lambda/\lambda_0)}{2\sigma^2}\right), \tag{4.5}$$

with the two fit-parameters λ_0 which is about the median value and the deviation σ.

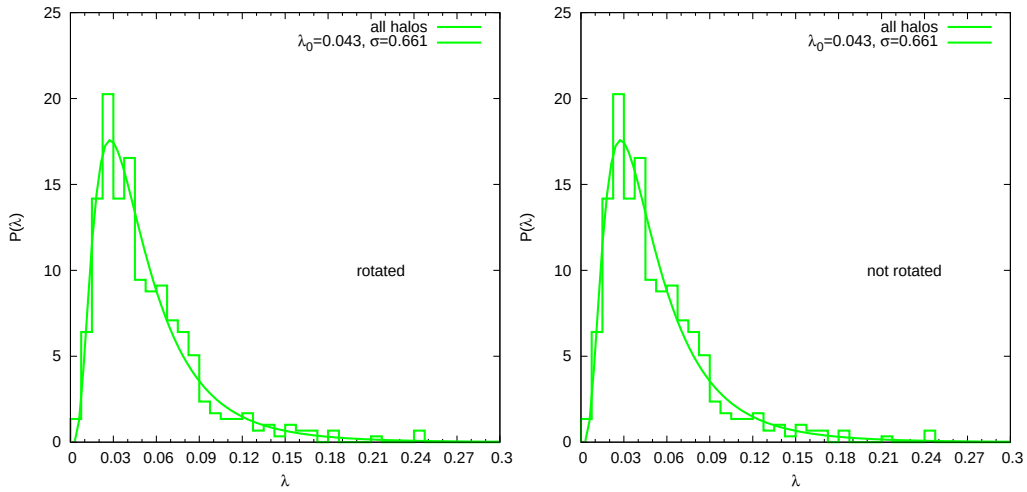

Fig. 4.14.: The λ-distribution for redshift $z = 1.98$ for all halos. On the left panel the halos were rotated whereas on the right plot the halos were not rotated. This makes no difference for the distribution of the λ-parameter.

Before we present the λ-distribution for several redshifts we want to check if it makes a difference if the halos have been rotated or not. The left plot of Fig. 4.14 shows the distribution of the λ-parameter for all halos at redshift $z = 1.98$ that were rotated. On the right panel the λ-distribution for the same redshift is shown but this time the halos were not rotated. The histograms are the calculated values and the curves are fits using formula (4.5). The two plots show exactly the same values and thus for the calculation of the λ-parameter it does not make a difference if the halos are rotated or not. This is an important finding with regard to the comparison of the dark matter only run and the run with baryons, since the halos in the dark matter only run are not rotated.

For Fig. 4.15 we calculated the λ-parameter of the halos in linear bins with a bin size of 0.0075 for different redshifts as indicated on the plots. The histograms and fit-curves are each normalized to the number of the considered halos. Green shows the distribution of λ for all 395 halos at $z = 1.98$ (upper left), 602 halos at $z = 0.99$ (upper right), 619 halos at $z = 0.47$ (lower left) and 607 halos at $z = 0.07$ (lower right). We note that there are 608 halos at the latter redshift but one seems to have an even higher value than the plotting range. This halo might be an interesting object for further studies. We find that for $z = 1.98$ there are two peaks, one located at $\lambda \approx 0.025$ and the other at ≈ 0.045 and also in the distribution at redshift $z = 0.07$ there is a double peak, a smaller one at $\lambda \approx 0.025$ and a broader one at ≈ 0.04. In order to check the reason for the two peaks we split the halos into elliptical (red) and disk (blue) galaxies. For this we take into account the ε-distribution of the gas as well as the star component as done above for the specific angular momentum of the gas versus that of the dark matter. The left peak can be identified with the ellipticals which have only little rotation. The right peak is associated with the disk galaxies. This splitting of the two galaxy types is seen at all four redshifts. The ellipticals have always lower median values than the disk galaxies, see also Table D.1. This is in contrast to the results from Sales et al. (2012) and Scannapieco et al. (2009), who did not find a correlation between galaxy type and the spin parameter.

From Table D.1 in the appendix we can also see that the fit values agree very well with the calculated median value of the λ-distributions.

The λ-distribution for all halos seems to be relatively constant with time, i.e. independent of redshift, which is in agreement with Peirani et al. (2004). However,

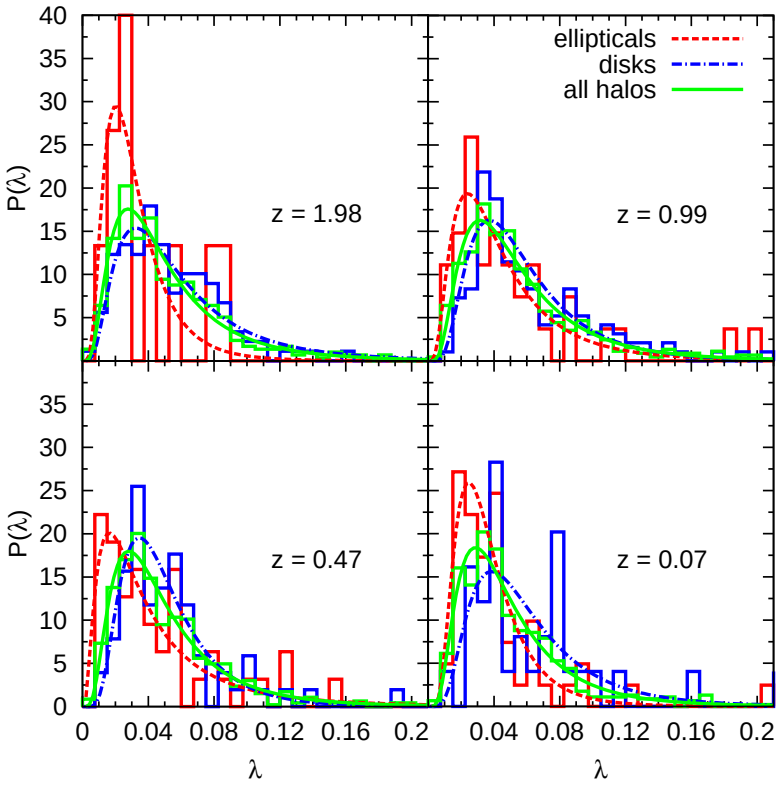

Fig. 4.15.: The λ-distribution calculated with formula (4.4) for the different redshifts as indicated in the plots. Green takes into account all halos. Ellipticals are red and disks are blue. The curves are the fits given by equation (4.5). We chose a bin size of 0.0075.

for the different galaxy types λ_{med} fluctuates between 0.048 and 0.058 for the disks and between 0.028 and 0.038 for ellipticals.

We now want to see how the curves change when taking different bin sizes. Fig. 4.16 shows the same as Fig. 4.15 but on the left panels of Fig. 4.16 we chose a bin size of 0.01 and on the right panels a bin size of 0.005. The fit curves are almost identical. There is a tendency that with smaller bin sizes the double peak in the distribution for all halos at redshifts 1.98 and 0.07 is better resolved. We note that even at $z = 0.99$ there is a small hint for a second peak at lower λ-values. A disadvantage of this high resolution is that the histograms make this plot confusing. Thus, for the following plots we will always use a bin size of 0.075 since the splitting of the galaxy types is resolved sufficiently and it does not make a huge difference for the fit values.

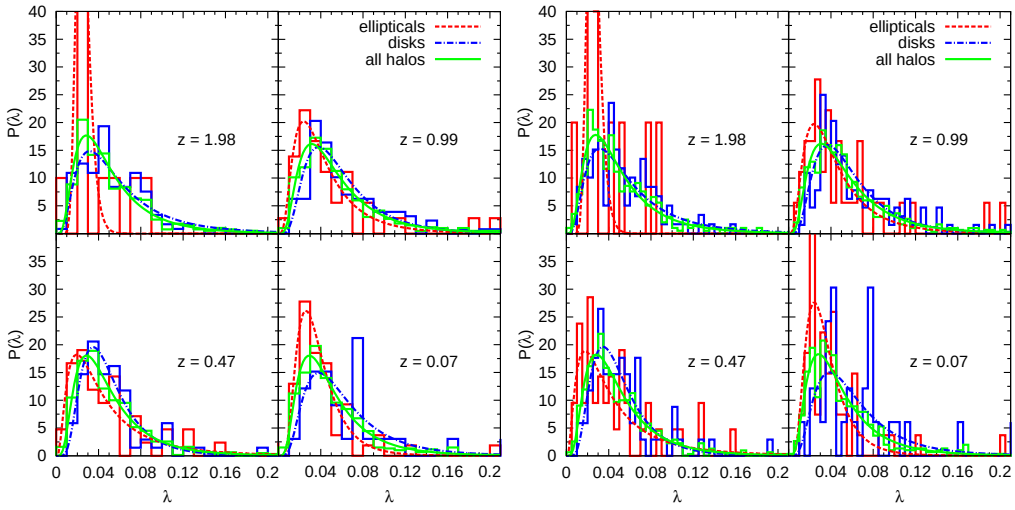

Fig. 4.16.: The λ-distribution for four redshifts as indicated in the plots. Left: The bin size is 0.01. Right: A bin size of 0.005 was used.

For statistical reasons it is interesting to check if the two curves for the disk and elliptical galaxies are following the same distribution. Hence we make use of the Kolmogorov-Smirnov (K-S) test. This test is applied to the two unbinned distributions for the disks and the ellipticals. An advantage of this test is that it is invariant under parametrization of the independent variable, in our case λ, in other words it is unimportant if we perform the K-S test with λ or $log(\lambda)$. We follow the routines from Press et al. (1996). The significance level that two distributions originate from the same distribution is given by

$$\text{probability} = Q_{\text{KS}}(x) = 2\sum_{i=1}^{\infty}(-1)^{i-1}e^{-2i^2x^2}, \tag{4.6}$$

where $x = [\sqrt{N_e} + 0.12 + 0.11/\sqrt{N_e}] \cdot D$ and D is the maximum distance of the two distributions and N_e is the effective number of data points, i.e. $N_e = N_1N_2/(N_1+N_2)$ with N_1 being the number of the data points of the first and N_2 that of the second distribution.

Table 4.1 shows the calculated values for the maximum distance D and the probability. At redshift $z = 1.98$ the probability that the distributions come from the same distribution is relatively high with nine per cent. This might be due to the small sample size of the ellipticals. However, at the other redshifts the probability is below five per cent which is a strong indication that these two distributions are

different ones.

Tab. 4.1.: The maximum distance D and the significance level (probability) resulting from the K-S test that the λ-distributions for disks and ellipticals at different redshifts for our sample of galaxies are from the same distribution

redshift	D	probability
1.98	0.3899	0.0900
0.99	0.2639	0.0324
0.47	0.2633	0.0446
0.07	0.3367	0.0142

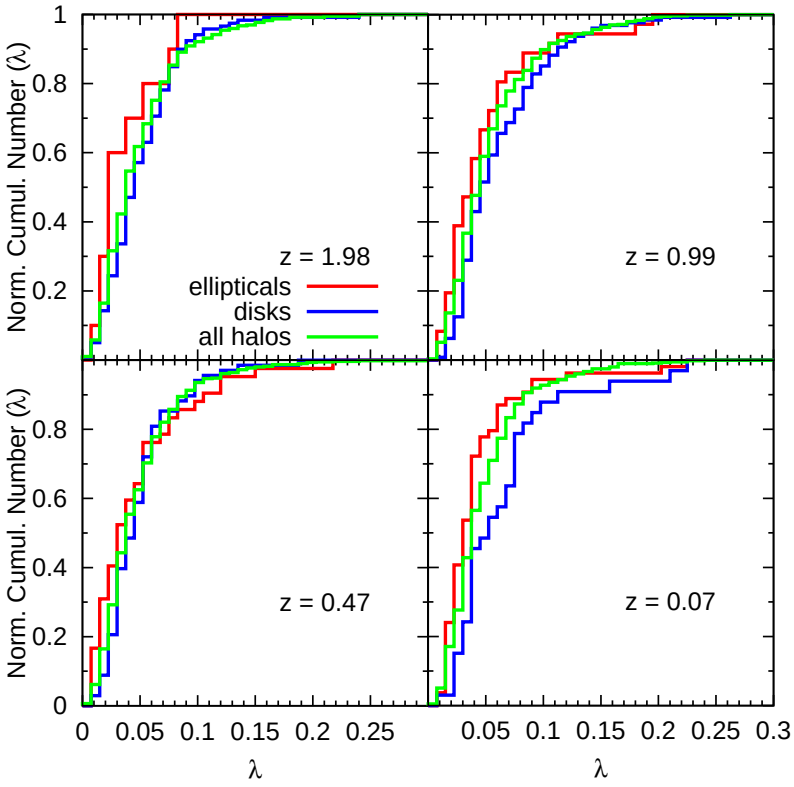

Fig. 4.17.: The λ-parameter plotted against the normalized cumulative number of halos. Green takes into account all halos, red the ellipticals and blue the disk galaxies.

Fig. 4.17 shows the λ-values against the normalized cumulative number of halos, where we used linear bins of bin size 0.0075. This illustrates the distances between the two distributions. At redshift 1.98 and 0.07 the two distributions are always separated and while the disks stay right, i.e. at higher values with respect to the

distribution of all halos, the ellipticals are at lower values. At the other two redshifts there is an overlap between the distributions. At redshift $z = 0.47$ the distribution for the ellipticals even ends at higher values than that of the disks, i.e. there are also ellipticals that have high λ-values. The distribution for all halos has the same shape at all four redshifts.

We now want to compare the λ-distribution of the dark matter only runs with that of previous works. Fig. 4.18 shows the λ-distribution for the dark matter only runs, linearly binned: The black histogram shows Box4 uhr, the blue histogram Box3 hr, both at $z = 1.48$, while the other lines are according to the fit values of several authors, as indicated in the legend (see also Table D.2). The fit curves of the two different resolutions lie very close to each other. Thus, the properties do not severely depend on the resolution and the size of the simulated box. In comparison to previous studies (i.e. Bullock et al. (2001), Bryan et al. (2013) and Trowland et al. (2013)) the distribution in our simulation is slightly broader. It comes closest to the results of Bryan et al. (2013).

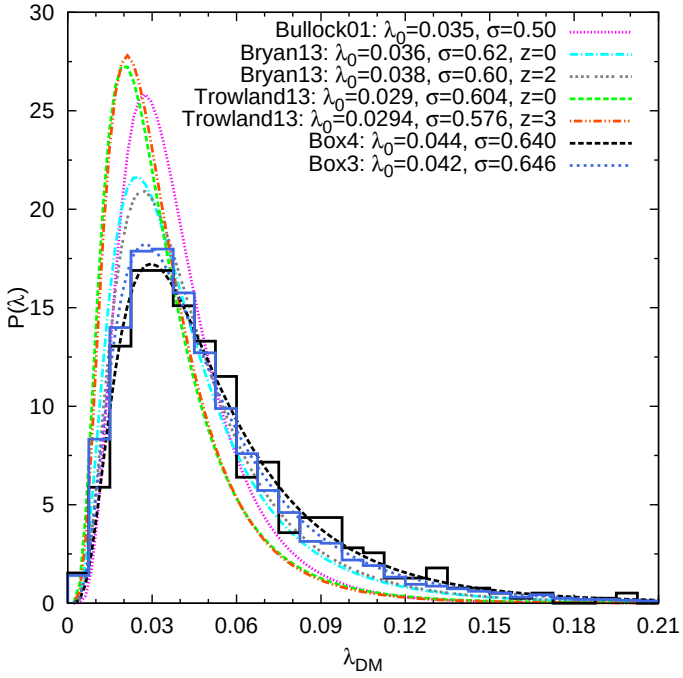

Fig. 4.18.: The λ-parameter in the DM-only simulations: the black histogram shows the distribution for Box4 uhr with a sample of 521 halos and the blue one in the Box3 hr with a sample of 9881 halos at $z = 1.48$.

In this section we have seen that there is a statistical correlation between the

morphological type and the overall distribution of the spin parameter λ. At all four considered redshifts the distributions for the ellipticals have lower median values than that of the disks. According to the K-S test there is a strong indication that they do not originate from the same distribution. On the other hand, we have also found that there are ellipticals with even higher λ-values than disk galaxies.

4.3.2. The λ – Distribution for Single Components of the Halos

In order to illustrate the influence of the baryons on the dark matter component we evaluate the λ-parameter for the different components. Therefore we use the modified spin parameter λ', which is defined by Bullock et al. (2001) as follows:

$$\lambda'(r) := \frac{J(r)}{\sqrt{2}M(r)V_{\mathrm{circ}}(r)r}, \tag{4.7}$$

where $J(r)$ is the angular momentum, $M(r)$ the mass and $V_{\mathrm{circ}} = \sqrt{GM(r)/r}$ the circular velocity within a radius r. The advantage of $\lambda'(r)$ is that it can be used for the calculation at different radii. When calculated over the entire virial radius it reduces to the general λ. For the evaluation of the different components it can be written in the following form, as done by van den Bosch et al. (2002):

$$\lambda_k = \frac{j_k}{\sqrt{2}R_{\mathrm{vir}}V_{\mathrm{circ}}}, \tag{4.8}$$

where k stands for the different components. In the following we only use this definition, so we drop the prime.

The left panels of Fig. 4.19 show λ for stars (yellow), dark matter (black) and gas (turquoise) for redshift $z = 1.98$ (upper panels) and $z = 0.07$ (lower panels). The star component has low values which is not surprising, since in elliptical galaxies stars do not show ordered rotation and in disk galaxies most stars within the innermost ten per cent of the virial radius are found in the bulge. As seen for the total λ in Fig. 4.15 we again find an indicated double peak in the distribution of the dark matter, which is the dominating component. This reinforces the assumption that the baryons influence the dark matter's rotation. The stellar component has the lowest λ-values and the highest standard deviation which is in agreement with Danovich et al. (2014). The λ-distribution for the gas has the highest median value. Sharma and Steinmetz (2005), Kimm et al. (2011), Sharma et al. (2012) and

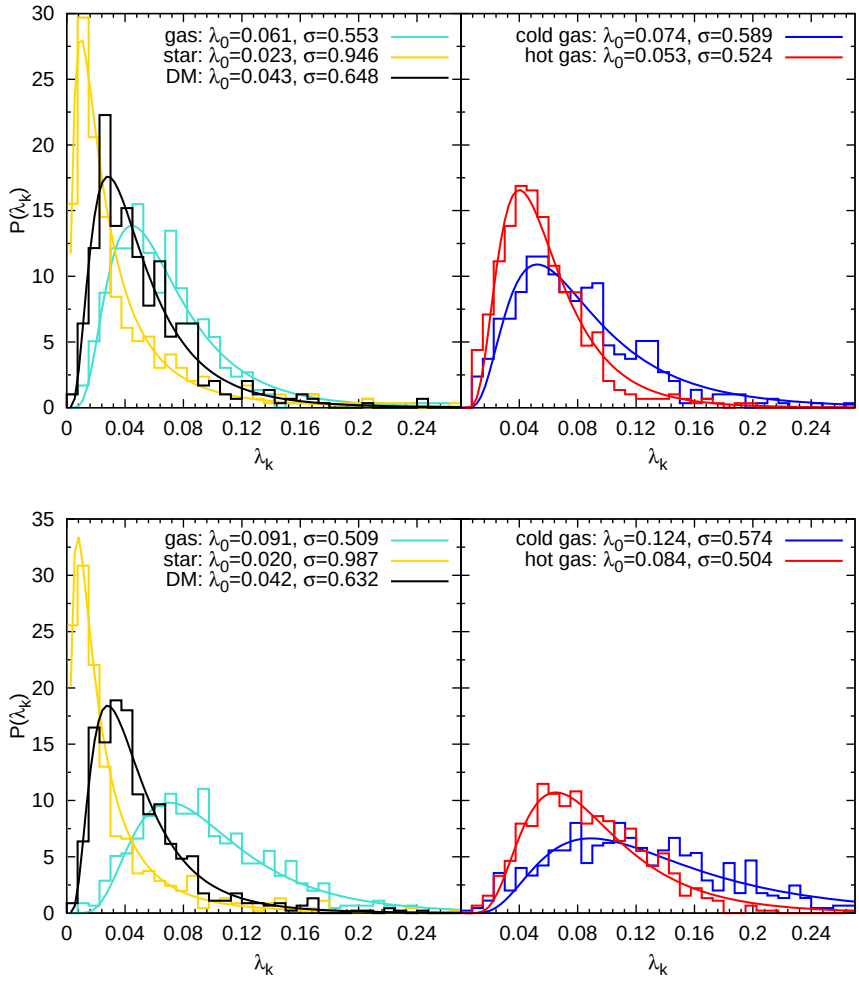

Fig. 4.19.: Left panel: the λ-parameter for the different components within R_{vir}: The dark matter (black) is the dominant component, the stars (yellow) peak at the lower values, whereas the gas is distributed around the higher values. Right panel: the gas component split into hot (red) and cold (blue) gas. The upper panels show redshift $z = 1.98$ and the lower ones $z = 0.07$.

Danovich et al. (2014) also found that the gas component has a higher spin parameter than the dark matter, in contrast to van den Bosch et al. (2002) and Chen et al. (2003), who got nearly the same value for the two components. We find a different behavior of the two gas components on the right panels of Fig. 4.19. The hot gas (red) has lower values than the cold gas (blue) which has a long tail to high λ-values. This is not in agreement with Chen et al. (2003), who found that the spin parameter for the hot gas is higher than that of the cold gas. On the other hand, our results agree well with Danovich et al. (2014). This trend for the cold gas to

high values was also seen by Stewart et al. (2011), who calculated λ-values for the cold gas around $0.1 - 0.2$. This in addition to the findings of the lower panels of Fig. 4.9, that in disk galaxies there is more cold gas in the center than in ellipticals, gives us the reason for the double peak in the λ-distribution.

Tab. 4.2.: The λ_0 fit value for the different components at different redshifts for our sample of galaxies

redshift	$\lambda_{\rm stars}$	$\lambda_{\rm DM}$	$\lambda_{\rm gas}$	$\lambda_{\rm hot}$	$\lambda_{\rm cold}$
1.98	0.023	0.043	0.061	0.053	0.074
0.99	0.026	0.046	0.078	0.070	0.098
0.47	0.021	0.042	0.085	0.079	0.108
0.07	0.020	0.042	0.091	0.084	0.124

For a better overview we have listed the fit values of the λ-distribution for the different components in Table 4.2. We immediately note that the values for the gas components are rising steadily with decreasing redshift, whereas the values for the stars and dark matter remain relatively constant. This illustrates the spin up of gas with time which we have already seen in e.g. Fig. 4.4.

We now want to check the λ-distribution for the dark matter component in the run with baryons, splitting the galaxies into ellipticals and disks, and then compare it to the distribution of the dark matter only run.

Fig. 4.20 shows $\lambda_{\rm DM}$ for the baryon run for the four redshifts as indicated in the plots. The green histogram shows $\lambda_{\rm DM}$ for all halos (as in the left panels of Fig. 4.19 and Fig. D.1), the red one stands for the ellipticals and the blue one for disk galaxies. Here again, especially at redshifts $z = 0.99$ and 0.47, there is a splitting of the two different galaxy types, the distribution of the ellipticals peaks at lower values and that of the disks at higher values. We also perform a K-S test on the two distribution (see Table 4.3). The values are similar to that of the general λ-distribution (Table 4.1). This is not surprising since the dark matter is the dominant component.

We now want to compare the run with the baryons and that with the dark matter only. Fig. 4.21 shows the λ-distribution for the dark matter component at three different redshifts as indicated on the panels. We remark that at redshift $z = 0.99$ there was no corresponding snap shot available for the dark matter only run. Green are the values for all halos in the run with the baryons and black is the control run with dark matter only. The distributions are similar but the fit values λ_0 for the

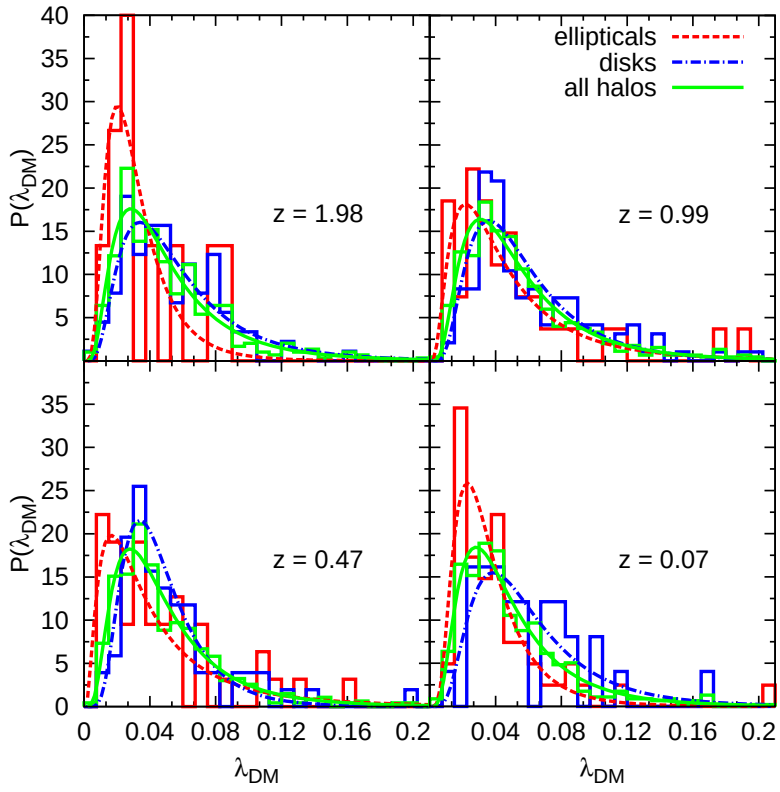

Fig. 4.20.: The λ-parameter for the dark matter component within $R_{\rm vir}$: Also in the dark matter component of all halos (green) there is a broad distribution, which is split into ellipticals (red) at lower values, while disks (blue) peak at higher values.

Tab. 4.3.: The maximum distance D and the significance level (probability) resulting from the K-S test that the $\lambda_{\rm DM}$-distributions for disks and ellipticals at different redshifts are drawn from the same distribution

redshift	D	probability
1.98	0.3815	0.1027
0.99	0.2595	0.0370
0.47	0.2507	0.0636
0.07	0.3401	0.0129

dark matter only run are slightly lower than for the run with baryons.

In order to see how the λ-parameter behaves for individual halos in the two different runs, we identified the same halos in the baryonic and the dark matter only run. We searched for the halos in a range of 200 kpc and they were allowed only to differ by 30 per cent in their virial masses. At redshift $z = 1.98$ we found for 363 halos in the baryon run a match in the DM-only run and at redshift $z = 0.07$

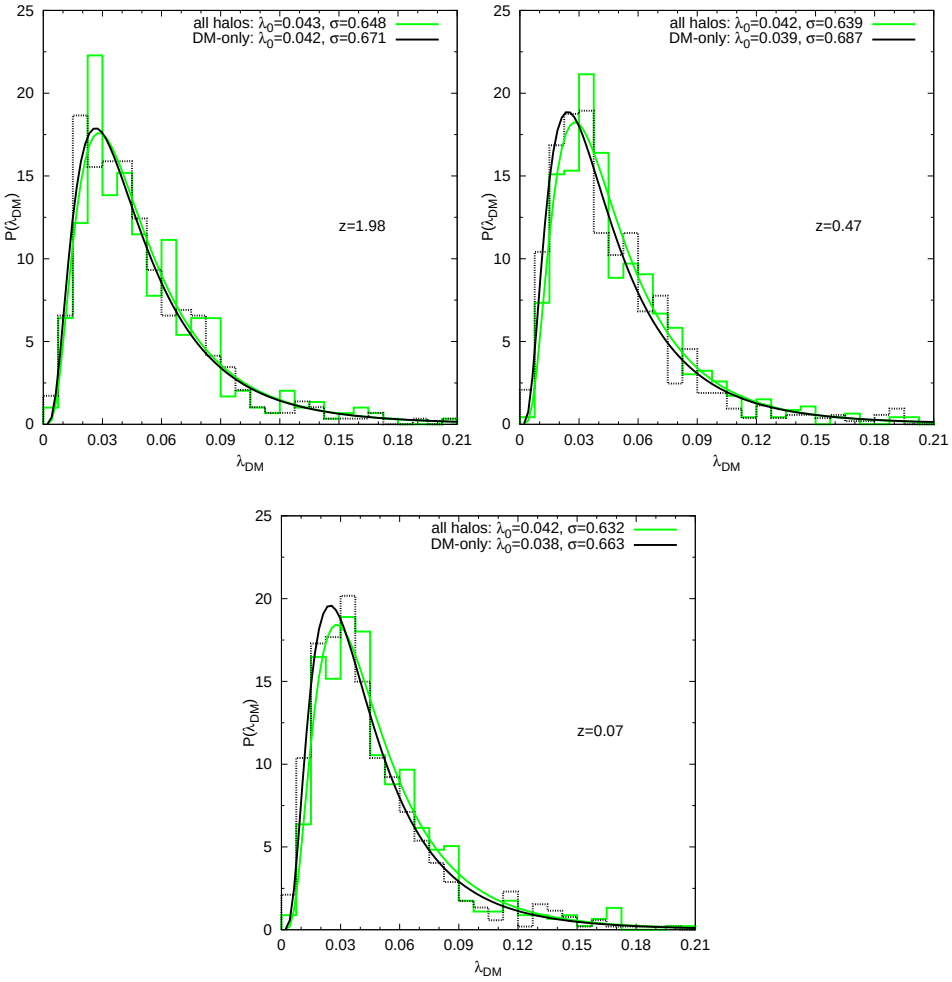

Fig. 4.21.: The λ-parameter for the dark matter component within for the baryon run (green) and for the DM-only run (black) at three redshifts.

we could assign 560 halos. Since baryons have an effect on the dark matter, in one run halos merge and in the other one at other times or not at all. The left panels of Fig. 4.22 show the λ-parameter of the dark matter component against the λ-parameter of the DM-only run in logarithmic scaling for ellipticals at redshifts $z = 1.98$ (upper panels) and $z = 0.07$ (lower panels). The values of the λ-parameter of the corresponding halos in both runs are similar. The stellar mass within ten per cent of the virial radius of the baryon run is color-coded. On the right panels we find $\lambda_{\rm DM}$-values for the disks. At a redshift $z = 1.98$ (upper panel) we note a slight tendency for the $\lambda_{\rm DM}$ to decrease with increasing stellar mass. The less massive disks tend to have higher λ-values. This is in agreement with Berta et al. (2008), who computed the dark matter spin parameter of ≈ 52000 disk galaxies from the Sloan

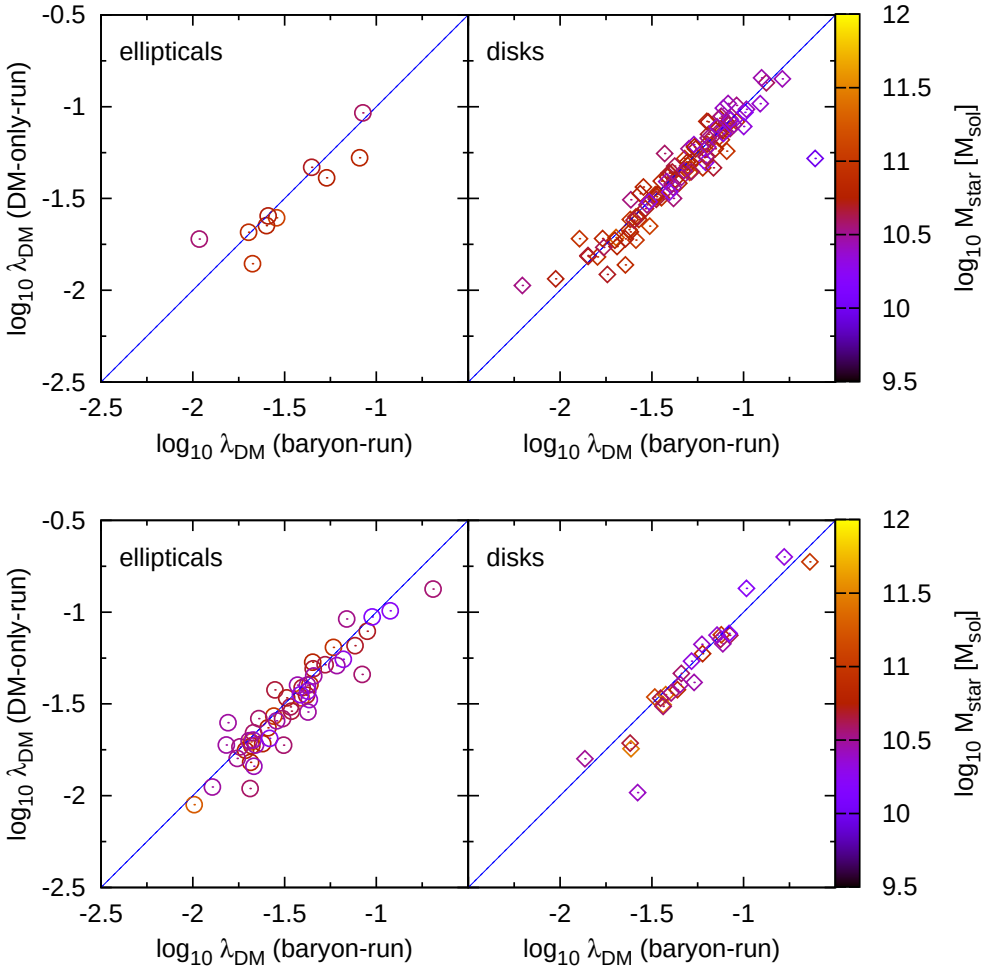

Fig. 4.22.: The λ-parameter plotted logarithmically for the dark matter component, on the x-axis the λ for the baryon-run and on the y-axis for the DM-only run, the color codes the stellar mass within the inner ten per cent of the virial radius. Left are the ellipticals and on the right panels the disks. The upper panels show redshift $z = 1.98$ and the lower ones $z = 0.07$.

Digital Sky Survey (SDSS) (for details of the sample see references in Berta et al. (2008)). They found a clear anti-correlation between the dark matter spin and the stellar mass, i.e. that galaxies with a low mass in general have higher dark matter spins. For the elliptical galaxies we do not see this trend. On the other hand, this figure also demonstrates that a high λ does not automatically lead to a disk galaxy and a small λ is no guarantee for an elliptical galaxy. The scatter is equal for both galaxy types. The fact that $\lambda_{\rm DM}$ in the whole virial radius is similar in the DM-only and the baryon run, is in good agreement with Bryan et al. (2013).

We want to check if we find an anti-correlation when directly plotting λ_{DM} against the stellar mass, as done in Fig. 4.23. The left panels show the ellipticals and the right panels the disk galaxies. The upper panels show a redshift of $z = 1.98$ and the lower ones $z = 0.07$. Indeed, we see a small trend for the disk galaxies at $z = 1.98$. At lower redshifts this trend gets weaker, which is probably due to the smaller sample size. The two redshifts in between, for which plots are shown in the appendix (Fig. D.3), also show a tendency for the disk galaxies. For elliptical galaxies there is no apparent trend of the spin parameter with stellar mass.

At last we want to see the relation of the λ-parameter of the different components

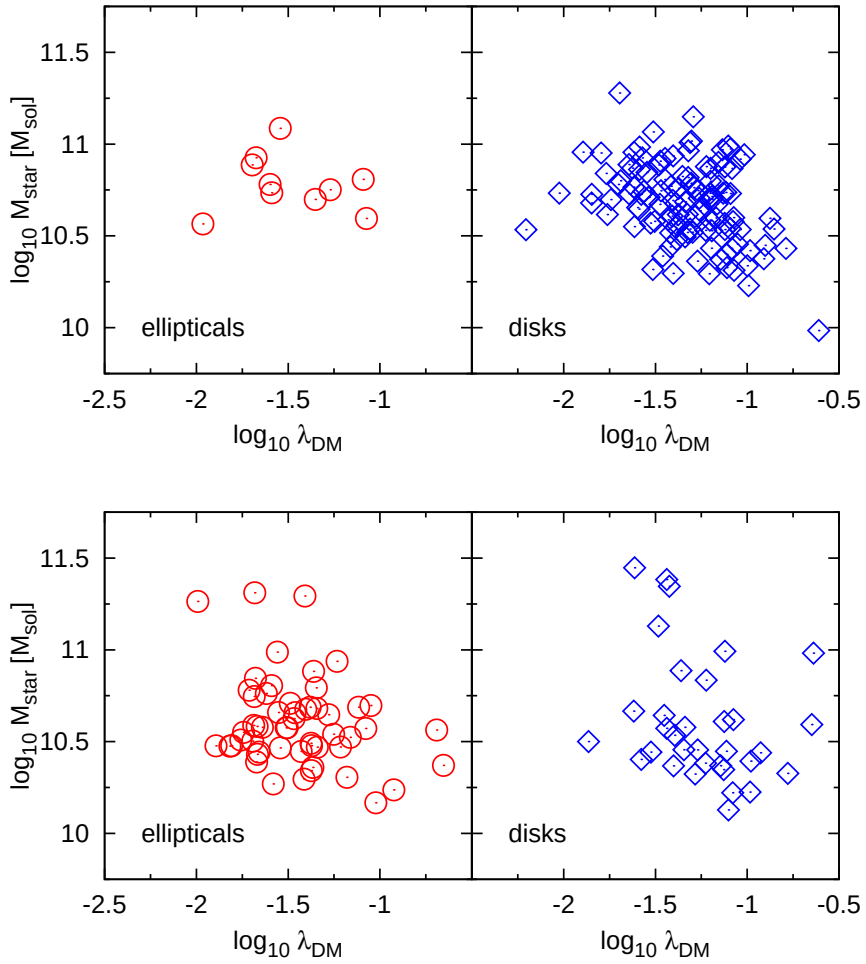

Fig. 4.23.: The λ-parameter plotted logarithmically for the dark matter component within for the baryon-run and on the y-axis the stellar mass within the inner ten per cent of the virial radius. Left are the ellipticals and on the right panels the disks. The upper panels show redshift $z = 1.98$ and the lower ones $z = 0.07$.

of individual halos. The left panels of Fig. 4.24 show the relation of the λ-parameter of the baryonic component, which includes gas as well as stars, against that of the dark matter for redshift $z = 1.98$ and $z = 0.07$, respectively. Each point represents a halo where red stands for ellipticals and blue for disk galaxies. At the higher redshift (upper panel), overall, the values seem to have the same order of magnitude but the scatter at the lower values is very high. The scatter becomes worse for the lower redshift (lower panel) and it almost seems like the ellipticals have higher spin parameter for the baryons than for the dark matter.

The right panels of Fig. 4.24 show the λ-parameter of the stars against that of the dark matter. In general λ_{DM} is higher than λ_{star}. We note that the halos with the

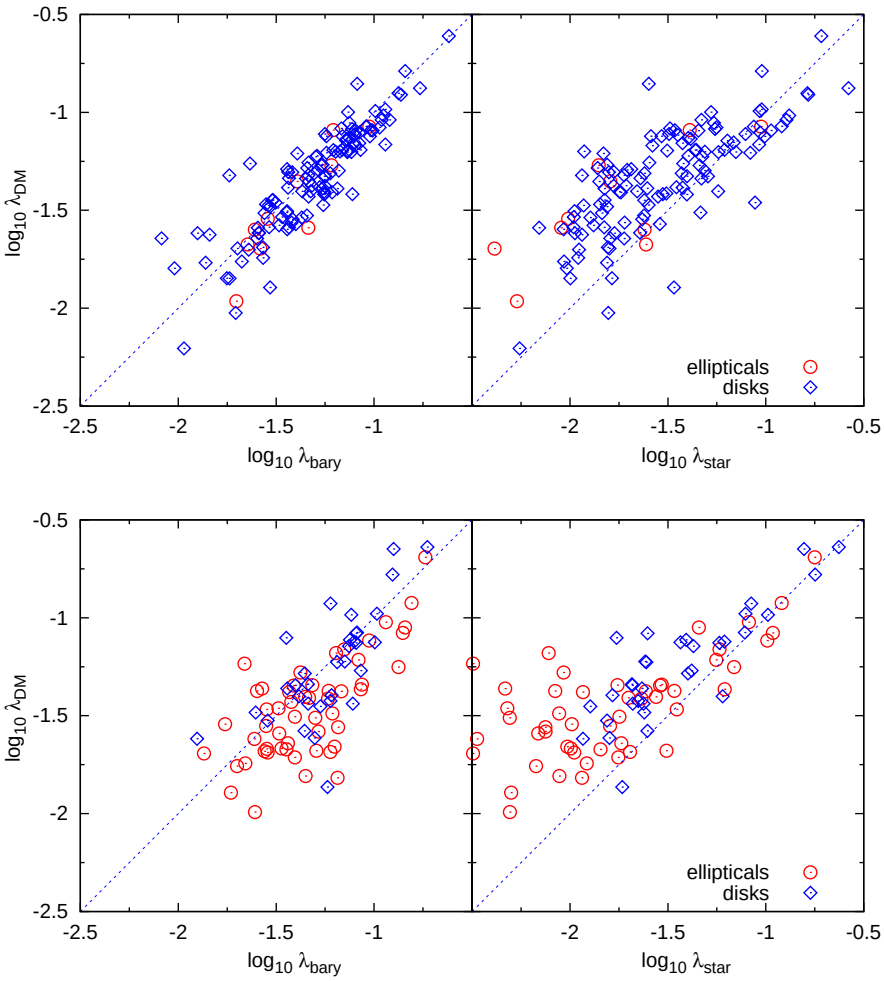

Fig. 4.24.: Left panels: the λ-parameter for the baryons (gas and stars) against that of the dark matter. Right panels: the λ-parameter for the stars against that of the dark matter. The upper panels show redshift 1.98 and the lower ones $z = 0.07$.

lowest $\lambda_{\rm star}$ values belong to halos hosting elliptical galaxies. We also see that if halos have low $\lambda_{\rm star}$ they tend to have comparatively higher $\lambda_{\rm DM}$ and on the other hand if they have high $\lambda_{\rm star}$ their spin parameter for the dark matter is comparatively lower.

The left panels of Fig. 4.25 show the relation of the λ-parameter of the dark matter component against that of the gas component for redshift $z = 1.98$ and $z = 0.07$, respectively. We can see that $\lambda_{\rm gas}$ is higher than $\lambda_{\rm DM}$, which is in agreement with Chen et al. (2003). They noted that this trend is strongest for the adiabatic case and becomes weaker with increased cooling. In our simulation, this trend becomes stronger with decreasing redshift, see also the two redshifts in between shown in Fig. D.5 of the appendix. This tendency was also found by Sharma and Steinmetz

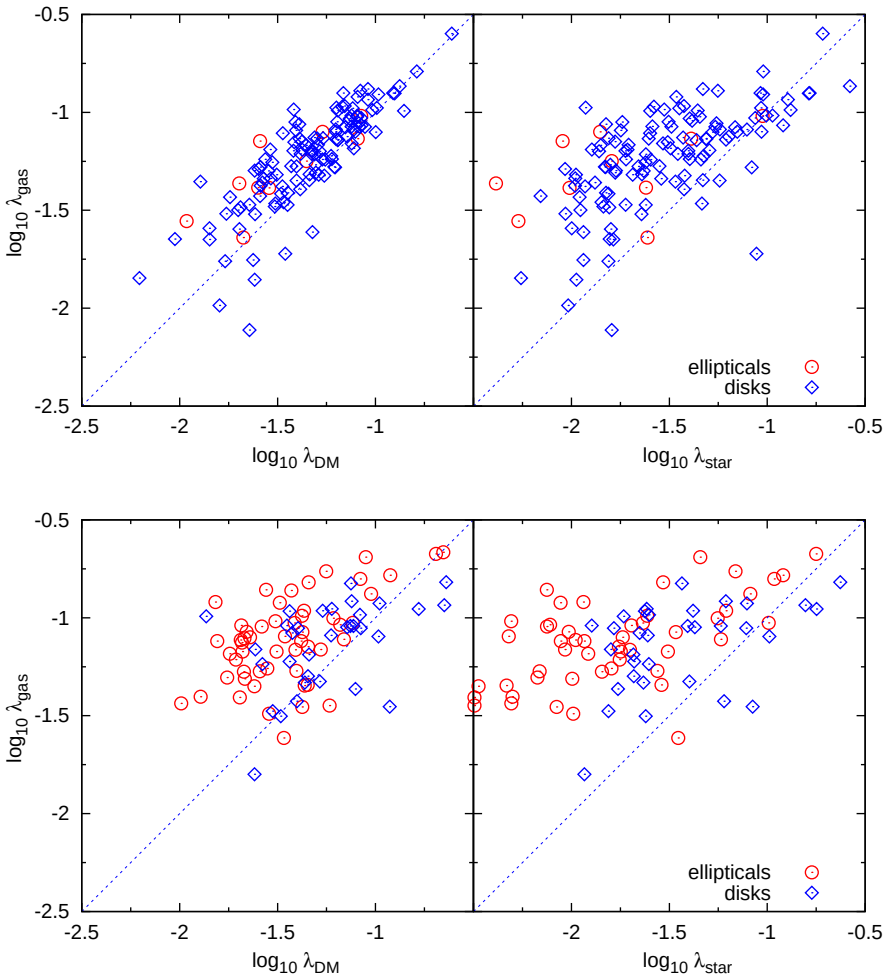

Fig. 4.25.: Left panels: the λ-parameter for the dark matter against that of the gas. Right panels: the λ-parameter for the stars against that of the gas. The upper panels show redshift $z = 1.98$ and the lower panels show $z = 0.07$.

(2005). We assume that this is due to the spin up of the gas with time. Hence, the baryonic component spins up with decreasing redshift, as seen in the left panels of Fig. 4.24.

The right panels of Fig. 4.25 show the λ-parameter of the stars against that of the gas. The spin parameter of the gas is higher than that of the stars. Most of the halos where the spin parameter of the stars is higher than that of the gas are classified as disk galaxies.

In this section we have found that the λ-distribution for the stars have the lowest values and that of the gas has the highest values. In addition, we have seen the spin up of the gas components with decreasing redshift. The cold gas has the highest spin values, which is explained by the fact that cold gas is mostly found in rotating disks. The hot gas has lower values than the cold gas, since in the halo it is more spherically distributed. The distribution of the λ-parameter for the dark matter reflects the overall λ-distribution, which is not surprising since it is the dominant component. The influence of the baryonic component, especially the gas, is displayed by a broader λ-distribution of the baryon run compared to the dark matter only control run. We also find an anti-correlation between λ_{DM} and the stellar mass for disks but not for ellipticals.

Summary

We extracted about $400 - 620$ halos at four different redshifts in a total halo mass range from $5 \cdot 10^{11} M_{\odot} - 2 \cdot 10^{13} M_{\odot}$ from a hydrodynamic cosmological state-of-the-art simulation, which includes detailed treatment of star formation, chemical enrichment and evolution of super massive black holes. We first rotated the halos to align them according to the angular momentum of their central part, where the galaxies are forming. Then we classified the morphological types of the formed galaxies via the distribution of the circularity parameter ε. Here, we focused on the subset of galaxies, which were clearly identified as pure elliptical or disk galaxies, where we always required this classification to hold in both, the stellar and the gas component. For these two classes of galaxies that have formed in our simulations we calculated the specific angular momentum of the different components as well as their alignments and studied the spin parameter λ. We additionally performed dark matter control simulations to evaluate the role of the baryons on the angular momentum within the simulations. We summarize our findings as follows:

- The rotation curves of the extended gas disks in our simulations compare well with the HI/Hα observations of local galaxies.

- Our simulations reproduce well the observed relations between the stellar mass and the specific angular momentum of the stars for both, the elliptical as well as the disk galaxies.

- In general, the spin parameter of the gas is noticeably larger than the spin parameter of the dark matter, mainly driven due to the cold gas component. This leads to a continuous growth of the spin parameter of the gas component during the evolution of the halo.

- In the inner region of disk galaxies the specific angular momentum of the gas is slightly higher than that of stars, which is in good agreement with recent observations (Obreschkow and Glazebrook, 2014). This is due to the fact that

the gas component has contributions from freshly accreted gas with higher $j_{\rm gas}$ which will be turned into stars later. This is also reflected in our finding that the specific angular momentum of the young stars shows larger values than that of the total $j_{\rm star}$.

- In general, $j_{\rm DM}$ of the total halo is higher than $j_{\rm gas}$ of the galaxy. $j_{\rm gas}$ of the elliptical galaxies is smaller than that of the disk galaxies. This arises from the fact that the cold gas can maintain its angular momentum while being accreted onto the forming disk in the halo center.

- The general alignment of the dark matter angular momentum vector of the halo with that of the angular momentum of its central part is weak for the DM-only and the baryon run. Disc galaxies preferentially form in halos with better aligned dark matter angular momentum vectors, whereas ellipticals form in halos with less alignment.

- The angular momentum vectors of the gas and star component within the whole virial radius have a median misalignment angle of $\approx 13^\circ$ and 23°, respectively, with that of the whole dark matter halo, for all halos at $z = 1.98$.

- The splitting of the overall distribution of λ reveals a dichotomy: The halos hosting disk galaxies have slightly larger spin than the ellipticals. When looking at the inner parts of the halo we find that the angular momenta of the gas and star component of disk galaxies are better aligned with the dark matter halo than that of elliptical galaxies. This is in broad agreement with earlier findings of van den Bosch et al. (2002), who reported a weak tendency that halos with better aligned gas and dark matter angular momentum vectors have higher spin parameters.

Our results are based on the poster child galaxies of the simulation which fulfill the selection criteria in both components. But many galaxies which by eye would be classified as disk galaxies due to their extended gaseous disk and their stellar disk of bright young stars do not pass the selection criteria since they also have a dominant bulge of old stars, especially at low redshift. Therefore the selection criteria have to be refined, so a galaxy with a bright disk of young stars and a bulge consisting of old faint stars is classified as a disk galaxy. Even hybrid forms of galaxy types could be classified and one can check if they behave more like one than the other galaxy type or even totally different.

In any case, the forthcoming years will be very exciting and will bring us nearer to the whole story of galaxy formation.

Acknowledgements

I would like to thank:

- PD Klaus Dolag, for giving me the opportunity to work with these fascinating simulations, to write a master thesis and for always taking the time to answer questions
- Rhea-Silvia Remus for always having an open ear and very useful ideas
- Prof. Andi Burkert for the fruitful discussions and for the input on which this thesis is partly based
- the CAST-group members, especially (in alphabetical order): Alex B., Anna, David, Felix, Katharina, Lisa, Madhura, Mathias G., Max B., Stefan, Tadziu, for useful discussions, looking over the programs, helping me with gnuplot, etc.
- the other students at the USM, especially Björn, Dominika, Georg, Hanna (for providing me with cookies), Markus and Max I.
- Andi Schmidt for encouraging and always helping me with problems throughout my entire studies
- Flo Semrau for the "Vollheulen-Lassen"

There are a lot of other people that made the last years a nice time and each of them helped me to understand a little bit more of physics, I just mention some of them here: Andi M., Christian K., Daniel, Flo Stecker, Jessy, Julia, Manuel N., Maxi, Susanne, Torben, ...

I want to thank my children for bearing me in these sometimes stressful times.

A. Appendix: Angular Momentum-Mass Relation at $z = 0.99$ and $z = 0.47$

For the sake of completeness we also show the plots for the two redshifts that were partially left out, namely $z = 0.99$ and $z = 0.47$. These are just to illustrate the time evolution of different properties discussed above.

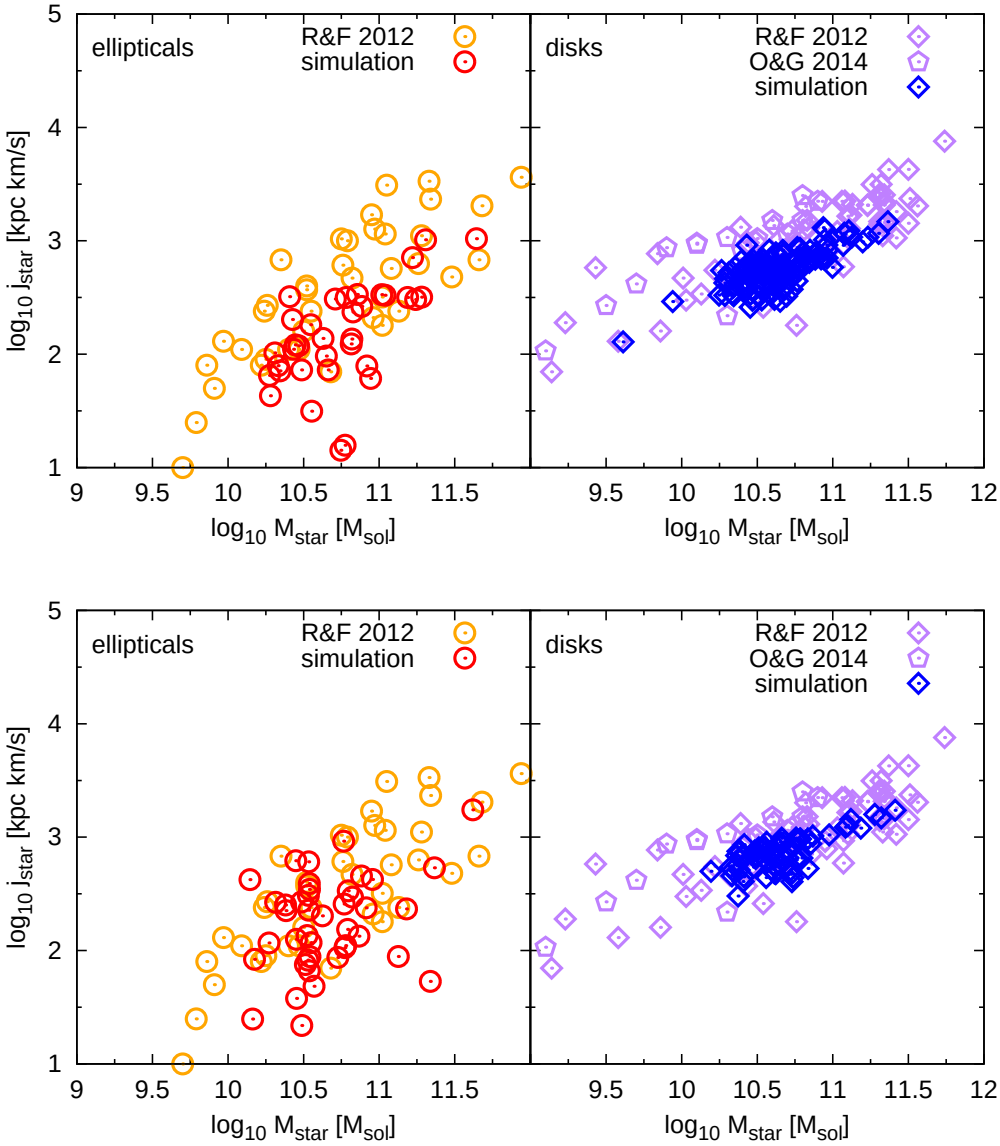

Fig. A.1.: The stellar mass within the innermost ten per cent of the virial radius against the specific angular momentum of the stars within the central region at redshift $z = 0.99$ (upper panels) and $z = 0.47$ (lower panels). Left for galaxies in our simulation, which are classified as ellipticals (red circles) compared to data from observed elliptical galaxies by Romanowsky and Fall (2012) (orange circles, denoted by "R&F 2012"). Right: Discs in our simulation (blue diamonds) compared to observational data of spiral galaxies by Romanowsky and Fall (2012) (purple diamonds, denoted by "R&F 2012") and Obreschkow and Glazebrook (2014) (magenta pentagons, denoted by "O&G 2014").

B. Appendix: Angular Momentum Profiles at $z = 0.99$ and $z = 0.47$

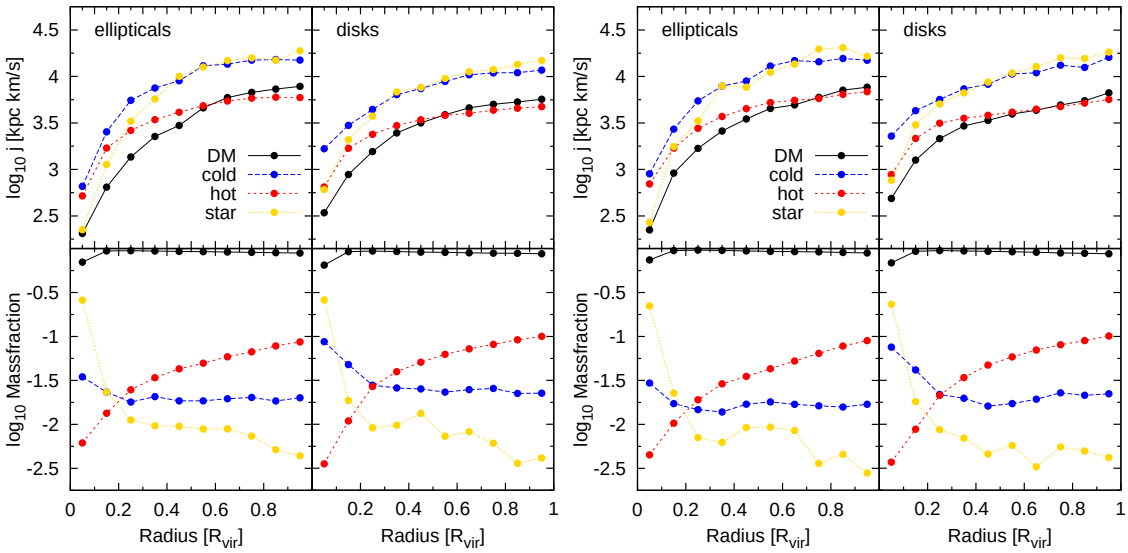

Fig. B.1.: The specific angular momentum (top panels) and the mass fractions (bottom panels) against distance from the center of mass for the cold gas, hot gas, stars and dark matter components of our sample of galaxies at redshift $z = 0.99$ (left) and $z = 0.47$ (right). On each left hand side we show the analysis for the elliptical galaxies and on each right hand side we show the analysis for the disc galaxies.

C. Appendix: Alignment Angles

C.1. Tables for $z = 1.98$ and 0.07

Tab. C.1.: The median and mean misalignment angles between the different components classified only by the circularity of both the gas and star component at redshift $z = 1.98$. DMO are the angles for the dark matter only run.

Median	all halos	discs	ellipticals
$\theta_{\mathrm{gas-stars}}$	24.8	24.8	19.7
$\theta_{\mathrm{gas,0.1-stars,0.1}}$	14.3	6.7	82.6
$\theta_{\mathrm{gas-DM}}$	12.8	14.8	20.6
$\theta_{\mathrm{gas,0.1-DM}}$	53.4	47.2	65.7
$\theta_{\mathrm{stars-DM}}$	22.6	22.7	35.1
$\theta_{\mathrm{stars,0.1-DM}}$	61.4	52.9	59.1
$\theta_{\mathrm{DM,0.1-DM}}$	56.5	50.3	95
$\theta_{\mathrm{DM,0.1-DM}}$ (DMO)	66.4	-	-
Mean	all halos	discs	ellipticals
$\theta_{\mathrm{gas-stars}}$	34.1	31.1	40.4
$\theta_{\mathrm{gas,0.1-stars,0.1}}$	26.5	7.9	77.5
$\theta_{\mathrm{gas-DM}}$	19.6	21.2	28.2
$\theta_{\mathrm{gas,0.1-DM}}$	60.7	53.3	69
$\theta_{\mathrm{stars-DM}}$	31.5	26.9	53
$\theta_{\mathrm{stars,0.1-DM}}$	66.1	55.1	77.2
$\theta_{\mathrm{DM,0.1-DM}}$	62.7	52.2	91
$\theta_{\mathrm{DM,0.1-DM}}$ (DMO)	70.8	-	-

Tab. C.2.: The median and mean misalignment angles between the different components classified only by the circularity of both the gas and star component at redshift $z = 0.07$. DMO are the angles for the dark matter only run.

Median	all halos	discs	ellipticals
$\theta_{\mathrm{gas-stars}}$	30.1	26.1	37.1
$\theta_{\mathrm{gas,0.1-stars,0.1}}$	36.9	5.5	85
$\theta_{\mathrm{gas-DM}}$	25.1	19.4	33.5
$\theta_{\mathrm{gas,0.1-DM}}$	48.8	38.5	55.6
$\theta_{\mathrm{stars-DM}}$	23.9	22.9	27.7
$\theta_{\mathrm{stars,0.1-DM}}$	53.7	42.5	88.3
$\theta_{\mathrm{DM,0.1-DM}}$	46	40.6	74.9
$\theta_{\mathrm{DM,0.1-DM}}$ (DMO)	51.2	-	-
Mean	all halos	discs	ellipticals
$\theta_{\mathrm{gas-stars}}$	40.1	38.3	42.8
$\theta_{\mathrm{gas,0.1-stars,0.1}}$	49.3	5.8	85.8
$\theta_{\mathrm{gas-DM}}$	33	20	37.9
$\theta_{\mathrm{gas,0.1-DM}}$	55.2	47.2	63.6
$\theta_{\mathrm{stars-DM}}$	31.2	24.4	37.1
$\theta_{\mathrm{stars,0.1-DM}}$	61.4	47.8	85.4
$\theta_{\mathrm{DM,0.1-DM}}$	54.5	46	72.9
$\theta_{\mathrm{DM,0.1-DM}}$ (DMO)	56.5	-	-

C.2. Gas and Stars at $z = 0.99$ and $z = 0.47$

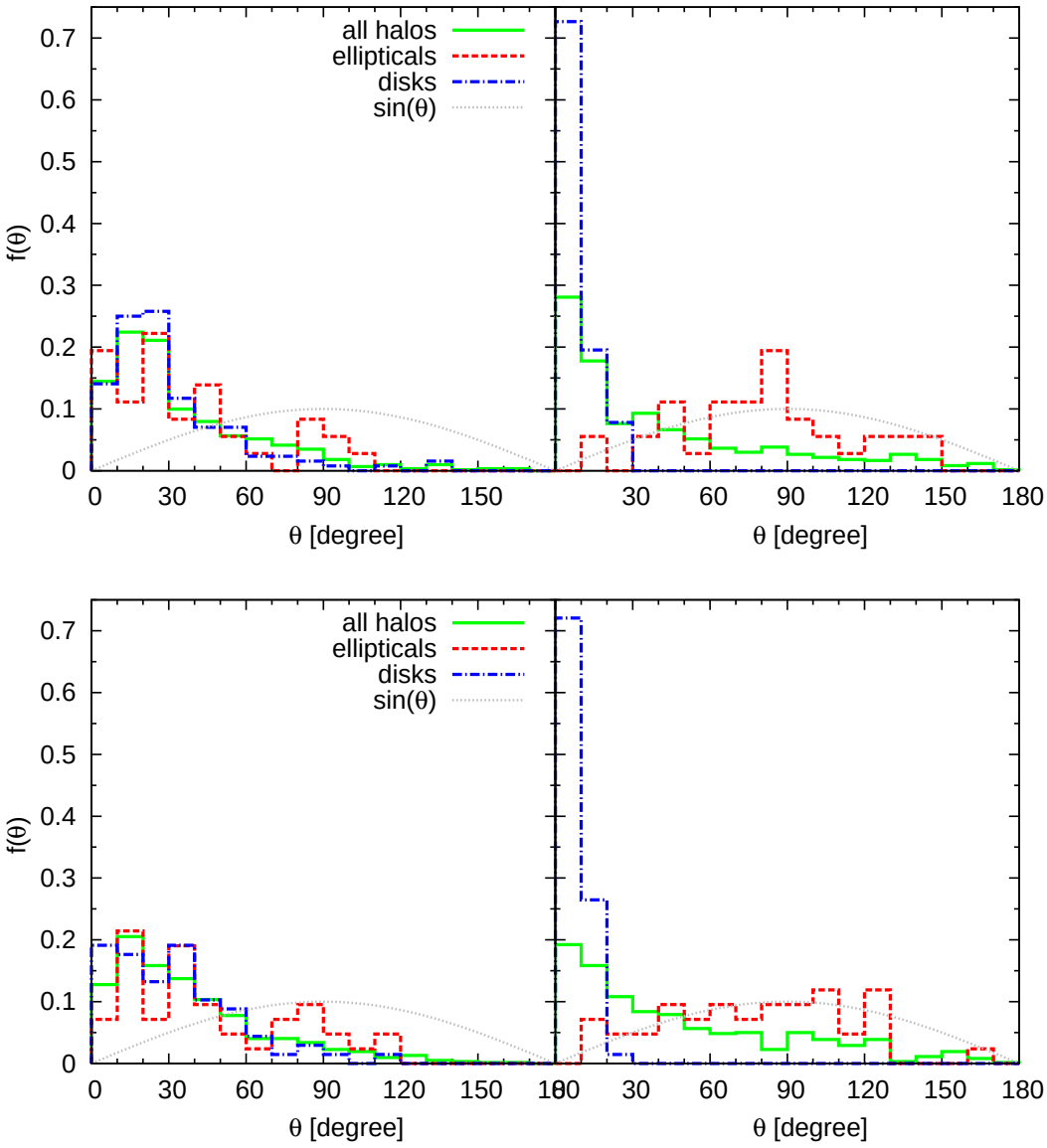

Fig. C.1.: Left: The angle between the total angular momentum vectors of gas and stars within the virial radius. Right: The angle between the total angular momentum vector of gas and stars, both within the innermost ten per cent of the virial radius. The upper panels show redshift $z = 0.99$ and the lower panels show $z = 0.47$.

C.3. Dark Matter and Gas at $z = 0.99$ and $z = 0.47$

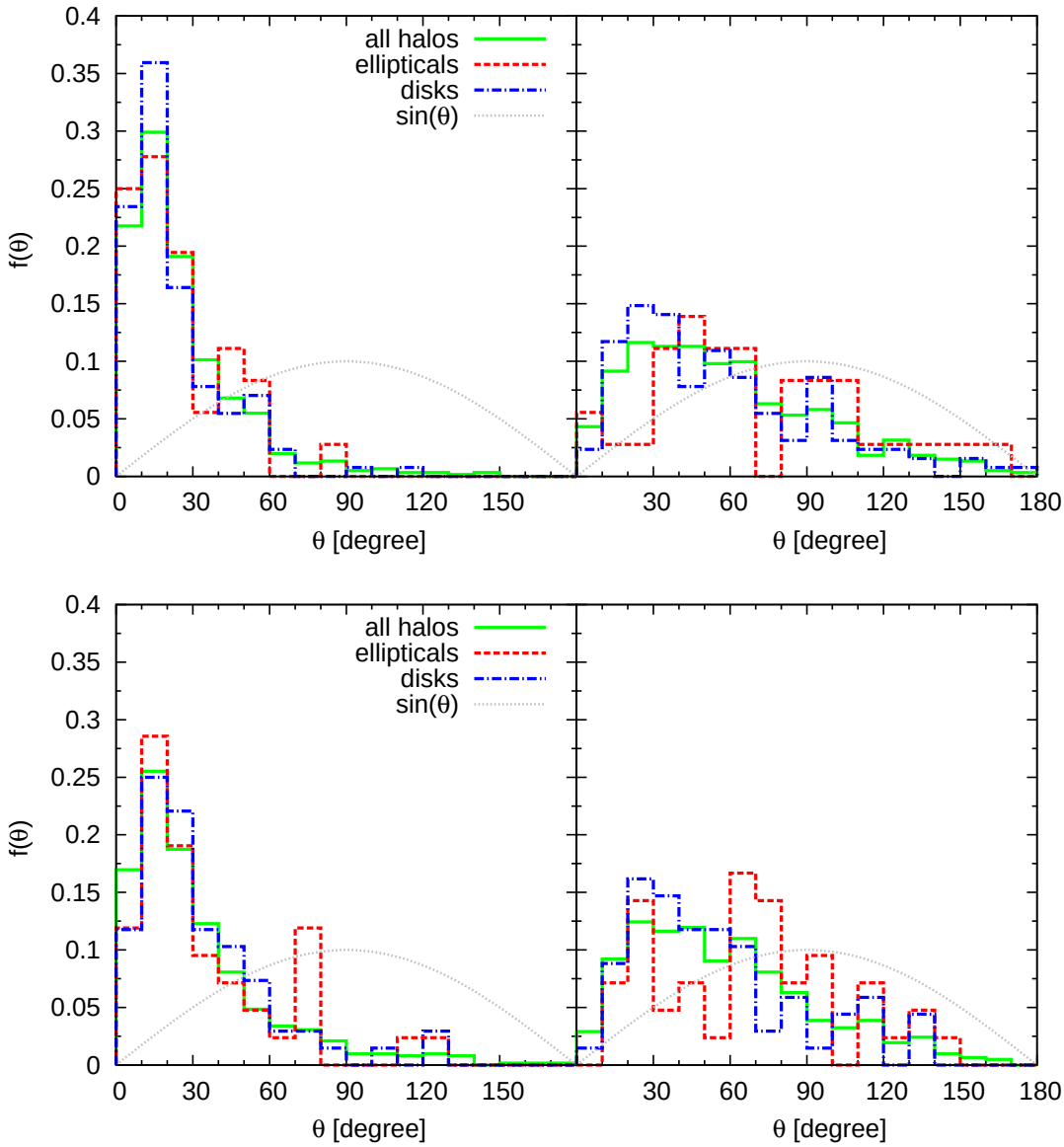

Fig. C.2.: Left: The angle between the total angular momentum vectors of DM and gas within the virial radius. Right: The angle between the total angular momentum vector of DM in $R_{\rm vir}$ and the gas within the innermost ten percent of the virial radius. The upper panels show redshift $z = 0.99$ and the lower panels show $z = 0.47$.

C.4. Dark Matter and Stars at $z = 0.99$ and $z = 0.47$

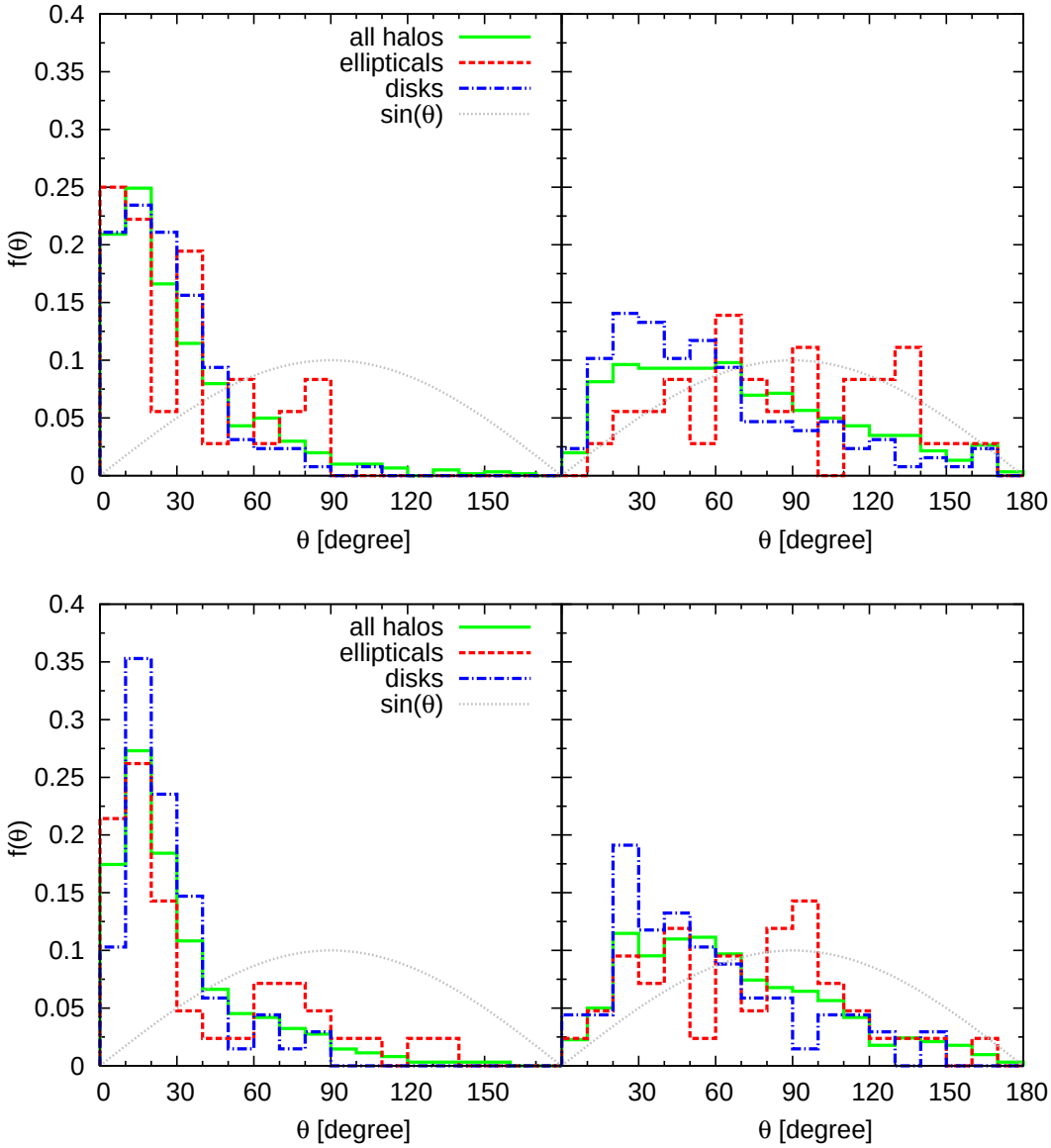

Fig. C.3.: Left: The angle between the total angular momentum vectors of DM and stars within the virial radius. Right: The angle between the total angular momentum vector of DM in $R_{\rm vir}$ and the stars within the innermost 10 per cent of the virial radius. The upper panels show redshift $z = 0.99$ and the lower panels show $z = 0.47$.

C.5. Dark Matter at Different Radii at $z = 0.99$ and $z = 0.47$

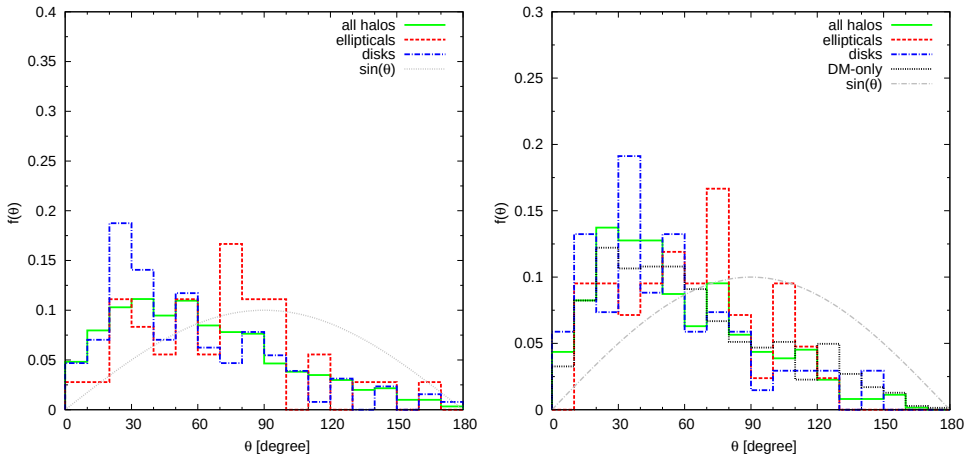

Fig. C.4.: The angle between the total angular momentum vector of DM in $R_{\rm vir}$ and that of the DM within the innermost 10 per cent of the virial radius. Left for $z = 0.99$ and right $z = 0.47$.

D. Appendix: λ – Distribution

D.1. Table for the Overall λ-Distribution

Tab. D.1.: The calculated median values λ_{med} and the fit values λ_0 and σ of the λ-distributions at different redshifts for our sample of galaxies

redshift	all halos
1.98	$\lambda_{\mathrm{med}} = 0.043$, $\lambda_0 = 0.043$, $\sigma = 0.661$
0.99	$\lambda_{\mathrm{med}} = 0.046$, $\lambda_0 = 0.047$, $\sigma = 0.636$
0.47	$\lambda_{\mathrm{med}} = 0.042$, $\lambda_0 = 0.042$, $\sigma = 0.641$
0.07	$\lambda_{\mathrm{med}} = 0.042$, $\lambda_0 = 0.042$, $\sigma = 0.623$
redshift	disks
1.98	$\lambda_{\mathrm{med}} = 0.048$, $\lambda_0 = 0.049$, $\sigma = 0.651$
0.99	$\lambda_{\mathrm{med}} = 0.051$, $\lambda_0 = 0.051$, $\sigma = 0.562$
0.47	$\lambda_{\mathrm{med}} = 0.045$, $\lambda_0 = 0.045$, $\sigma = 0.517$
0.07	$\lambda_{\mathrm{med}} = 0.058$, $\lambda_0 = 0.053$, $\sigma = 0.568$
redshift	ellipticals
1.98	$\lambda_{\mathrm{med}} = 0.028$, $\lambda_0 = 0.028$, $\sigma = 0.569$
0.99	$\lambda_{\mathrm{med}} = 0.038$, $\lambda_0 = 0.038$, $\sigma = 0.684$
0.47	$\lambda_{\mathrm{med}} = 0.036$, $\lambda_0 = 0.034$, $\sigma = 0.849$
0.07	$\lambda_{\mathrm{med}} = 0.034$, $\lambda_0 = 0.033$, $\sigma = 0.539$

D.2. λ for the Dark Matter Only

Tab. D.2.: λ-parameters from different authors using dark matter only simulations: Bullock et al. (2001) (B01), Bryan et al. (2013) (Bryan13), Trowland et al. (2013) (Trowland13)

author	λ_0	σ	redshift	sample size	remarks
B01	0.035±0.005	0.5±0.03	0	500	
Bryan13	0.036	0.62 ± 0.01	0	7094	
Bryan13	0.038	0.60	2	5334	
Trowland13	$0.0290\ ^{+0.00006}_{-0.00005}$	$0.604^{+0.001}_{-0.002}$	0		Millenium
Trowland13	$0.02940^{+0.00008}_{-0.0001}$	0.576 ± 0.002	3		Millenium

D.3. λ for Different Components at $z = 0.99$ and $z = 0.47$

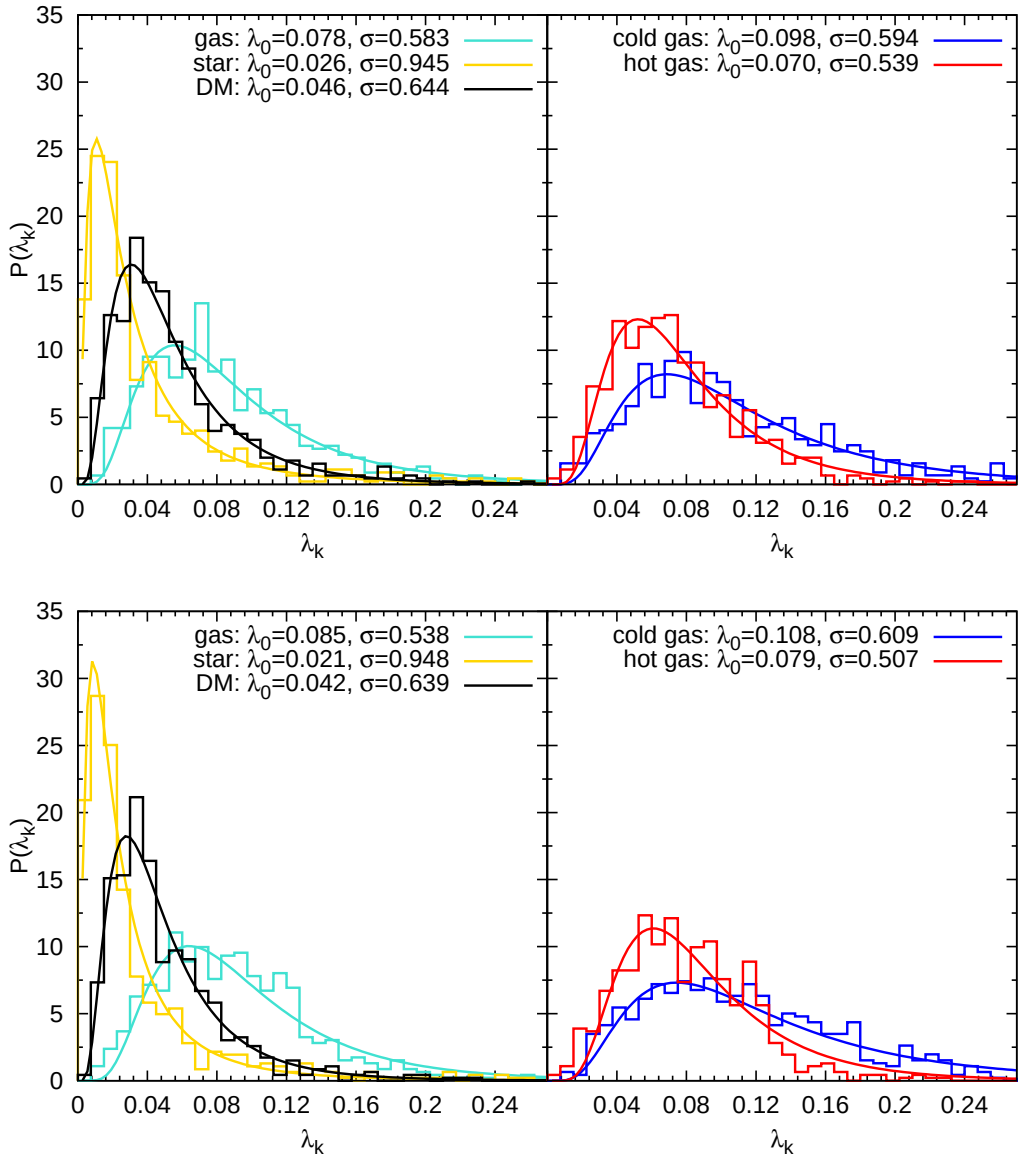

Fig. D.1.: Left panel: the λ-parameter for the different components within the virial radius: The DM (black) is the dominant component, the stars (yellow) peak at the lower values, whereas the gas is distributed around the higher values. Right panel: the gas component split into hot (red) and cold (blue) gas. The upper panels show redshift $z = 0.99$ and the lower ones $z = 0.47$.

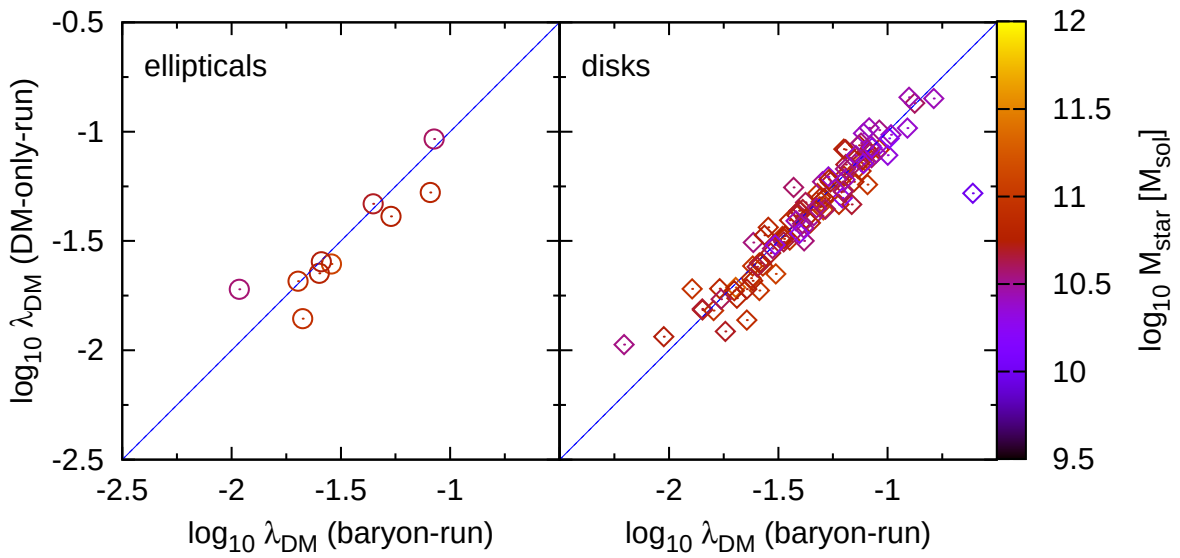

Fig. D.2.: The λ-parameter plotted logarithmically for the dark matter component within the virial radius, on the x-axis the λ for the baryon-run and on the y-axis for the DM-only run, the color codes the stellar mass within the inner 10 per cent of the virial radius. Left are the ellipticals and on the right panel the discs at redshift $z = 0.47$.

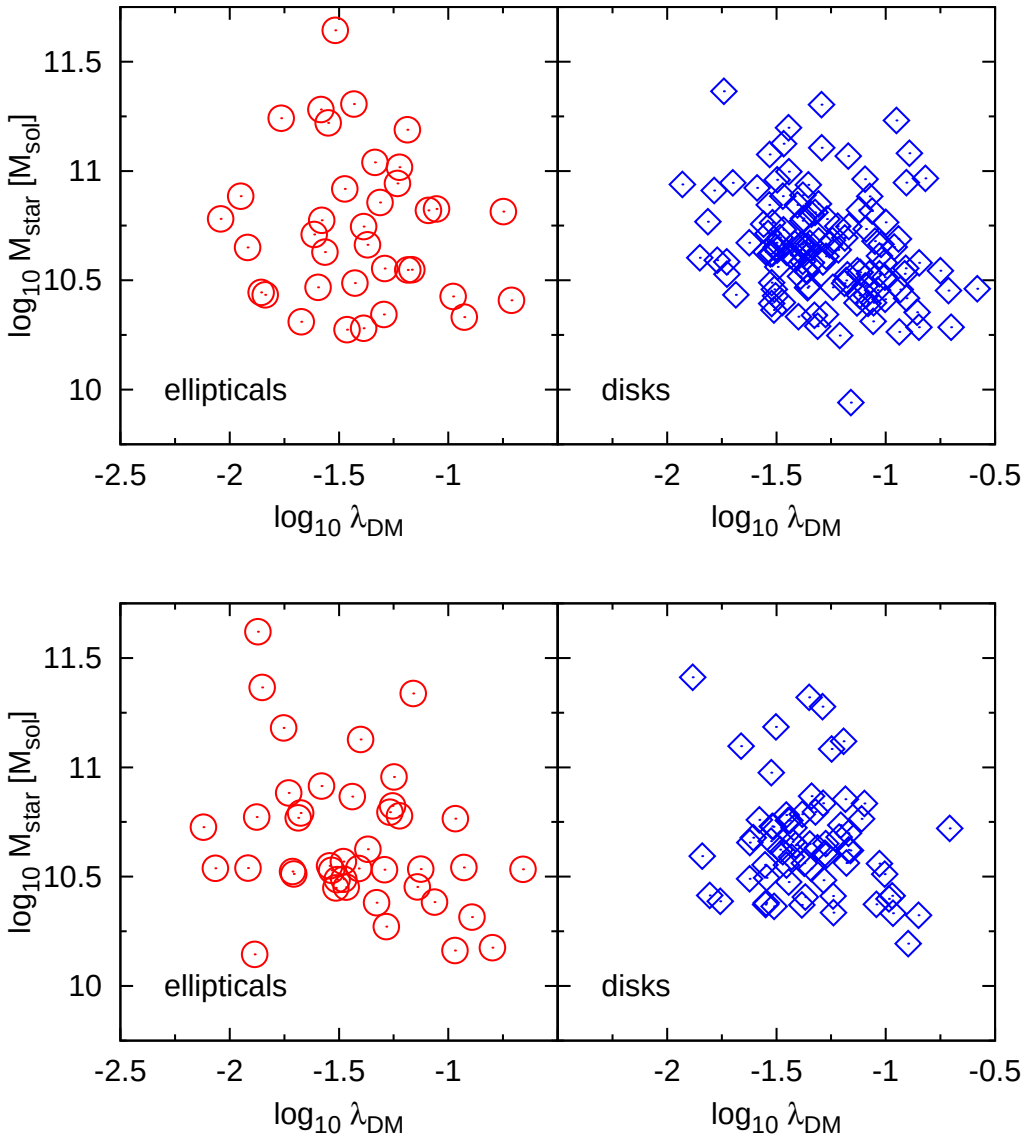

Fig. D.3.: The λ-parameter plotted logarithmically for the dark matter component within the virial radius for the baryon-run and on the y-axis the stellar mass within the inner 10 per cent of the virial radius. Left are the ellipticals and on the right panel the discs. The upper panels show redshift $z = 0.99$ and the lower ones $z = 0.47$.

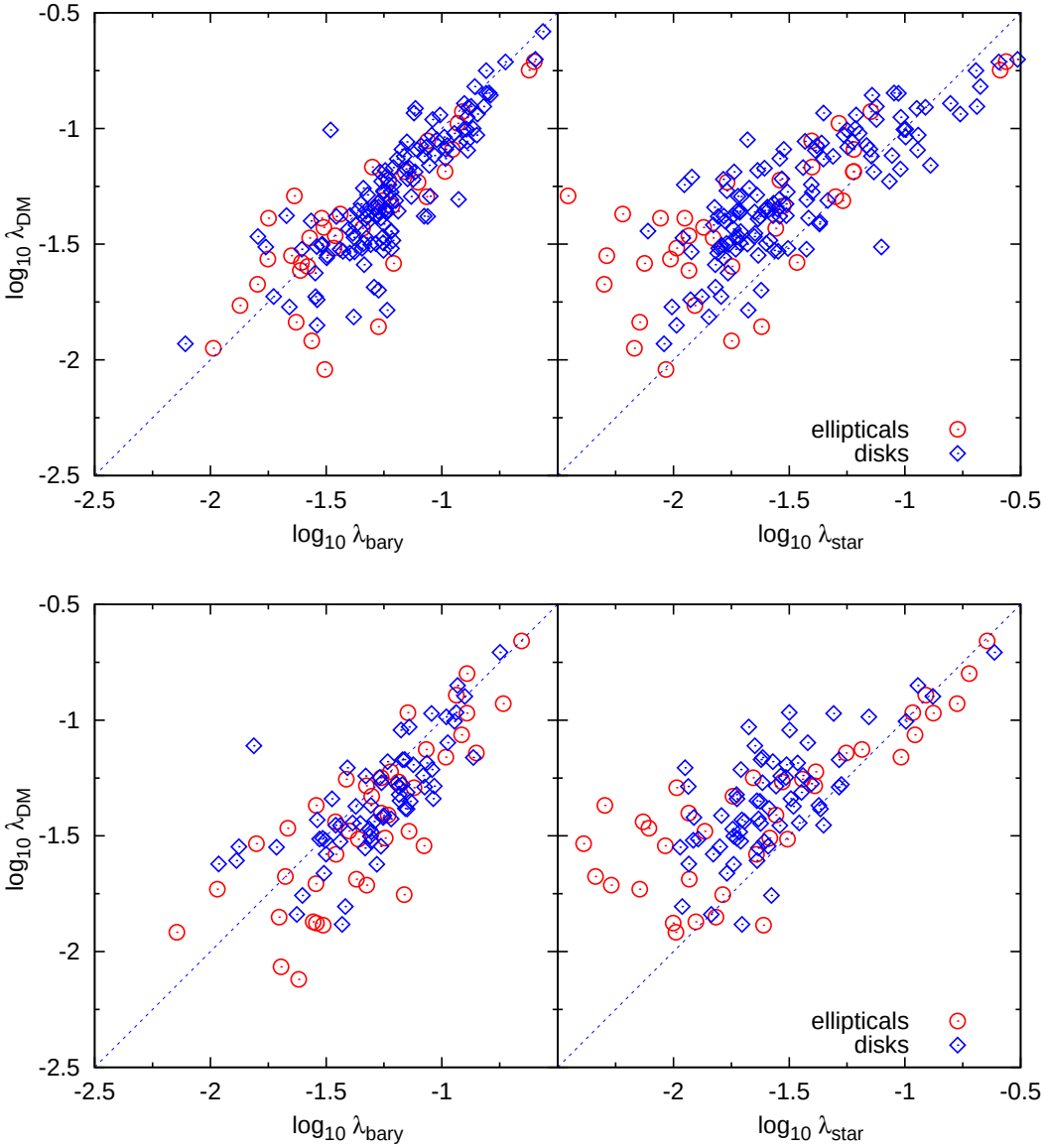

Fig. D.4.: Left panels: the λ-parameter for the baryons (gas and stars) against that of the dark matter. Right panels: the λ-parameter for the stars against that of the dark matter. The upper panels show $z = 0.99$ and the lower panels $z = 0.47$.

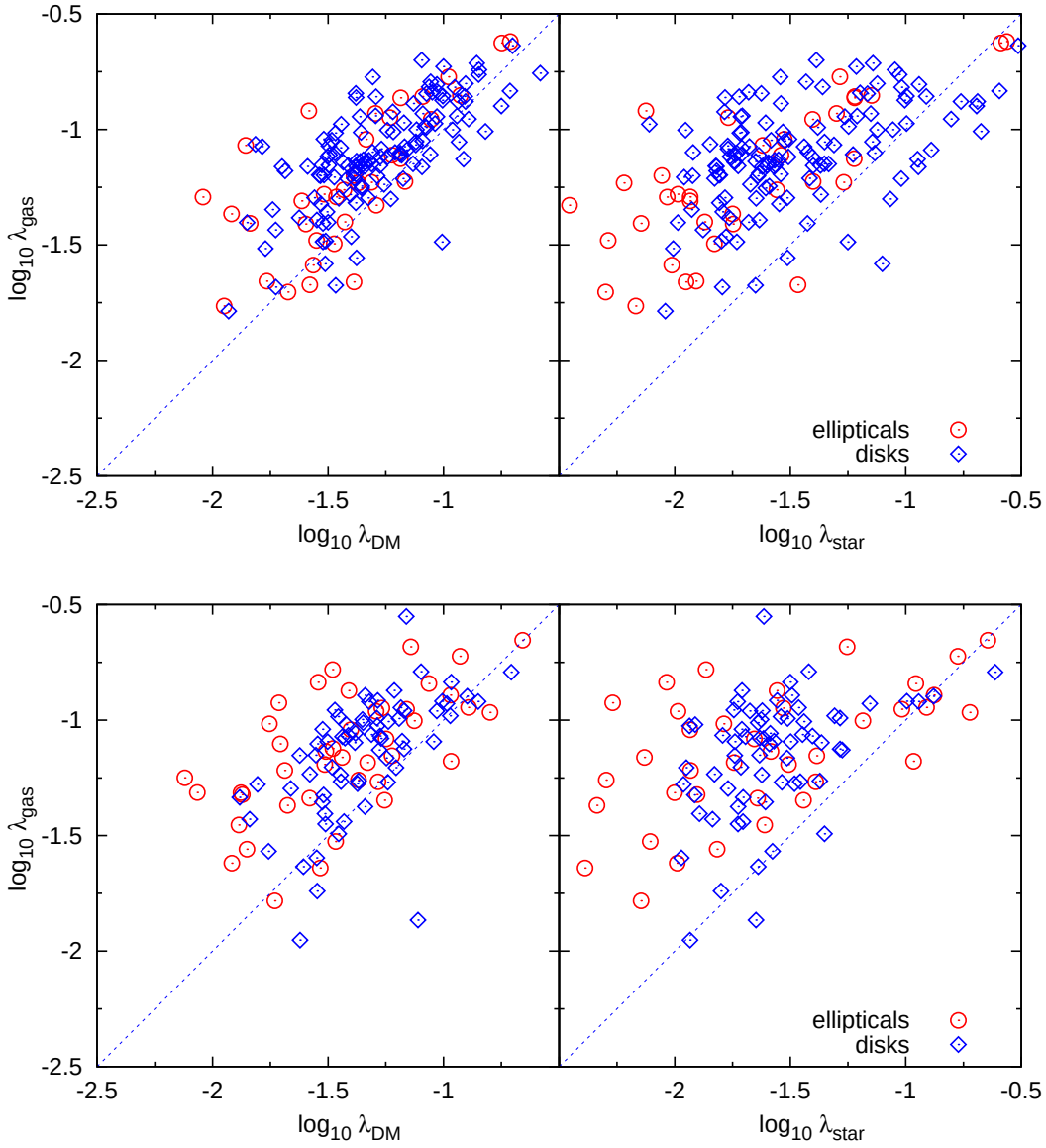

Fig. D.5.: Left panel: the λ-parameter for the dark matter against that of the gas. Right panel: the λ-parameter for the stars against that of the gas. The upper panels show redshift $z = 0.99$ and the lower panels $z = 0.47$.

Bibliography

Abadi, M. G., Navarro, J. F., Steinmetz, M., and Eke, V. R. (2003). Simulations of Galaxy Formation in a Λ Cold Dark Matter Universe. II. The Fine Structure of Simulated Galactic Disks. *The Astrophysical Journal*, 597:21–34.

Bachmann, L. K., Dolag, K., Hirschmann, M., Almudena Prieto, M., and Remus, R.-S. (2014). A refined sub-grid model for black hole accretion and AGN feedback in large cosmological simulations. *ArXiv e-prints*.

Bailin, J. and Steinmetz, M. (2005). Internal and External Alignment of the Shapes and Angular Momenta of ΛCDM Halos. *The Astrophysical Journal*, 627:647–665.

Barnes, J. and Efstathiou, G. (1987). Angular momentum from tidal torques. *The Astrophysical Journal*, 319:575–600.

Berta, Z. K., Jimenez, R., Heavens, A. F., and Panter, B. (2008). The role of spin in the formation and evolution of galaxies. *Monthly Notices of the Royal Astronomical Society*, 391:197–204.

Bett, P., Eke, V., Frenk, C. S., Jenkins, A., Helly, J., and Navarro, J. (2007). The spin and shape of dark matter haloes in the Millennium simulation of a Λ cold dark matter universe. *Monthly Notices of the Royal Astronomical Society*, 376:215–232.

Bett, P., Eke, V., Frenk, C. S., Jenkins, A., and Okamoto, T. (2010). The angular momentum of cold dark matter haloes with and without baryons. *Monthly Notices of the Royal Astronomical Society*, 404:1137–1156.

Binney, J. and Tremaine, S. (2008). *Galactic Dynamics*. Princeton University Press, second edition.

Blais-Ouellette, S., Amram, P., Carignan, C., and Swaters, R. (2004). Accurate determination of the mass distribution in spiral galaxies. III. Fabry-Perot imaging spectroscopy of 6 spiral galaxies. *Astronomy and Astrophysics*, 420:147–161.

Brook, C. B., Kawata, D., Gibson, B. K., and Flynn, C. (2004). Stellar halo constraints on simulated late-type galaxies. *Monthly Notices of the Royal Astronomical Society*, 349:52–56.

Bryan, S. E., Kay, S. T., Duffy, A. R., Schaye, J., Dalla Vecchia, C., and Booth, C. M. (2013). The impact of baryons on the spins and shapes of dark matter haloes. *Monthly Notices of the Royal Astronomical Society*, 429:3316–3329.

Bullock, J. S., Dekel, A., Kolatt, T. S., Kravtsov, A. V., Klypin, A. A., Porciani, C., and Primack, J. R. (2001). A Universal Angular Momentum Profile for Galactic Halos. *The Astrophysical Journal*, 555:240–257.

Cappellari, M., Emsellem, E., Krajnović, D., McDermid, R. M., Scott, N., Verdoes Kleijn, G. A., Young, L. M., Alatalo, K., Bacon, R., Blitz, L., Bois, M., Bournaud, F., Bureau, M., Davies, R. L., Davis, T. A., de Zeeuw, P. T., Duc, P.-A., Khochfar, S., Kuntschner, H., Lablanche, P.-Y., Morganti, R., Naab, T., Oosterloo, T., Sarzi, M., Serra, P., and Weijmans, A.-M. (2011). The ATLAS^{3D} project - I. A volume-limited sample of 260 nearby early-type galaxies: science goals and selection criteria. *Monthly Notices of the Royal Astronomical Society*, 413:813–836.

Catinella, B., Giovanelli, R., and Haynes, M. P. (2006). Template Rotation Curves for Disk Galaxies. *The Astrophysical Journal*, 640:751–761.

Chen, D. N., Jing, Y. P., and Yoshikaw, K. (2003). Angular Momentum Distribution of Hot Gas and Implications for Disk Galaxy Formation. *The Astrophysical Journal*, 597:35–47.

Corbelli, E., Lorenzoni, S., Walterbos, R., Braun, R., and Thilker, D. (2010). A wide-field H I mosaic of Messier 31. II. The disk warp, rotation, and the dark matter halo. *Astronomy and Astrophysics*, 511:A89.

Croft, R. A. C., Di Matteo, T., Springel, V., and Hernquist, L. (2009). Galaxy morphology, kinematics and clustering in a hydrodynamic simulation of a Λ cold dark matter universe. *Monthly Notices of the Royal Astronomical Society*, 400:43–67.

Danovich, M., Dekel, A., Hahn, O., Ceverino, D., and Primack, J. (2014). Four phases of angular-momentum buildup in high-z galaxies: from cosmic-web streams to an extended tilted ring, disc and bulge. *ArXiv e-prints*.

Davis, M., Efstathiou, G., Frenk, C. S., and White, S. D. M. (1985). The evolution of large-scale structure in a universe dominated by cold dark matter. *The Astrophysical Journal*, 292:371–394.

Dolag, K., Borgani, S., Murante, G., and Springel, V. (2009). Substructures in hydrodynamical cluster simulations. *Monthly Notices of the Royal Astronomical Society*, 399:497–514.

Dolag, K., Jubelgas, M., Springel, V., Borgani, S., and Rasia, E. (2004). Thermal Conduction in Simulated Galaxy Clusters. *The Astrophysical Journal*, 606:L97–L100.

Dolag, K., Vazza, F., Brunetti, G., and Tormen, G. (2005). Turbulent gas motions in galaxy cluster simulations: the role of smoothed particle hydrodynamics viscosity. *Monthly Notices of the Royal Astronomical Society*, 364:753–772.

Doroshkevich, A. G. (1970). The space structure of perturbations and the origin of rotation of galaxies in the theory of fluctuation. *Astrofizika*, 6:581–600.

Dressler, A. (1980). Galaxy morphology in rich clusters - Implications for the formation and evolution of galaxies. *The Astrophysical Journal*, 236:351–365.

Eke, V. R., Cole, S., and Frenk, C. S. (1996). Cluster evolution as a diagnostic for Omega. *Monthly Notices of the Royal Astronomical Society*, 282:263–280.

Fabjan, D., Borgani, S., Tornatore, L., Saro, A., Murante, G., and Dolag, K. (2010). Simulating the effect of active galactic nuclei feedback on the metal enrichment of galaxy clusters. *Monthly Notices of the Royal Astronomical Society*, 401:1670–1690.

Fall, S. M. (1983). Galaxy formation - Some comparisons between theory and observation. In Athanassoula, E., editor, *Internal Kinematics and Dynamics of Galaxies*, volume 100 of *IAU Symposium*, pages 391–398.

Fall, S. M. and Efstathiou, G. (1980). Formation and rotation of disc galaxies with haloes. *Monthly Notices of the Royal Astronomical Society*, 193:189–206.

Fall, S. M. and Romanowsky, A. J. (2013). Angular Momentum and Galaxy Formation Revisited: Effects of Variable Mass-to-light Ratios. *The Astrophysical Journal*, 769:L26.

Goto, T., Yamauchi, C., Fujita, Y., Okamura, S., Sekiguchi, M., Smail, I., Bernardi, M., and Gomez, P. L. (2003). The morphology-density relation in the Sloan Digital Sky Survey. *Monthly Notices of the Royal Astronomical Society*, 346:601–614.

Governato, F., Willman, B., Mayer, L., Brooks, A., Stinson, G., Valenzuela, O., Wadsley, J., and Quinn, T. (2007). Forming disc galaxies in ΛCDM simulations. *Monthly Notices of the Royal Astronomical Society*, 374:1479–1494.

Hahn, O., Teyssier, R., and Carollo, C. M. (2010). The large-scale orientations of disc galaxies. *Monthly Notices of the Royal Astronomical Society*, 405:274–290.

Hetznecker, H. (2009). *Kosmologische Strukturbildung*. Spektrum Akademischer Verlag, first edition.

Hirschmann, M., Dolag, K., Saro, A., Bachmann, L., Borgani, S., and Burkert, A. (2014). Cosmological simulations of black hole growth: AGN luminosities and downsizing. *Monthly Notices of the Royal Astronomical Society*, 442:2304–2324.

Kimm, T., Devriendt, J., Slyz, A., Pichon, C., Kassin, S. A., and Dubois, Y. (2011). The angular momentum of baryons and dark matter halos revisited. *ArXiv e-prints*.

Komatsu, E., Smith, K. M., Dunkley, J., Bennett, C. L., Gold, B., Hinshaw, G., Jarosik, N., Larson, D., Nolta, M. R., Page, L., Spergel, D. N., Halpern, M., Hill, R. S., Kogut, A., Limon, M., Meyer, S. S., Odegard, N., Tucker, G. S., Weiland, J. L., Wollack, E., and Wright, E. L. (2011). Seven-year Wilkinson Microwave Anisotropy Probe (WMAP) Observations: Cosmological Interpretation. *Astrophysical Journal Supplement Series*, 192:18.

Kregel, M. and van der Kruit, P. C. (2004). Structure and kinematics of edge-on galaxy discs - III. The rotation curves in the gas. *Monthly Notices of the Royal Astronomical Society*, 352:787–803.

Leroy, A. K., Walter, F., Brinks, E., Bigiel, F., de Blok, W. J. G., Madore, B., and Thornley, M. D. (2008). The Star Formation Efficiency in Nearby Galaxies: Measuring Where Gas Forms Stars Effectively. *Astronomical Journal*, 136:2782–2845.

Macciò, A. V., Dutton, A. A., and van den Bosch, F. C. (2008). Concentration, spin and shape of dark matter haloes as a function of the cosmological model: WMAP1,

WMAP3 and WMAP5 results. *Monthly Notices of the Royal Astronomical Society*, 391:1940–1954.

Meza, A., Navarro, J. F., Steinmetz, M., and Eke, V. R. (2003). Simulations of Galaxy Formation in a ΛCDM Universe. III. The Dissipative Formation of an Elliptical Galaxy. *The Astrophysical Journal*, 590:619–635.

Mo, H. J., Mao, S., and White, S. D. M. (1998). The formation of galactic discs. *Monthly Notices of the Royal Astronomical Society*, 295:319–336.

Navarro, J. F. and Benz, W. (1991). Dynamics of cooling gas in galactic dark halos. *The Astrophysical Journal*, 380:320–329.

Navarro, J. F. and Steinmetz, M. (1997). The Effects of a Photoionizing Ultraviolet Background on the Formation of Disk Galaxies. *The Astrophysical Journal*, 478:13–28.

Navarro, J. F. and White, S. D. M. (1994). Simulations of dissipative galaxy formation in hierarchically clustering universes-2. Dynamics of the baryonic component in galactic haloes. *Monthly Notices of the Royal Astronomical Society*, 267:401–412.

Obreschkow, D. and Glazebrook, K. (2014). Fundamental Mass-Spin-Morphology Relation Of Spiral Galaxies. *The Astrophysical Journal*, 784:26.

Okamoto, T., Eke, V. R., Frenk, C. S., and Jenkins, A. (2005). Effects of feedback on the morphology of galaxy discs. *Monthly Notices of the Royal Astronomical Society*, 363:1299–1314.

Peebles, P. J. E. (1969). Origin of the Angular Momentum of Galaxies. *The Astrophysical Journal*, 155:393.

Peebles, P. J. E. (1971). Rotation of Galaxies and the Gravitational Instability Picture. *Astronomy and Astrophysics*, 11:377.

Peebles, P. J. E. (1993). *Principles of Physical Cosmology*. Princeton University Press, first edition.

Peirani, S., Mohayaee, R., and de Freitas Pacheco, J. A. (2004). The angular momentum of dark haloes: merger and accretion effects. *Monthly Notices of the Royal Astronomical Society*, 348:921–931.

Persic, M., Salucci, P., and Stel, F. (1996). The universal rotation curve of spiral galaxies - I. The dark matter connection. *Monthly Notices of the Royal Astronomical Society*, 281:27–47.

Press, W. H., Teukolsky, S. A., Vetterling, W. T., and Flannery, B. P. (1996). *Numerical Recipes in Fortran 90*. Cambridge University Press, second edition.

Remus, R.-S., Burkert, A., Dolag, K., Johansson, P. H., Naab, T., Oser, L., and Thomas, J. (2013). The Dark Halo—Spheroid Conspiracy and the Origin of Elliptical Galaxies. *The Astrophysical Journal*, 766:71.

Romanowsky, A. J. and Fall, S. M. (2012). Angular Momentum and Galaxy Formation Revisited. *Astrophysical Journal Supplement Series*, 203:17.

Sales, L. V., Navarro, J. F., Theuns, T., Schaye, J., White, S. D. M., Frenk, C. S., Crain, R. A., and Dalla Vecchia, C. (2012). The origin of discs and spheroids in simulated galaxies. *Monthly Notices of the Royal Astronomical Society*, 423:1544–1555.

Scannapieco, C., Tissera, P. B., White, S. D. M., and Springel, V. (2008). Effects of supernova feedback on the formation of galaxy discs. *Monthly Notices of the Royal Astronomical Society*, 389:1137–1149.

Scannapieco, C., White, S. D. M., Springel, V., and Tissera, P. B. (2009). The formation and survival of discs in a ΛCDM universe. *Monthly Notices of the Royal Astronomical Society*, 396:696–708.

Schneider, P. (2008). *Einführung in die Extragalaktische Astronomie und Kosmologie*. Springer Berlin Heidelberg, first edition.

Sharma, S. and Steinmetz, M. (2005). The Angular Momentum Distribution of Gas and Dark Matter in Galactic Halos. *The Astrophysical Journal*, 628:21–44.

Sharma, S., Steinmetz, M., and Bland-Hawthorn, J. (2012). On the Origin of the Angular Momentum Properties of Gas and Dark Matter in Galactic Halos and Its Implications. *The Astrophysical Journal*, 750:107.

Spitzer, L. (1962). *Physics of Fully Ionized Gases*.

Springel, V. (2005). The cosmological simulation code GADGET-2. *Monthly Notices of the Royal Astronomical Society*, 364:1105–1134.

Springel, V., Di Matteo, T., and Hernquist, L. (2005). Modelling feedback from stars and black holes in galaxy mergers. *Monthly Notices of the Royal Astronomical Society*, 361:776–794.

Springel, V. and Hernquist, L. (2003). Cosmological smoothed particle hydrodynamics simulations: a hybrid multiphase model for star formation. *Monthly Notices of the Royal Astronomical Society*, 339:289–311.

Springel, V., White, S. D. M., Tormen, G., and Kauffmann, G. (2001a). Populating a cluster of galaxies - I. Results at [formmu2]z=0. *Monthly Notices of the Royal Astronomical Society*, 328:726–750.

Springel, V., Yoshida, N., and White, S. D. M. (2001b). GADGET: a code for collisionless and gasdynamical cosmological simulations. *Nature*, 6:79–117.

Stewart, K. R., Brooks, A. M., Bullock, J. S., Maller, A. H., Diemand, J., Wadsley, J., and Moustakas, L. A. (2013). Angular Momentum Acquisition in Galaxy Halos. *The Astrophysical Journal*, 769:74.

Stewart, K. R., Kaufmann, T., Bullock, J. S., Barton, E. J., Maller, A. H., Diemand, J., and Wadsley, J. (2011). Orbiting Circumgalactic Gas as a Signature of Cosmological Accretion. *The Astrophysical Journal*, 738:39.

Toomre, A. (1977). Mergers and Some Consequences. In Tinsley, B. M. and Larson, D. Campbell, R. B. G., editors, *Evolution of Galaxies and Stellar Populations*, page 401.

Tornatore, L., Borgani, S., Dolag, K., and Matteucci, F. (2007). Chemical enrichment of galaxy clusters from hydrodynamical simulations. *Monthly Notices of the Royal Astronomical Society*, 382:1050–1072.

Tornatore, L., Borgani, S., Matteucci, F., Recchi, S., and Tozzi, P. (2004). Simulating the metal enrichment of the intracluster medium. *Monthly Notices of the Royal Astronomical Society*, 349:L19–L24.

Trowland, H. E., Lewis, G. F., and Bland-Hawthorn, J. (2013). The Cosmic History of the Spin of Dark Matter Halos within the Large-scale Structure. *The Astrophysical Journal*, 762:72.

van den Bosch, F. C., Abel, T., Croft, R. A. C., Hernquist, L., and White, S. D. M. (2002). The Angular Momentum of Gas in Protogalaxies. I. Implications for the Formation of Disk Galaxies. *The Astrophysical Journal*, 576:21–35.

Vogt, N. P., Haynes, M. P., Herter, T., and Giovanelli, R. (2004). M/L, Hα Rotation Curves, and H I Measurements for 329 Nearby Cluster and Field Spirals. I. Data. *Astronomical Journal*, 127:3273–3299.

Walter, F., Brinks, E., de Blok, W. J. G., Bigiel, F., Kennicutt, Jr., R. C., Thornley, M. D., and Leroy, A. (2008). THINGS: The H I Nearby Galaxy Survey. *Astronomical Journal*, 136:2563–2647.

Welker, C., Devriendt, J., Dubois, Y., Pichon, C., and Peirani, S. (2014). Mergers drive spin swings along the cosmic web. *ArXiv e-prints*.

White, S. D. M. (1984). Angular momentum growth in protogalaxies. *The Astrophysical Journal*, 286:38–41.

White, S. D. M. and Rees, M. J. (1978). Core condensation in heavy halos - A two-stage theory for galaxy formation and clustering. *Monthly Notices of the Royal Astronomical Society*, 183:341–358.

Yegorova, I. A., Babic, A., Salucci, P., Spekkens, K., and Pizzella, A. (2011). Rotation curves of luminous spiral galaxies. *Astronomische Nachrichten*, 332:846–853.

Young, L. M., Scott, N., Serra, P., Alatalo, K., Bayet, E., Blitz, L., Bois, M., Bournaud, F., Bureau, M., Crocker, A. F., Cappellari, M., Davies, R. L., Davis, T. A., de Zeeuw, P. T., Duc, P.-A., Emsellem, E., Khochfar, S., Krajnović, D., Kuntschner, H., McDermid, R. M., Morganti, R., Naab, T., Oosterloo, T., Sarzi, M., and Weijmans, A.-M. (2014). The ATLAS^{3D} project - XXVII. Cold gas and the colours and ages of early-type galaxies. *Monthly Notices of the Royal Astronomical Society*, 444:3408–3426.

Zavala, J., Okamoto, T., and Frenk, C. S. (2008). Bulges versus discs: the evolution of angular momentum in cosmological simulations of galaxy formation. *Monthly Notices of the Royal Astronomical Society*, 387:364–370.

Selbstständigkeitserklärung

Hiermit erkläre ich, dass ich diese Masterarbeit zum Thema:

'Angular Momentum Distribution in Galactic Halos'

selbstständig verfasst habe. Ich habe keine anderen als die in der Arbeit angegebenen Quellen und Hilfsmittel benutzt.

München,	
Ort, Datum	Unterschrift